Overview about rock mechanical lab testing – part I: mechanical tests

Authors: Prof. Dr. habil. Heinz Konietzky (TU Bergakademie Freiberg, Geotechnical Institute) & Ass. Prof. Dr. Thomas Frühwirt (Montan-Universität Leoben, Chair of Mining Engineering and Mineral Economics)

1   Introduction

Rock mechanical lab testing provides basic parameters in respect to mechanical, hydraulic and thermal rock properties. This also includes the interaction of these properties, obtained by so-called hydro-thermal-mechanical coupled testing (HTM). Several tests are similar to those which are common in soil mechanics [e.g. Germaine & Germaine 2009], but due to the high stiffness and strength level of the rock material as well as the brittle characteristics of most of the rock forces, resolution in respect to deformation and displacement as well as reaction time of testing devices have to meet special requirements.

Rock mechanical lab testing can be subdivided into several types according to different criteria, for instance:

- Static vs. dynamic tests
- Uniaxial vs. triaxial tests
- Coupled vs. uncoupled tests
- Sophisticated tests vs. indicator tests
- Standardized tests vs. scientific tests
- Compression tests vs. tensile tests

Standards for rock mechanical lab tests are formulated in regulations or recommendations by national or international scientific organizations. Important documents are the following:

- Recommendation of the DGGT (German Geotechnical Society)

- Recommendations of the ISRM (Int. Society for Rock Mechanics)

- ASTM standard (American Society for Testing and Materials)

Because brittle rocks have similar parameters and show similar pattern during testing compared with concrete, standards and recommendation valid for concrete can be consulted in addition to the rock mechanical literature. Prerequisite to obtain reliable data from rock mechanical testing is the correct sample selection and preparation. Samples should be prepared according to the specific recommendations valid for the different tests. Important are size (e.g. length to height ratio or ratio of grain size to sample size) and the surface conditions (e.g. roughness or parallelism). The most important mechanical properties are related to strength (e.g. uniaxial compressive and tensile strength) and stiffness (e.g. Young's or Deformation Modulus and Poisson's ratio). The most important hydraulic parameters are porosity and permeability. The most important thermal parameters are thermal conductivity and thermal expansion coefficient.

The next chapters describe the most popular tests in detail. The authors are aware, that several other test procedures exist but this chapter can cover only a few and the most popular ones. Fig. 1.1 illustrates how strain rate, test apparatus and deformation type correlate to each other.
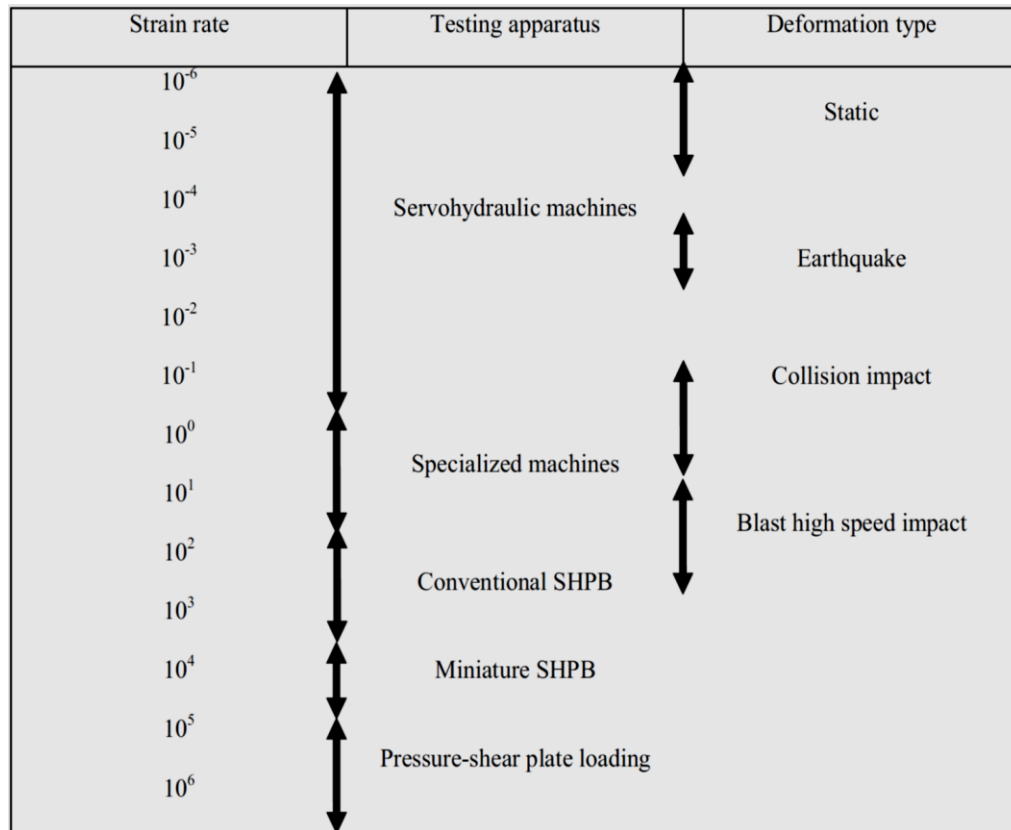
Overview about rock mechanical lab testing – part I mechanical tests

Only for private and internal use!   Updated: 12 August 2024

Strain rate	Testing apparatus	Deformation type
10^{-6}		Static
10^{-5}		
10^{-4}	Servohydraulic machines	
10^{-3}		Earthquake
10^{-2}		
10^{-1}		Collision impact
10^{0}		
10^{1}	Specialized machines	
10^{2}		Blast high speed impact
10^{3}	Conventional SHPB	
10^{4}	Miniature SHPB	
10^{5}		
10^{6}	Pressure-shear plate loading	

Fig. 1.1: Test apparatus vs. strain rate [Wong et al. 2017; SHPB = Split-Hopkinson-Pressure-Bar]

2   Basic tests

Before any more comprehensive test is performed, in most cases some basic parameters have to be determined, like density, porosity and water content using simple test procedures. Density values are obtained by determining the weight and the volume of the sample. One can distinguish between the following different types:

- Bulk density ρ
- Saturated density ρ_{sat}
- Dry density ρ_d
- Grain density ρ_s

The grains (solid components of the sample) are characterized by mass M_s and volume V_s. Pore water and corresponding mass are characterized by M_w and $\mathbf{V}_w$. Pore volume is given by V_v.

$$\rho = \frac{M}{V}$$

$$\rho_S = \frac{M_s}{V_s}$$

$$\rho_{sat} = \frac{M_s + \rho_w V_v}{V}$$

$$\rho_d = \frac{M_s}{V}$$

Based on these parameters also water content w, degree of saturation S_r, porosity n and void ratio e are given, respectively.

$$w = \frac{M_w}{M_s}$$

$$S_r = \frac{V_w}{V_v}$$

$$n = \frac{V_v}{V}$$

$$e = \frac{V_v}{V_s}$$

$$e = \frac{n}{1-n}$$

To determine dry density, samples have to be dried in an oven at 105 °C for at least 24 hours, but at least until equilibrium in mass is obtained. The volume (rock matrix and pores) can be determined by different methods: calliper method (volume determination by means of mechanical measuring devices, e.g. calliper), mercury displacement method (measurement of amount of mercury penetrating the dry sample), water displacement method (measurement of amount of water penetrating the dry sample) and buoyancy method (difference in weight between saturated and dry sample). More detailed information is given for instance in Ulusay & Hudson [2007].

3   Mechanical lab tests

3.1   Static Hardness determination

Static hardness testing is based on the indentation of a hard tool into the sample (see Fig. 3.1.1. Hard metal balls or diamond cones or pyramids can act as indentors. The test load is applied with a defined initial application time and duration and has to be applied perpendicular to the sample. The indentation is measured after removal of the load, either with integrated or separate optical devices (microscopes). The most popular methods applied in rock mechanics are the testing procedures according to Brinell (ball), Vickers (pyramid), Knoop (pyramid) and Rockwell (different shapes). Fig. 3.1.2 illustrates the most popular hardness testing methods incl. the measuring values. Either optical microscop or laser scanning can be used for these meassurements. Distance between two neighbouring testing locations should be at least 3 times the width of the imprints. Sample thickness should be at least ten times penetration depth of indentor. Load level and indentor size depend on material and considered resolution. Hardness testing is standardized by national and international regulations (e.g. ISO, DIN, ASTM). Fig. 3.1.3 shows the recommended force range according to different standards. According to the different procedures different dimensionless hardness parameters can be determined. Fig. 3.1.4 shows typical devices to measure the hardness.

Overview about rock mechanical lab testing – part I mechanical tests

Only for private and internal use!   Updated: 12 August 2024
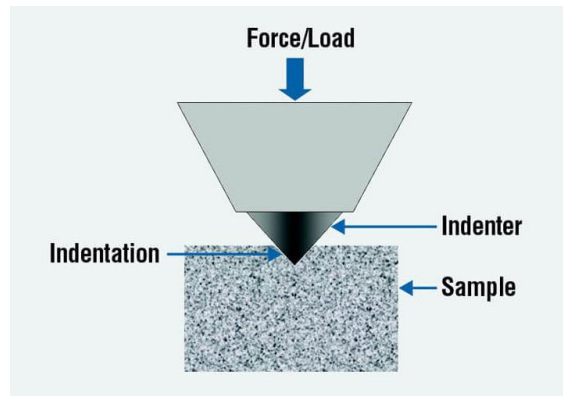
Fig. 3.1.1:   Principal set-up of hardness testing [company leaflets, Struers]
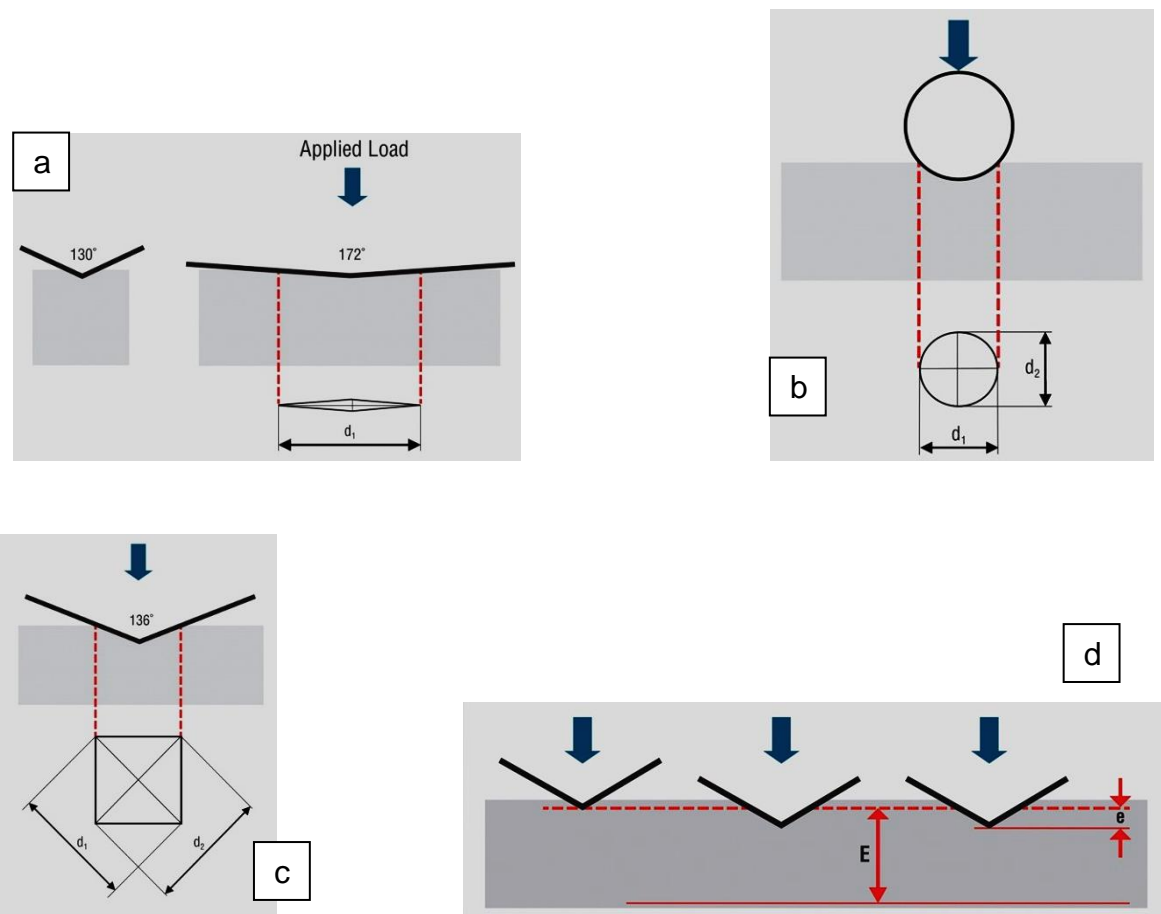

Fig. 3.1.2: Hardness testing according to Knoop (a), Brinell (b), Vickers (c) and Rockwell (d) [company leaflet, Struers]

Overview about rock mechanical lab testing – part I mechanical tests

Only for private and internal use!   Updated: 12 August 2024

Hardness Testing Method	Standard	Load Range	
Vickers	ISO 6507 ASTM E384 ASTM E384	10 gf - ≤100 kgf 1 gf - ≤1 kgf >1 gf - ≤120 kgf	(0.0981 - ≤9.807 N) (0.0098 - ≤9.807 N) (>9.807 - ≤1176.800 N)
Knoop	ISO 4545 ASTM E384	1 gf - 1 kgf 1 gf - 1 kgf	(0.0098 - ≤9.807 N) (0.0098 - ≤9.807 N)
Brinell	ISO 6506 ASTM E10	1 kgf - 3000 kgf 1 kgf - 3000 kgf	(9.807 - 29420 N) (9.807 - 29420 N)
Rockwell	ISO 6508 ASTM E18	15 kgf - 150 kgf 15 kgf - 150 kgf	(147.1 - 1471 N) (147.1 - 1471 N)

Fig. 3.1.3: Standards and force range for hardness testing [company leaflet, Struers]

Fig. 3.1.4:   Typical hardness testing devices [company leaflets]

Overview about rock mechanical lab testing – part I mechanical tests

Only for private and internal use!   Updated: 12 August 2024

Fig. 3.1.5:   Multi-functional hardness testing device with digital image analysis [RML 2016]
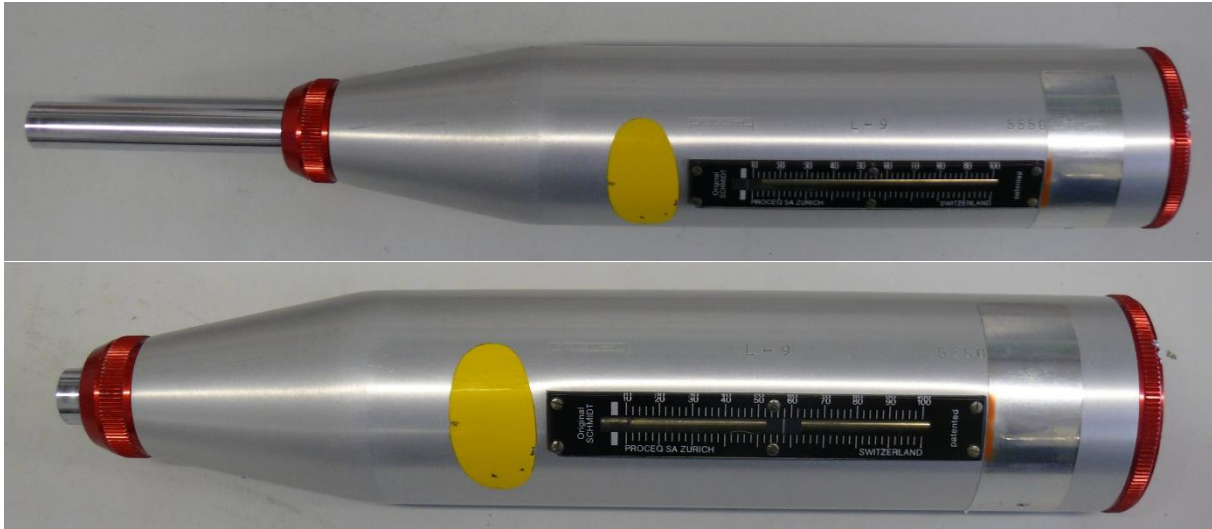
Fig. 3.2.1:   Schmidt Hammer after (top) and before (bottom) releasing the spring [RML 2016]

3.2   Rebound Hardness determination

The Schmidt Hammer (see Fig. 3.2.1) is the most popular portable device to measure the rebound hardness and is often used to estimate uniaxial compressive strength or Young's modulus via empirical relations [Ulusay 2015]. The Schmidt hammer consists of a spring loaded piston, which is released when the plunger is pressed against the surface. The percentage of maximum stretched length of the spring before the release of the piston to the length after rebound gives the so-called rebound hardness value R. Depending on rock strength two different types are used: L-type (0.735 Nm) and N-type (2.207 Nm).

3.3   Abrasion determination

Abrasion tests measure the resistance of steel pins to wear during defined interaction with rock. During the past decades several testing procedures were developed to specify the abrasion characteristics of rocks [e.g. Ulusay 2007]. The most popular procedure is the so-called Cherchar test. During the test a steel pin (Rockwell hardness of 54 – 56 and tensile strength of 2 GPa) with angle of 60° and loaded by 70 N is scratching the rock surface. A distance of at least 50 mm or even better 100 mm is recommended to determine the CAI (Cherchar Abrasiveness Index) according to Plinninger et al. [2003]. CAI itself is determined by microscopic inspection of the abrasion of the steel needle. CAI varies between 0.3 (not very abrasive) and 6.0 (extremely abrasive). By performing several scratch tests and rotating the sample anisotropy in abrasion can be determined.

Overview about rock mechanical lab testing – part I mechanical tests

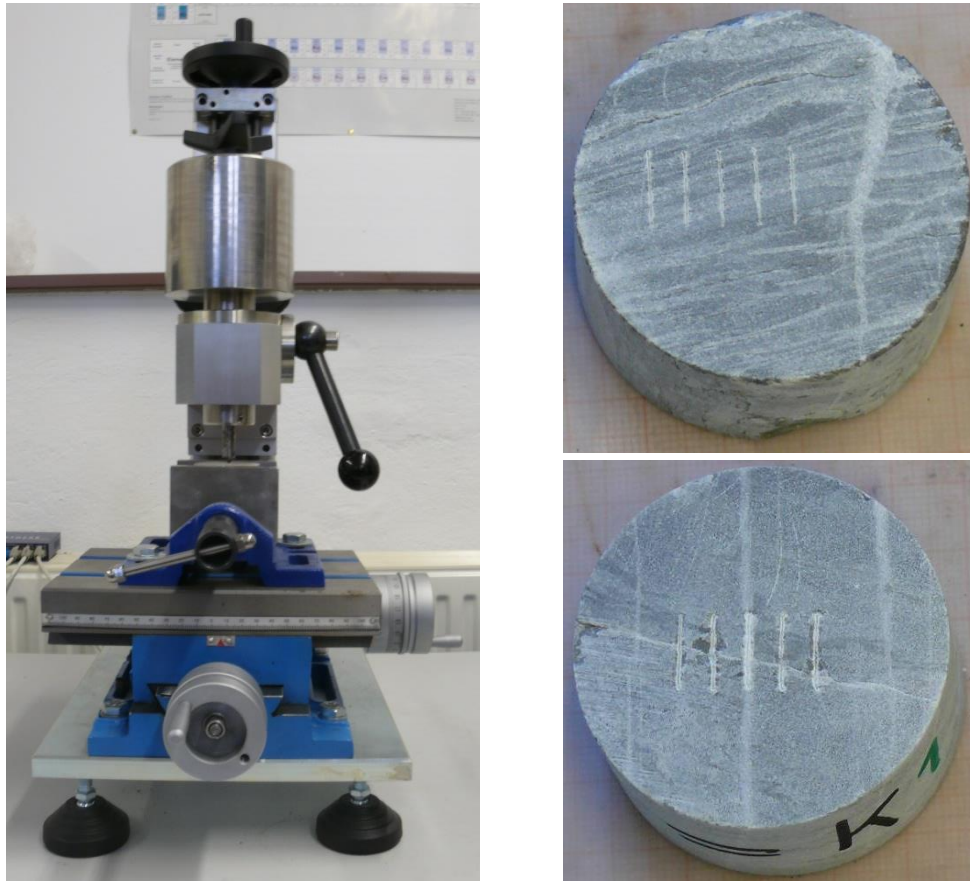Only for private and internal use! Updated: 12 August 2024

Fig. 3.3.1: Left side: Typical test device for determination of CAI. Right Side: Scratching traces on limestone specimen after testing perpendicular to bedding and in parallel to bedding planes, respectively [RML 2016]

3.4 Point load index test

The Point Load Index Test (PLT) is a simple alternative to the uniaxial compression test, but does not deliver directly uniaxial or tensile compressive strength data, but rather an index about rock strength, which can be either correlated to more precise parameters or directly used in empirical design procedures. During PLT a rock sample is compressed between conical steel platens (pins) until failure occurs. The PLT index I_S is calculated according to the following formulae:

$$I_S = \frac{F_S}{A}$$

where: F_S is the failure load (force)

A is the corresponding area of the fracture plane (sometimes also the square of the equivalent sample radius is used)

The PLT device (Fig. 3.4.1) should meet several requirements in respect to size, shape and stiffness and allow to monitor the applied pressure including the determination of peak pressure. Also, only those tests, which show unique fracture pattern should be used for evaluation (Fig. 3.4.2). Because PLT index shows a significant scale effect (increase with increasing sample size), a size correction has to be performed by log-log-plots or the LOGAR-procedure [Thuro 2008]. If enough reliable data for one specific rock type exist,

Overview about rock mechanical lab testing – part I mechanical tests

Only for private and internal use! Updated: 12 August 2024

a correlation between PLT index and uniaxial compressive strength (UCS) can be established in terms of a linear relation: $UCS = c \cdot I_s$, where c is a correlation factor. Fig. 3.4.3 and 3.4.4 show such correlations for Cottaer Sandstone and Innsbrucker Quarzphyllit, respectively. More detailed information about PLT testing are given in Ulusay & Hudson [2007] or Thuro [2008].

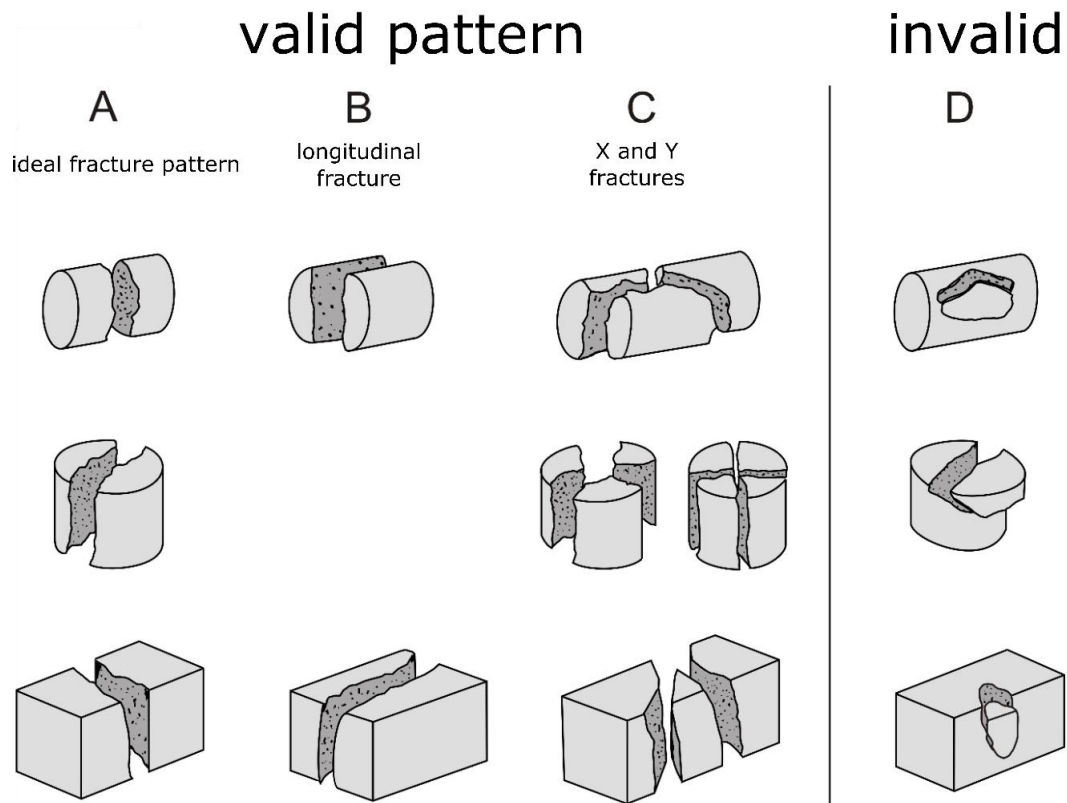Fig. 3.4.1: Point Load Index Device (loading frame, pump with manometer and data aquisition unit) [RML 2016]

Overview about rock mechanical lab testing – part I mechanical tests

Only for private and internal use!   Updated: 12 August 2024

valid pattern   invalid

A   B   C   D

ideal fracture pattern   longitudinal   X and Y
                            fracture   fractures

Fig. 3.4.2: Valid and invalid fracture patterns [Thuro 2008]

$I_s = 2.8 \pm 0.5 \, [\text{N/mm}^2]$

$\sigma_u = 43.2 \pm 7.6 \, [\text{N/mm}^2]$

Postaer Sandstone

n = 200	I_S [N/mm²]	σ_u* [N/mm²]
Average Value	2.8	43.2
Standard Deviation	0.49	7.6
Coefficient of Variation	0.18	0.18

Factor of Correlation for σ_u*:

c=   15.4   [-]
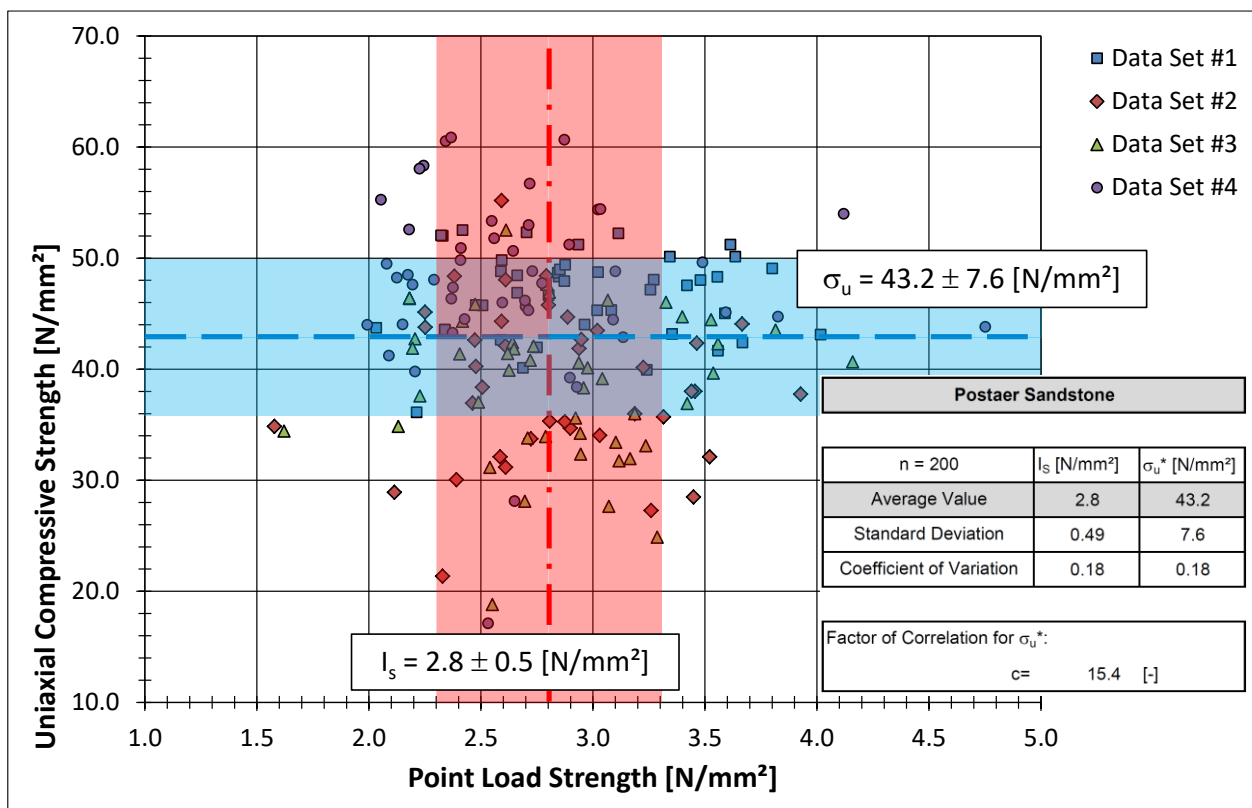
Fig. 3.4.3:   Correlation between Point Load Index and UCS, Postaer Sandstone [RML 2016]

Overview about rock mechanical lab testing – part I mechanical tests

Only for private and internal use!   Updated: 12 August 2024

Innsbrucker Quarzphyllit
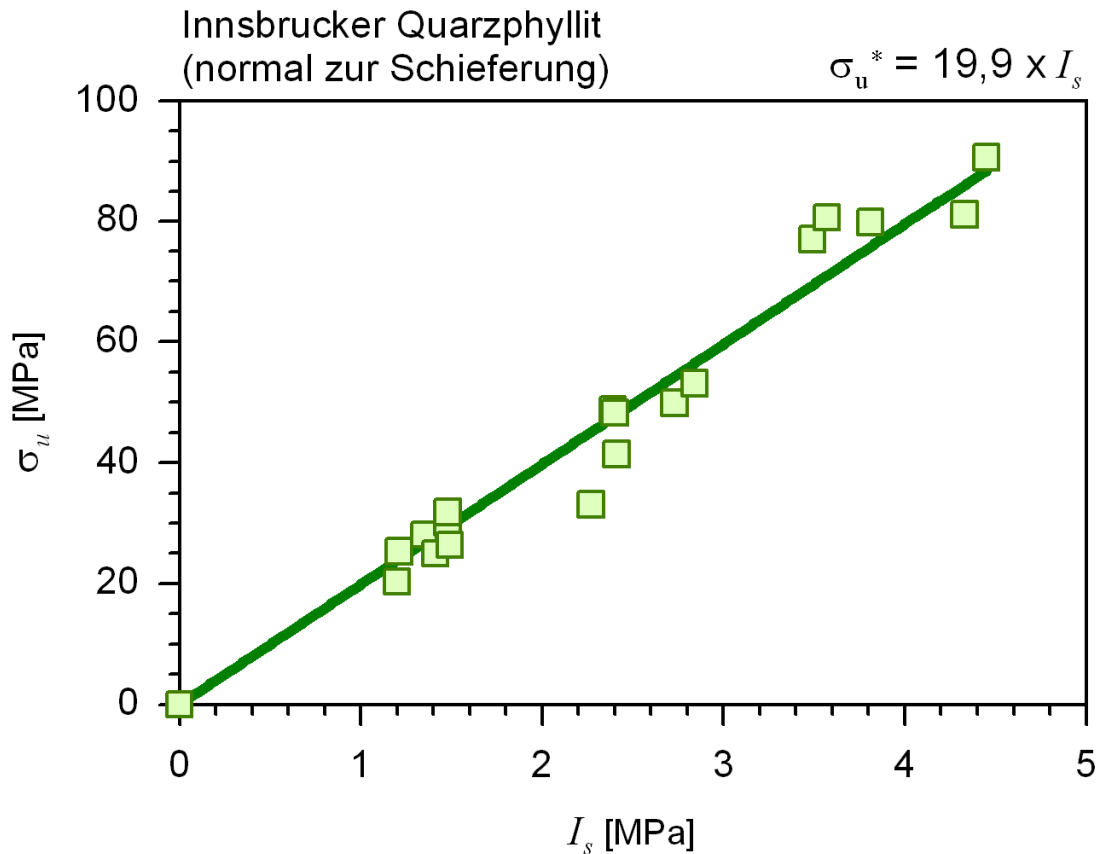(normal zur Schieferung) $\sigma_u^* = 19{,}9 \times I_s$

Fig. 3.4.4: Correlation between Point Load Index and UCS, Innsbrucker Quarzphyllit [Thuro 2008]

3.5   Needle penetration test

The needle penetration test (NPT) is only applicable for soft rocks and was developed as a fast and cheap index test for the estimation of UCS. Fig. 3.5.1 shows a sketch of such a device. Handling and data evaluation are described by ISRM Suggetsed Methods (Ulusay et al., 2014). The NPT can be used at any kind or rock piece without any preparation. The needle penetration index (NPI) is calculated as follows:

NPI=100/D in case F=100 N and D≤10 mm or NPI=F/10 in case D=10 mm and F<100 N

Fig. 1 Needle penetrometer and its parts: *1* presser, *2* chuck, *3* penetration scale, *4* load scale, *5* load indicating ring, *6* cap, *7* penetration needle and *8* spring
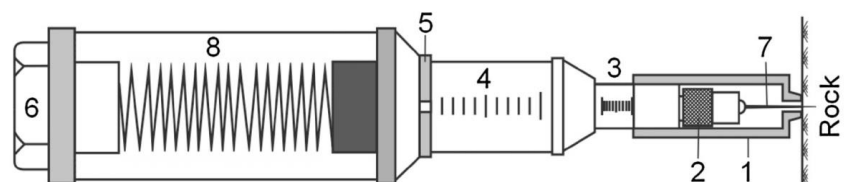
Fig. 3.5.1: Needle petrenometer (Ulusay et al., 2014)

Many correlations are established with UCS, Young's moduls, cohesion, P-wave velocity, S-wave velocity, friction angle etc. (e.g. Ulusay et al. 2014; Rabat et al., 2020). However, the use of NPI to estimate UCS or other parameters needs a reliable calibration.

Overview about rock mechanical lab testing – part I mechanical tests

Only for private and internal use!   Updated: 12 August 2024
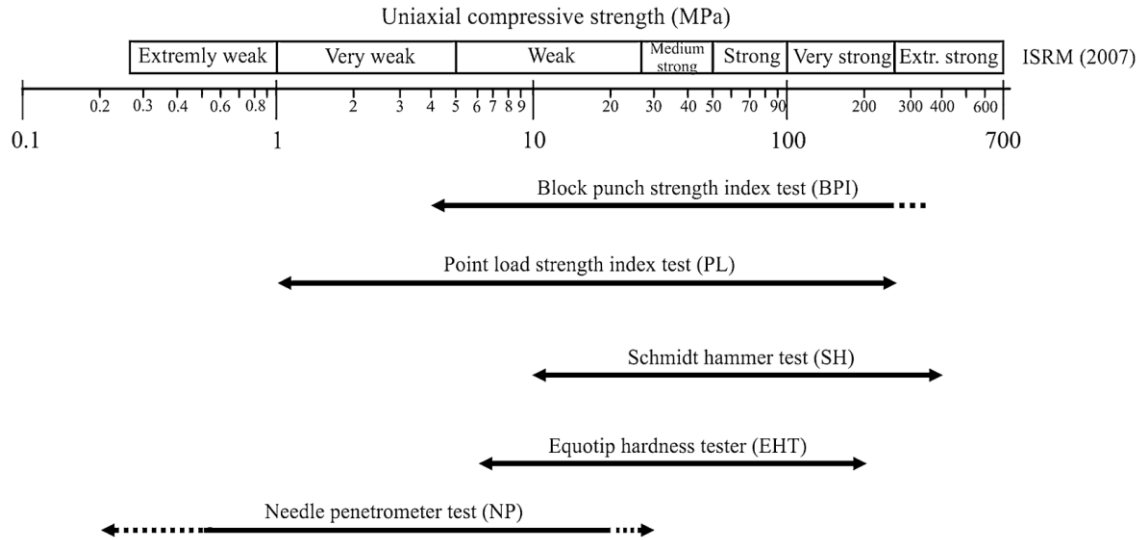
Fig. 3.5.2: Range of application of NPT and other index tests in relation to UCS (Ulusay et al., 2014)
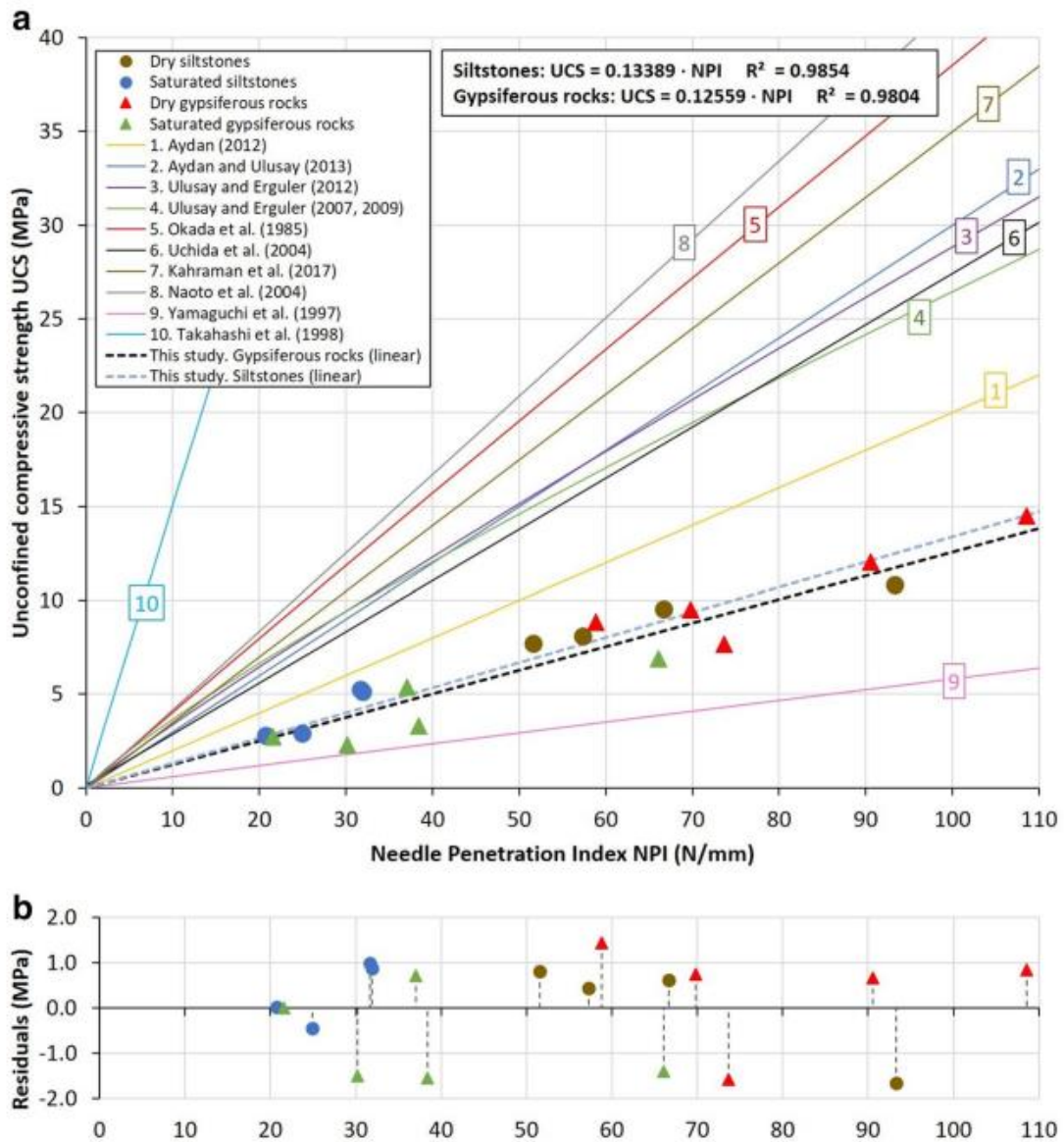
Fig. 3.5.3: Correlation between NPI and UCS (Rabat et al., 2020)

Overview about rock mechanical lab testing – part I mechanical tests

Only for private and internal use!   Updated: 12 August 2024

3.6 Sound velocity tests

Sound velocity is closely related to dynamic elastic constants by the following formulae:

$$v_p = \sqrt{\frac{E(1-v)}{\rho(1+v)(1-2v)}}$$

$$v_s = \sqrt{\frac{E(1-v)}{\rho \cdot 2(1+v)}}$$

where:
v_p	Compressional wave speed
v_s	Transversal wave speed
E	Dynamic Young's modulus
v	Dynamic Possion's ratio
ρ	Density

Sound velocity is usually measured by piezo-electric sensors (transmitter and receiver) on prepared cores samples, bars or bigger rock blocks. Frequencies are typically in the order of several 100 kHz. Three different measuring procedures are common:

- Determination of wave speed of longitudinal and transversal wave
- Determination of velocity of dilatational and torsional waves in bar of rode-like specimen
- Determination of resonant frequency of dilatational and torsional waves in bar of rode-like specimen

Velocity of P- and S-waves are determined by dividing distance by travel time or multiplying two times the length of the bar with resonance frequency. Despite the determination of dynamic elastic constants (E, v) sound velocity measurements can also be used to estimate the damage state, the anisotropy ratio or to classify rocks.

Overview about rock mechanical lab testing – part I mechanical tests

Only for private and internal use!   Updated: 12 August 2024

Fig. 3.6.1: Typical equipment to measure sound velocity on core samples [RML 2016]

3.7 Uniaxial compression tests

The aim of uniaxial compression testing is to determine compressive strength and stiffness of intact rock samples.

A suitable testing machine has to be used, which should have the following features (see also specifications according to ASTM, DIN or ISRM / DGGT recommendations):

- Sufficient stiffness and load capacity
- Spherical seat and sufficient hardness of loading platens
- Sufficient size of loading platens (diameter of loading platen > sample diameter)
- High accuracy in measuring axial load and vertical displacement incl. display and storage of data (measurement error < 1 %)

The rock samples should meet several requirements:

- Cylindrical shape with height to diameter ration of about 2 to 3
- Diameter of specimen should be related to the largest grain diameter by a ratio of 10:1 or larger
- The ends of the specimen should be flat and not depart from perpendicularity (parallel with high precision)

The testing shall be performed according to the following rules:

- Constant stress rate of about 0.5 to 1.0 MPa/s until failure
- To determine any kind of deformation modulus, Young's modulus and Poisson's ratio, it is recommended to use separate high-precision measuring devices, like LVDT's, strain gauges or optical devices (accuracy in strain determination should be better than 2 %)

Overview about rock mechanical lab testing – part I mechanical tests

Only for private and internal use!   Updated: 12 August 2024

Test reporting should contain information about the following items:

- Source of sample incl. lithological description and basic parameters (density, water content etc.)
- Orientation of sample axis in respect to planes of anisotropy
- Sample geometry
- Date of testing, used machine and loading rate
- Failure pattern
- Measured (forces and displacements) and deduced values (peak strength, deformations modulus etc.)
- Photo documentation of sample before and after testing

Uniaxial compressive strength is determined by dividing the peak load P by the initial cross sectional area A_0:

$$UCS = \frac{P}{A_0}$$

Axial strain ε_a is measured by dividing change in axial length Δl by original axial length l_0:

$$\varepsilon_a = \frac{\Delta l}{l_0}$$

The lateral deformation can be given either as diametric strain ε_a (change in diameter) or circumferential strain ε_c (change in circumference):

$$\varepsilon_d = \Delta d / d_0 \quad \text{or} \quad \varepsilon_c = \Delta c / c_0 \quad \text{(both give identical results)}$$

Deformation moduli incl. Young's modulus are given by the slope of the axial strain – axial deformation curve, whereby according to the definitions different regions (parts) of the stress – strain curves are used. Poisson's ratio is given by dividing the horizontal strain ε_h by vertical strain ε_a:

$$\nu = \frac{\varepsilon_h}{\varepsilon_a}$$

Due to the inhomogeneity of the samples and measurement errors in general, it is recommended to perform at least 3 or better 5 tests per rock type. Scale (size) effects should be taken into account (see also Fig. 3.7.5).

Fig. 3.7.1: Typical machine for uniaxial compression tests [RML 2016]

Fig. 3.7.2: Sample, prepared for uniaxial compression testing with longitudinal and lateral strain measurement direct on the sample [RML 2016]
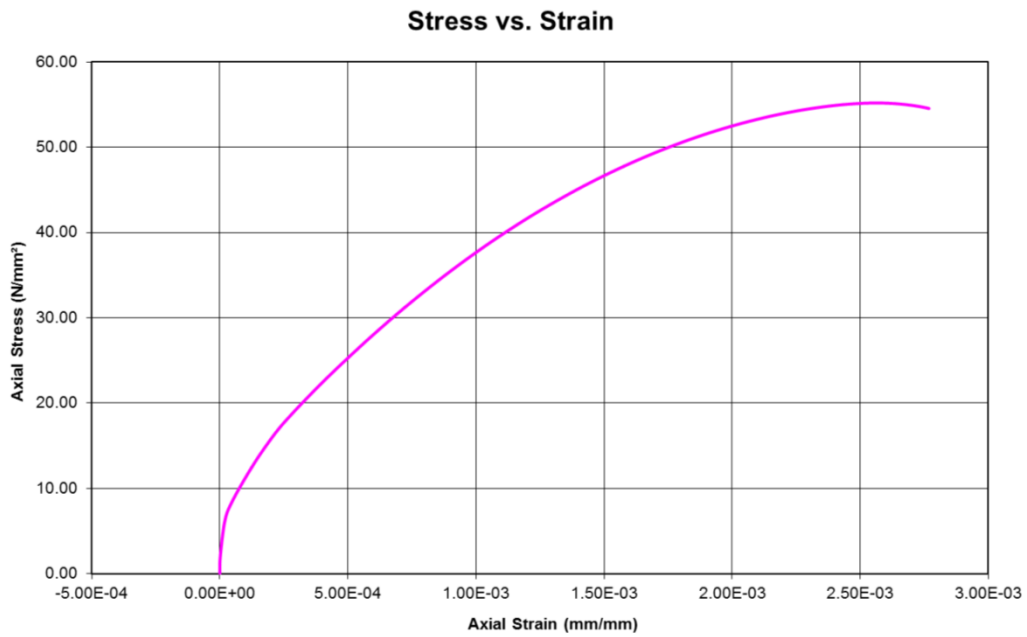
Fig. 3.7.3: Typical recording during uniaxial compression testing: vertical stress vs. vertical strain [RML 2016]
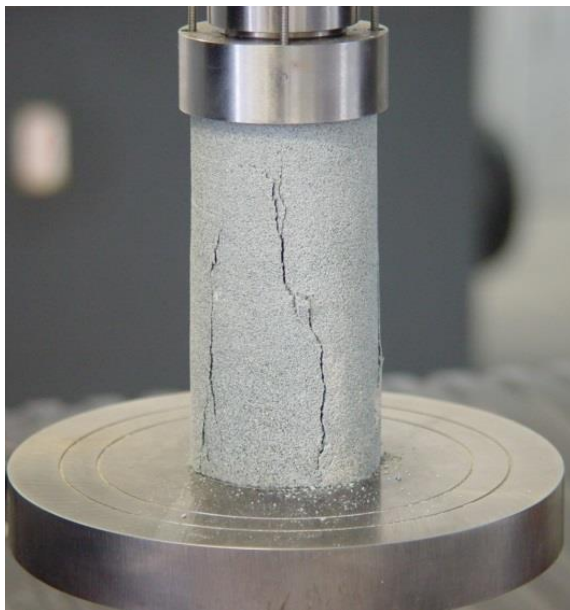

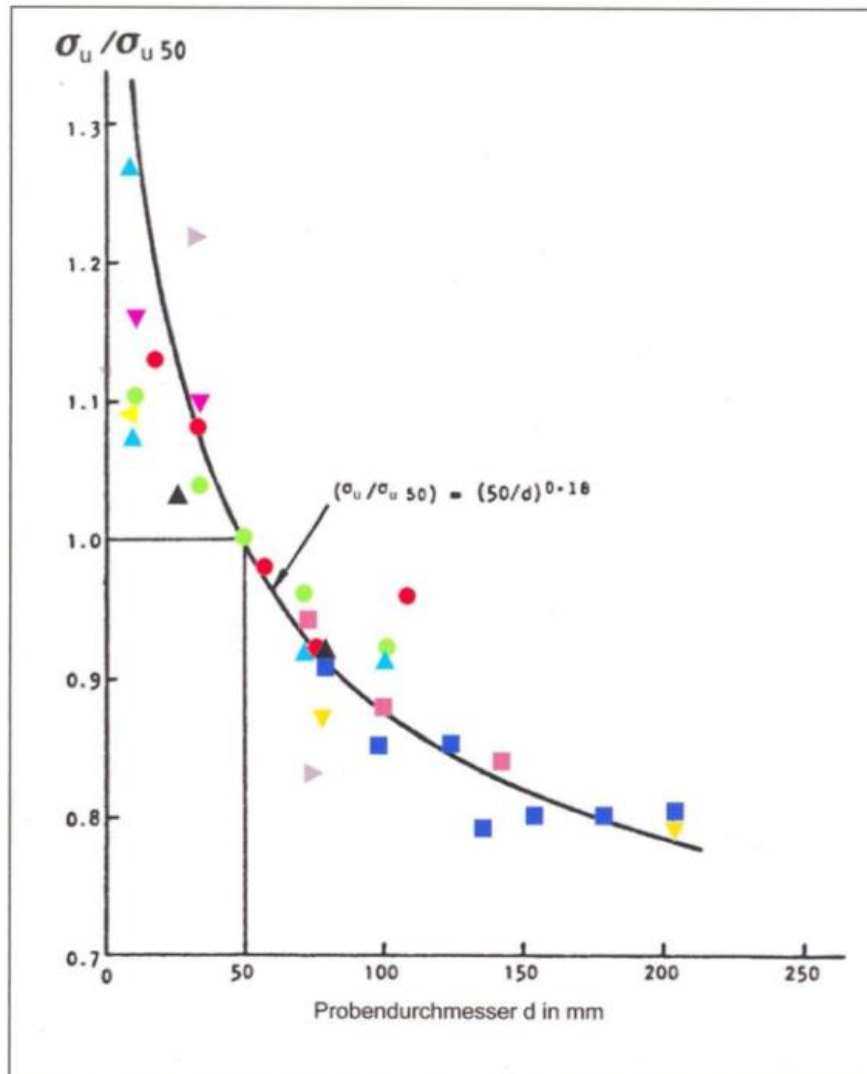Fig. 3.7.4: Typical fracture pattern: axial splitting (left) and shear fracturing (right) [RML 2016]

Overview about rock mechanical lab testing – part I mechanical tests

Only for private and internal use!   Updated: 12 August 2024

Fig. 3.7.5: Example for scale effect of sample size [Pinto, 1990]

A big issue is the question how many tests should be performed to get a reliable result. Ruffolo & Shakoor have investigated the UCS for 5 different types of rock using up to 50 samples. They have determined mean, standard deviation, 95% confidence interval and coefficient of vaiation for each group (3, 5, 10, 15, 20, 25, ….50).

Fig. 3.7.6 shows the evaluation result for Milba granite and Fig. 3.6.7. shows the uppermost and lowermost 95% confidence intervals and accepted strength variations for different types of rock.

Ruffolo & Shakoor (2009) concluded, that 9 to 10 samples are necessary for a 95% confidence interval amd a 20% acceptable strengtg deviation from the mean based on their statistical analysis.

Fig. 3.7.8 documents the minimum number of samples needed to reach a certain coefficient of variation.

Please note, that similar relations are also valid for other rockmechanical tests.
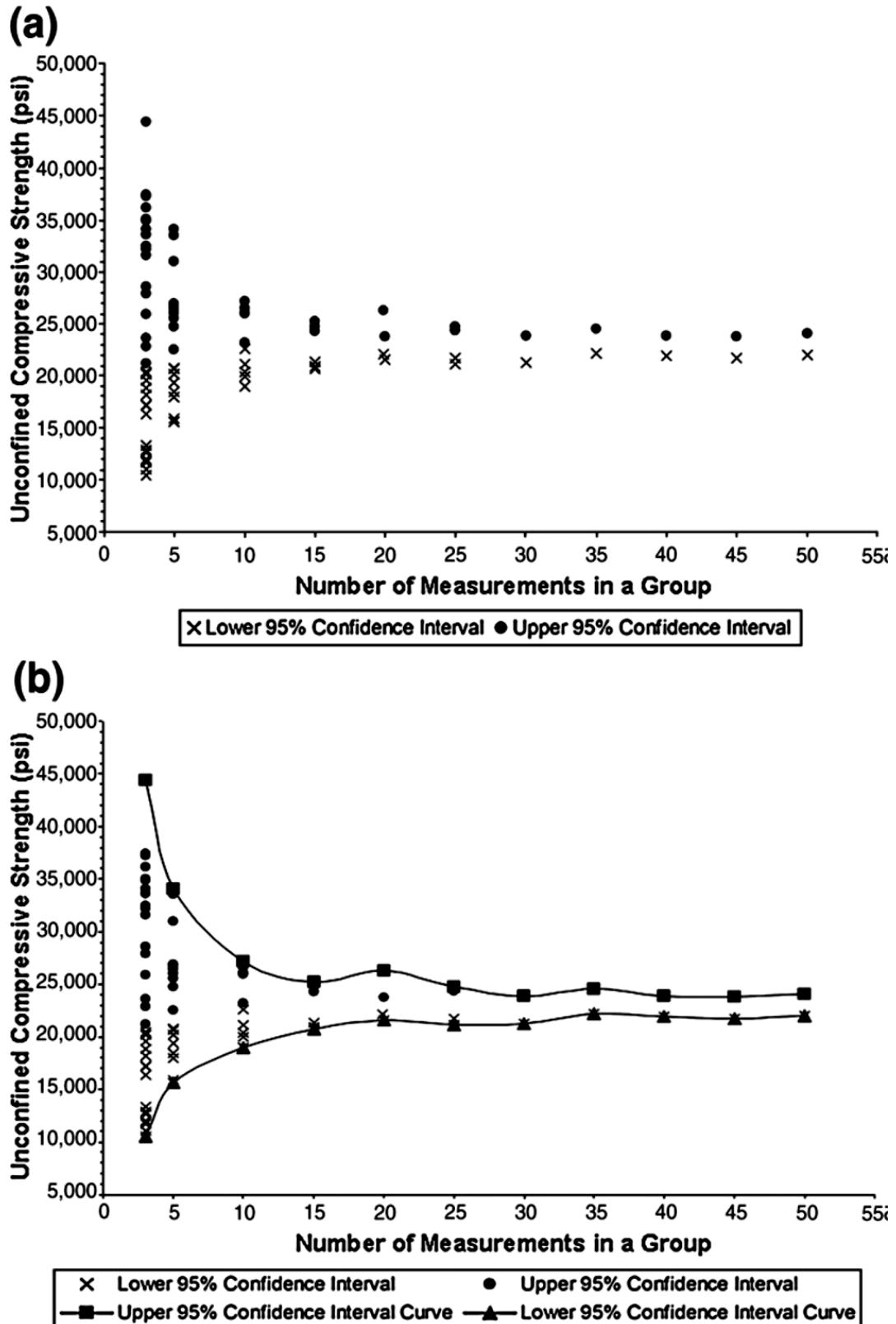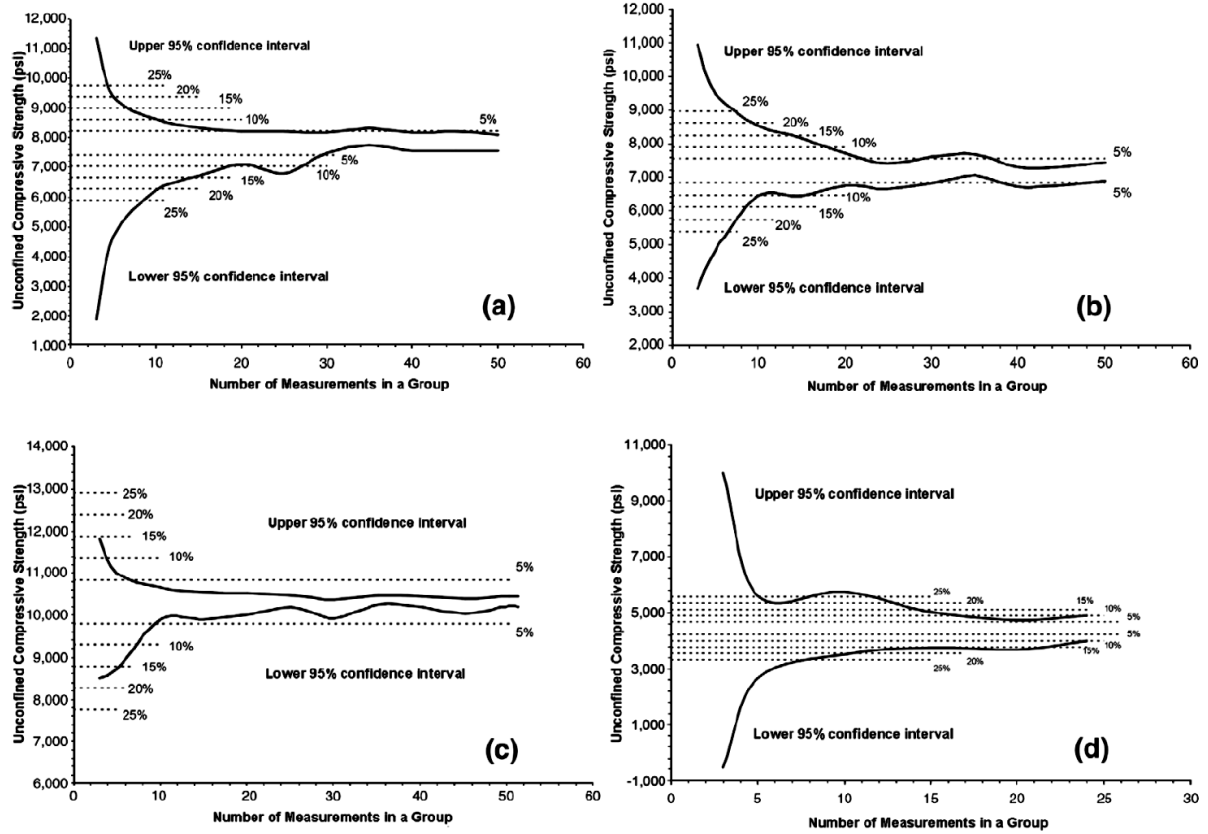
Overview about rock mechanical lab testing – part I mechanical tests

Only for private and internal use!   Updated: 12 August 2024

Fig. 3.7.6: Upper and lower 95% confidence intervals for each group of Milban granite [Ruffolo & Shakoor, 2009]

Overview about rock mechanical lab testing – part I mechanical tests

Only for private and internal use!   Updated: 12 August 2024

Fig. 3.7.7: Uppermost and lowermost 95% confidence intervals and accepted strength variations for different types of rock [Ruffolo & Shakoor, 2009]
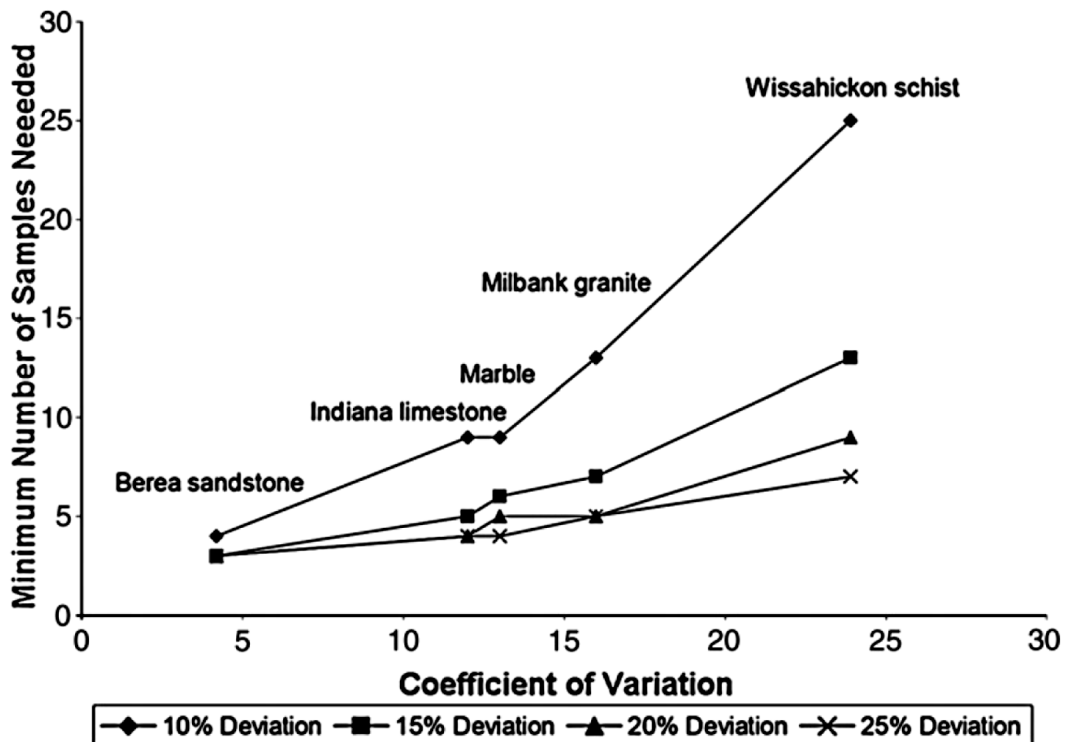
Fig. 3.7.8: Minimum number of samples needed to reach a certain coefficient of variation [Ruffolo & Shakoor, 2009]

Please, note also that (a) loading velocity has some influence on the UCS value and (b) different recommendations in respect to the applied loading velocity are given by different organizations (see Fig. 3.7.9).
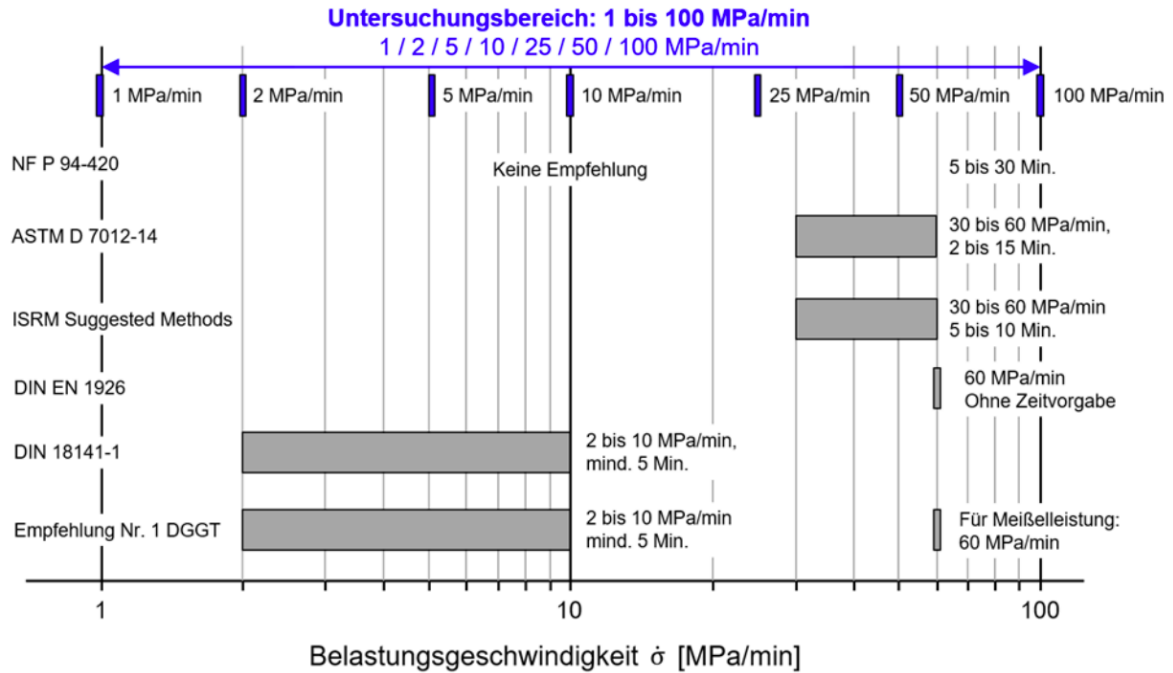
Fig. 3.7.9: Recommendations for UCS test loading velocities from different organizations (Burbach, 2021)

Burbach (2021) has investigated the UCS for different types of rock applying different loading velocities. A summary of his investigations is shon in Fig. 3.7.10.
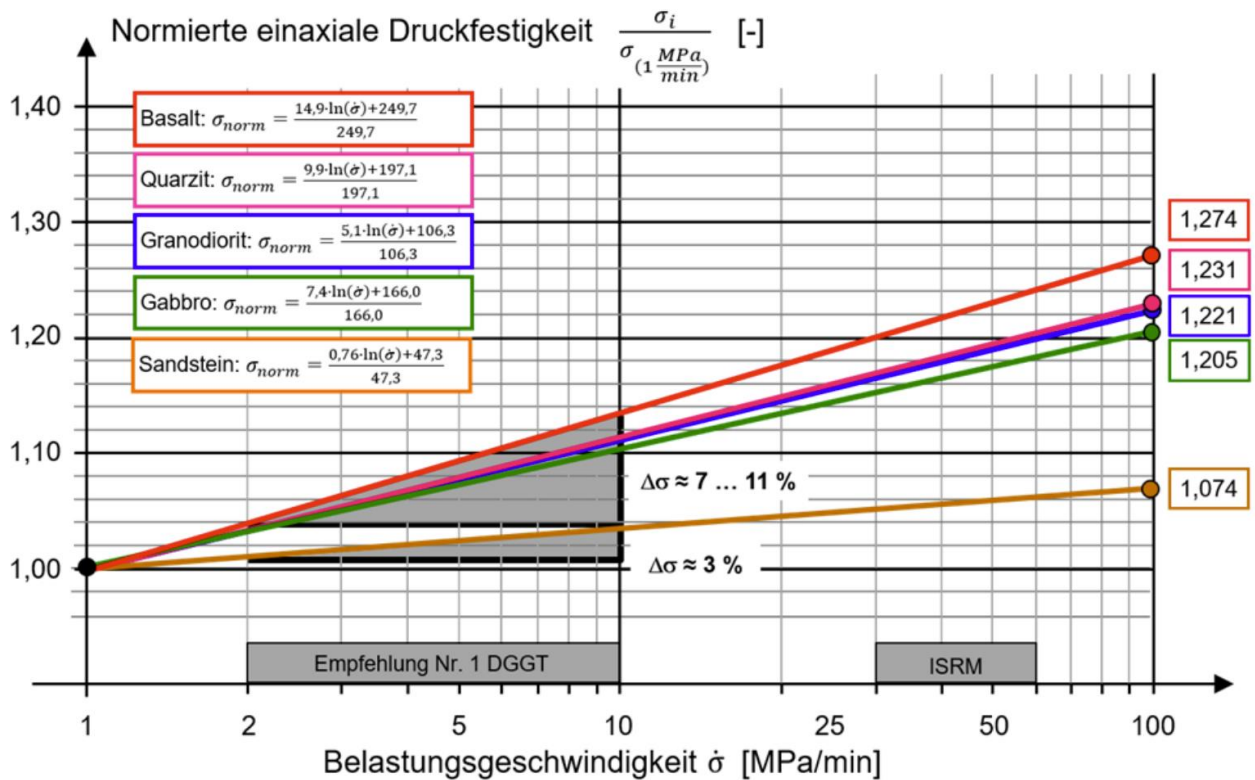

Fig. 3.7.10: Normalized UCS versus loading velocity for different types of rock (Burbach, 2021)

3.8   Uniaxial tension test

For the uniaxial tension test, the same general rules and recommendations are valid as for the uniaxial compression test (see chapter 3.6). After sample preparation cylindrical metal caps shall be cemented to the specimen ends, so that tensile stress can be applied. Care should be taken by cementation of the end caps and the load transfer system, so that alignment of the whole system (sample + end caps) with the load axis is guaranteed and any torsion or bending is avoided.
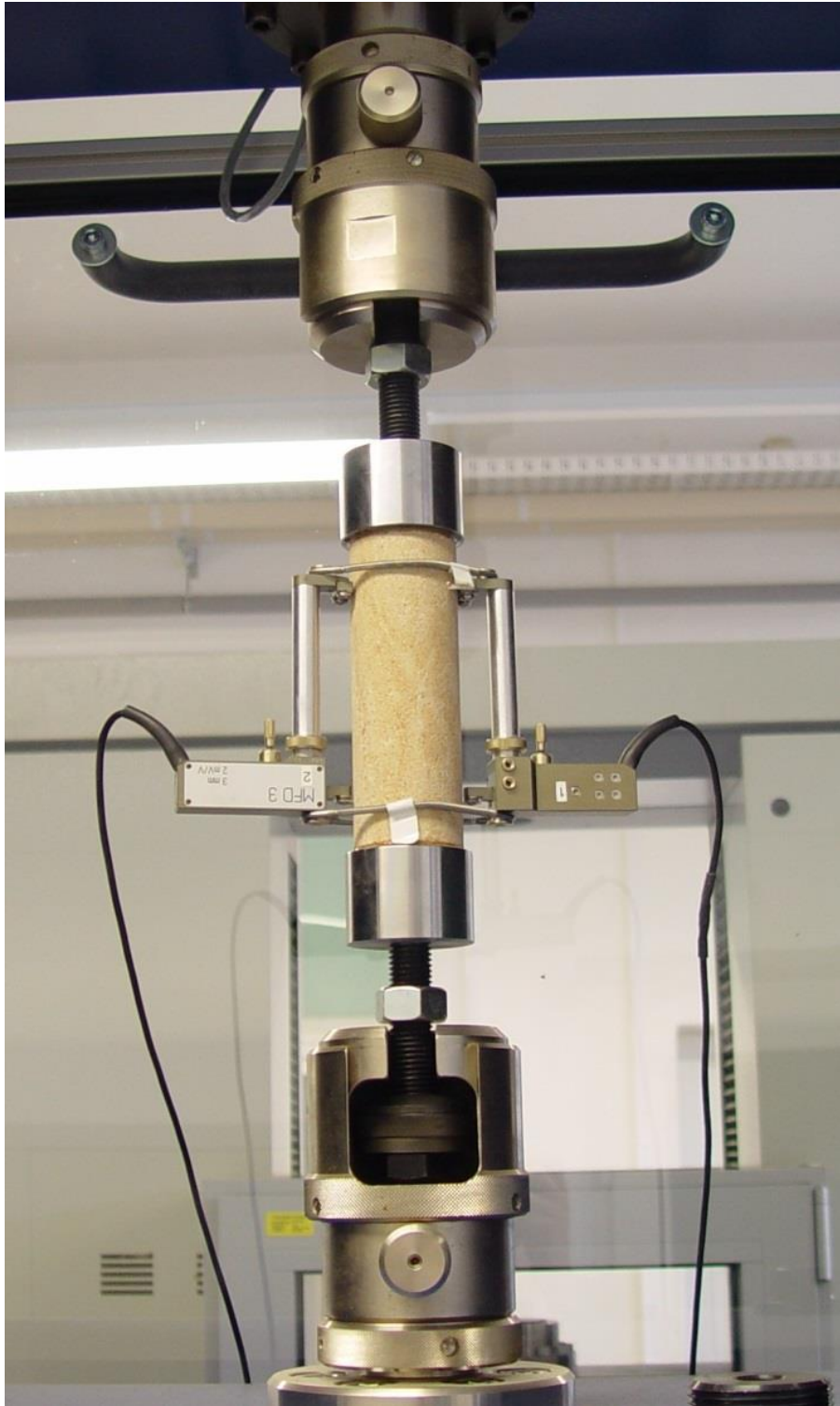

Fig. 3.8.1: Uniaxial tension test: machine with sample during testing [RML 2016]

Overview about rock mechanical lab testing – part I mechanical tests

Only for private and internal use!   Updated: 12 August 2024

Fig. 3.8.2: Uniaxial tension test: Samples with typical failure pattern [RML 2016]

Overview about rock mechanical lab testing – part I mechanical tests

Only for private and internal use!   Updated: 12 August 2024
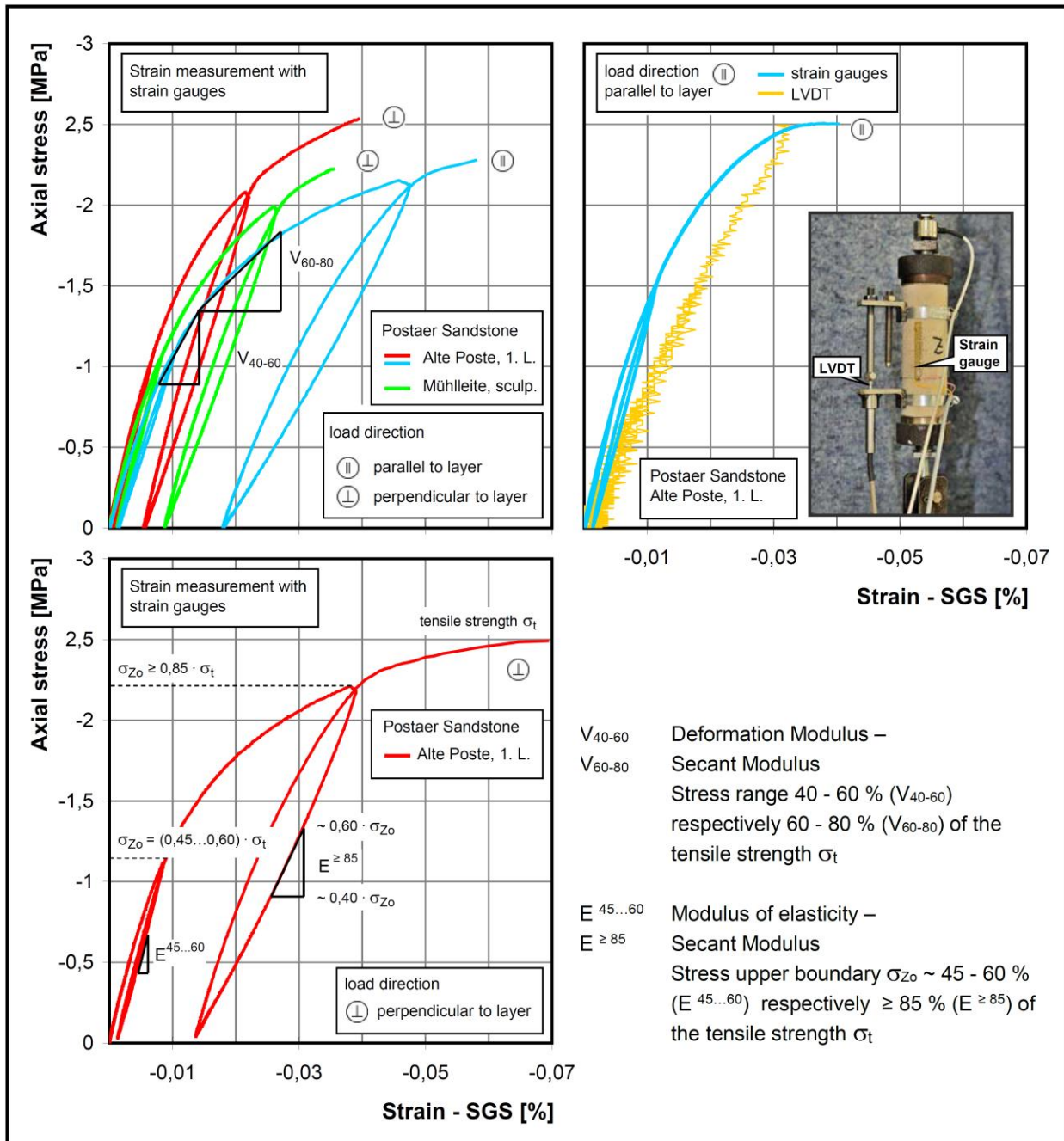
Fig. 3.8.3: Uniaxial tension test: typical results obtained for Postaer Sandstone [Baumgarten & Konietzky, 2012]

Perez-Rey et al. (2024) have a direct tension benchmark test conducted using two different types of rock: sandstone and granite. They describe in detail the used equipment and dicuss results including advantage and disadvantages to measure deformation. Fig. 3.8.4 and 3.8.5 show the obtained results in form boxplots.
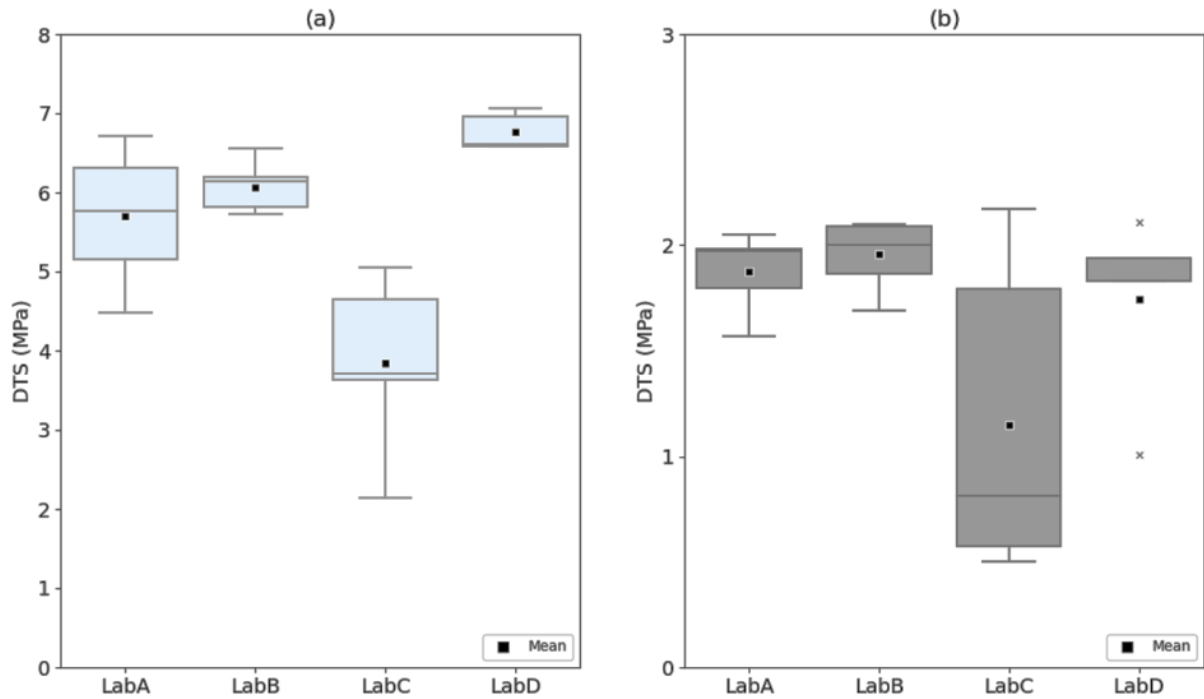
Fig. 3.8.4: Boxplot for direct tensile strength obtained by 4 different labs, (a) Blaco Mera granite, (b) Cotta sandstone
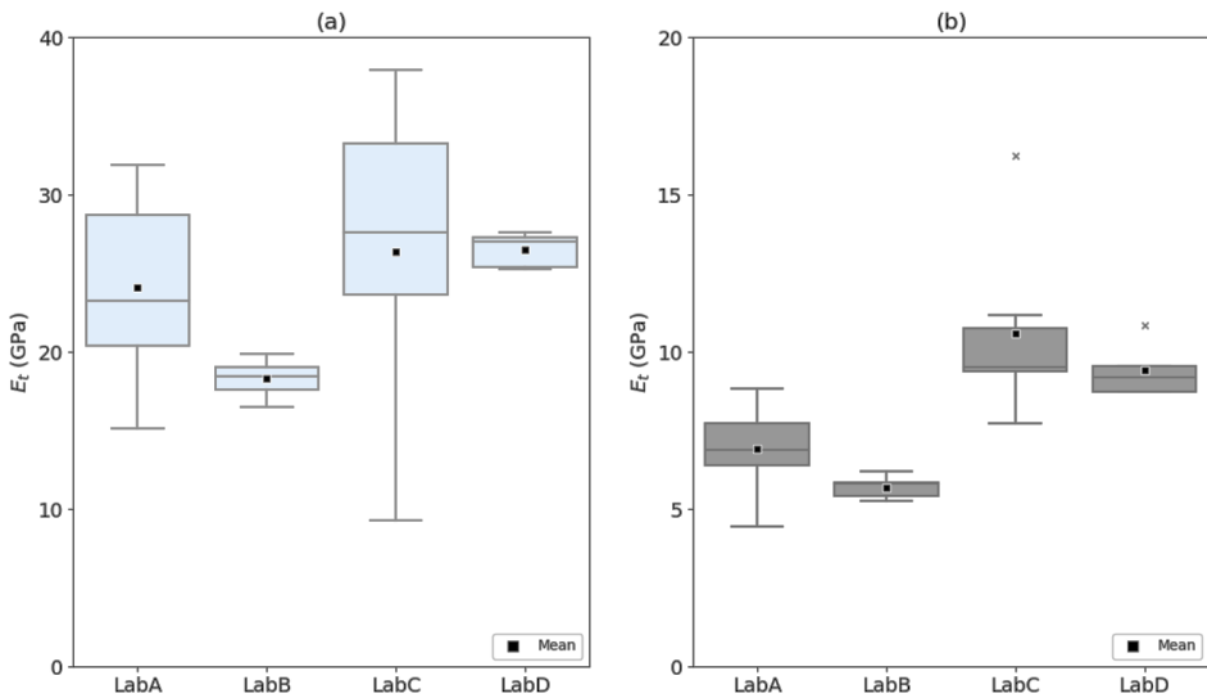

Fig. 3.8.5: Boxplot for Young*s moduls obtained by 4 different labs using direct tension tests, (a) Blaco Mera granite, (b) Cotta sandstone

Overview about rock mechanical lab testing – part I mechanical tests

Only for private and internal use!   Updated: 12 August 2024

3.9 Brazilian test

The Brazilian test (also called tensile splitting test) is an indirect method to determine the tensile strength. This method is very popular, because sample preparation is easy and standard compressive testing equipment can be used. During a Brazilian test a circular rock disc is compressed by two diametrically applied forces (Fig. 3.9.1). The applied compressive load should be transmitted to the sample only through a very small arc of contact (< 10°). Thickness if disc should be half the diameter. Based on a simplified analytical solution the splitting tensile strength σ_t can be calculated according to the following formulae:
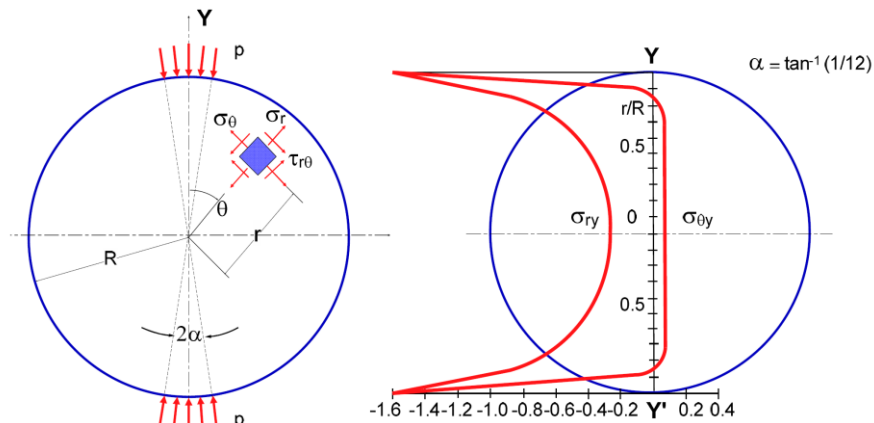

Fig. 3.9.1: Stress situation during Brazilian test [Dinh 2011]

$$\sigma_t = \frac{2P}{\pi Dt}$$

where: P = maximum (peak) load at failure
             D = diameter of disc
             t = thickness of disc

The above mentioned formulae is only valid, if a central tensile crack is observed. For anisotropic material, especially if plane of anisotropy is inclined to the loading direction, mixed-mode or even predominant shear failure can occur (see Fig. 3.9.2). Also, sometimes shear failure is observed at the load entry points under the loading jaws. In these cases the above mentioned formulae is not valid. More detailed information, especially under consideration of anisotropic rocks and influence of testing parameters, is given by Dinh [2011], Dinh et al. [2013], Vervoort et al. [2014] and Dinh & Konietzky [2014].

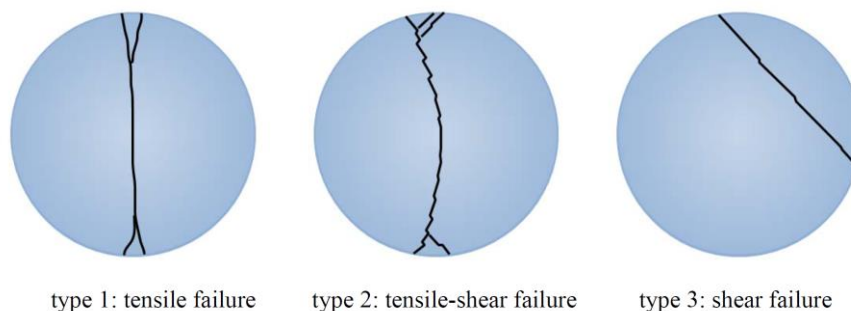type 1: tensile failure   type 2: tensile-shear failure   type 3: shear failure

Fig. 3.9.2: Typical potential failure pattern for anisotropic material [Dinh & Konietzky 2014]

Fig. 3.9.3: Typical test arrangement with arc-formed loading jaws and cylindrical samples [RML 2016]
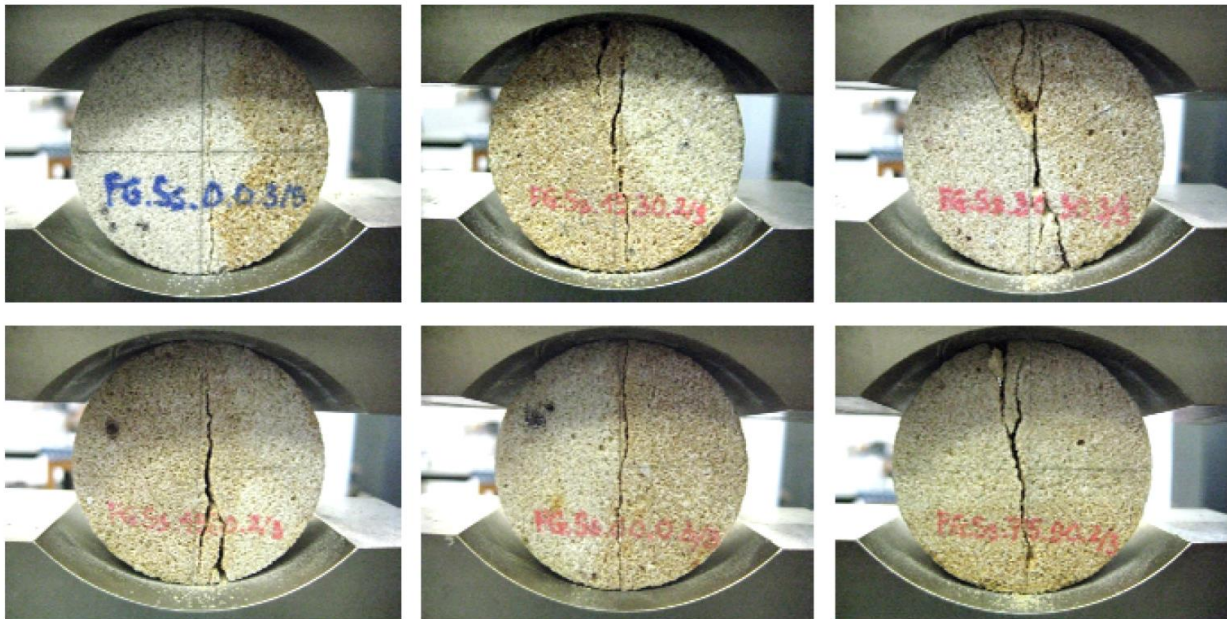

Fig. 3.9.4: Typical fracture pattern during Brazilian tests for quasi-isotropic rocks (Postaer Sandstone) [RML 2016]

3.10 Comparison between different types to measure tensile strength

The tensile strength of rocks can be determined by different types of measurement. Besides the direct tensile strength (DTS) measurement and the very popular Brazilian test method (BTS) – both are explained above - also other methods are applicable like three or four point bending tests, hydraulic fracturing or ring tests. In general these methods deliver slightly different values. These differences become even more pronounced if the rock is anisotropic like documented in Fig. 3.10.1.

Perras & Diederichs (2014) have evaluated tensile strength data from literature and performed a statistical analysis. Besides some remarkable scatter they found also that in general the DTS is the smallest value compared with values determined by indirect methods. Therefore, it is recommended to use only about 80% of the tensile strength value determined by indirect methods if DST has to be determined. Typically the ratio between UCS and tensile strength for a specific type of rock is between 5 and 20. This is also confirmed by Perras & Diederichs (2014) as documented in Fig. 3.10.2.

Overview about rock mechanical lab testing – part I mechanical tests

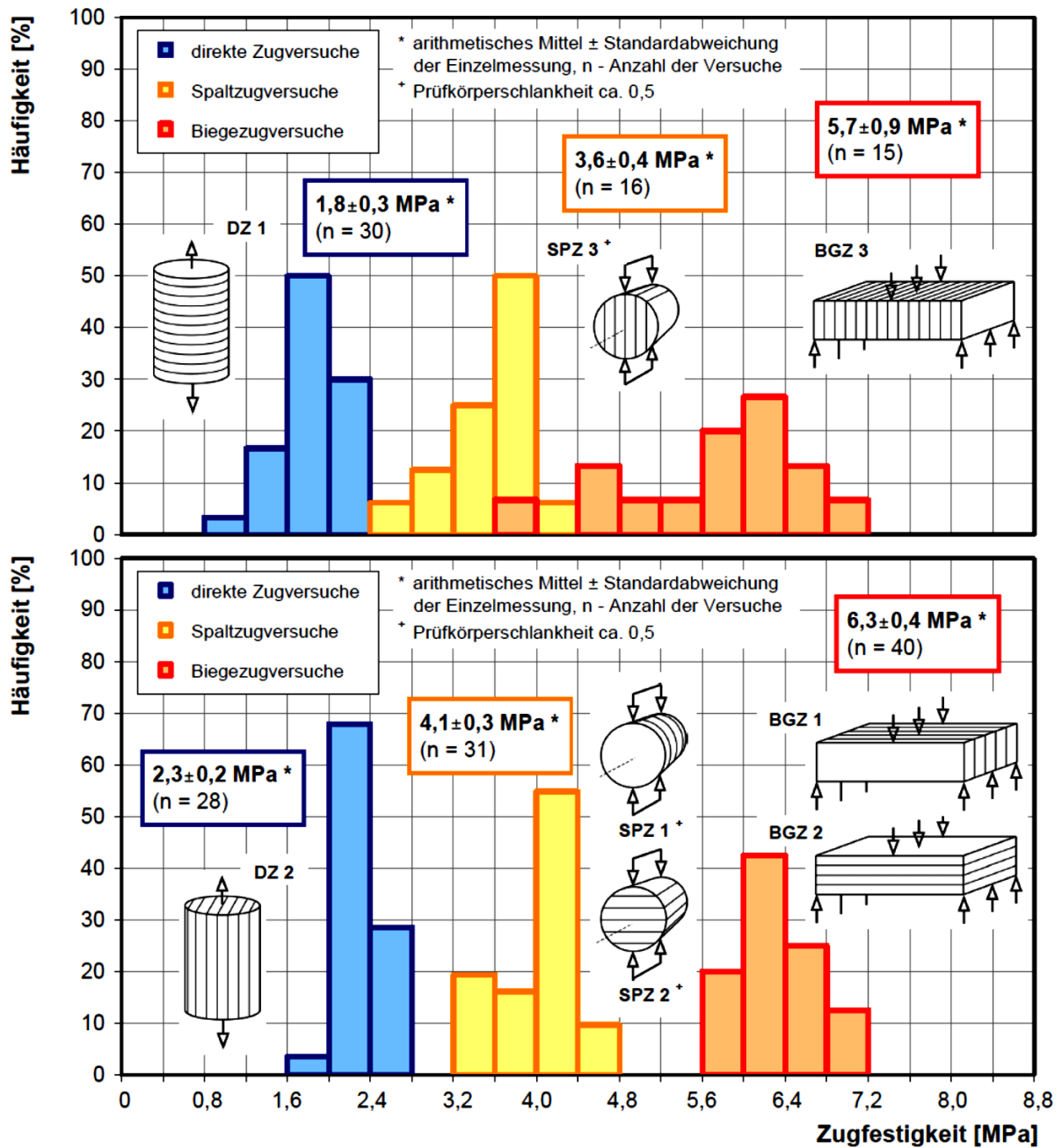Only for private and internal use!   Updated: 12 August 2024

Fig. 3.10.1: Tensile strength of anisotropic sandstone measured via DTS method, BTS method and three-point bending method (given are mean value and standard deviation as well as number of samples)

Overview about rock mechanical lab testing – part I mechanical tests

Only for private and internal use!   Updated: 12 August 2024
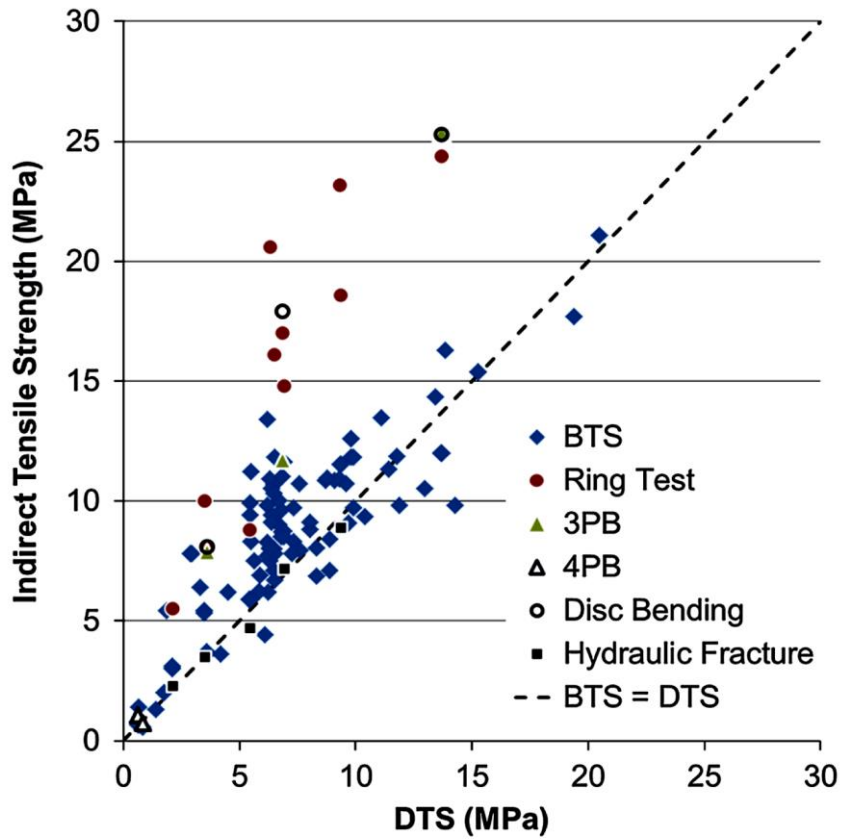
Fig. 3.10.2: DTS versus indirect determined tensile strength (Perras & Diederichs, 2014)
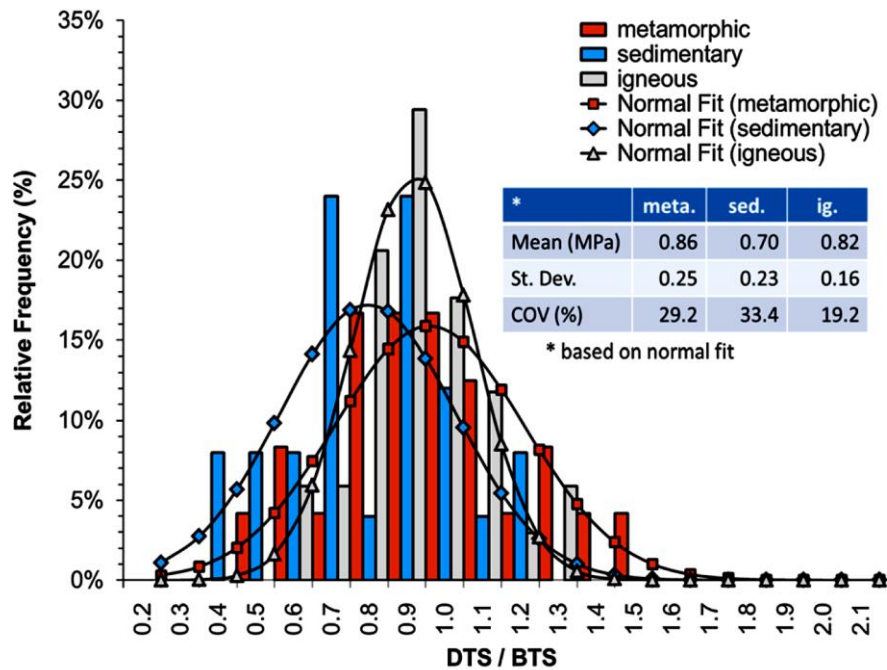
Fig. 3.10.3: Histogram of ratio between DTS and BTS (Perras & Diederichs, 2014)

Overview about rock mechanical lab testing – part I mechanical tests

Only for private and internal use!   Updated: 12 August 2024

Fig. 3.10.4: Relation between UCS and tensile strength (Perras & Diederichs, 2014)

Sainsbury & McDonald (2023) have analysed different methods to characterize the tensile strength. They found the empirical relations between UCS and tensile strength shown in Fig. 3.10.5 and 3.10.6.

Overview about rock mechanical lab testing – part I mechanical tests

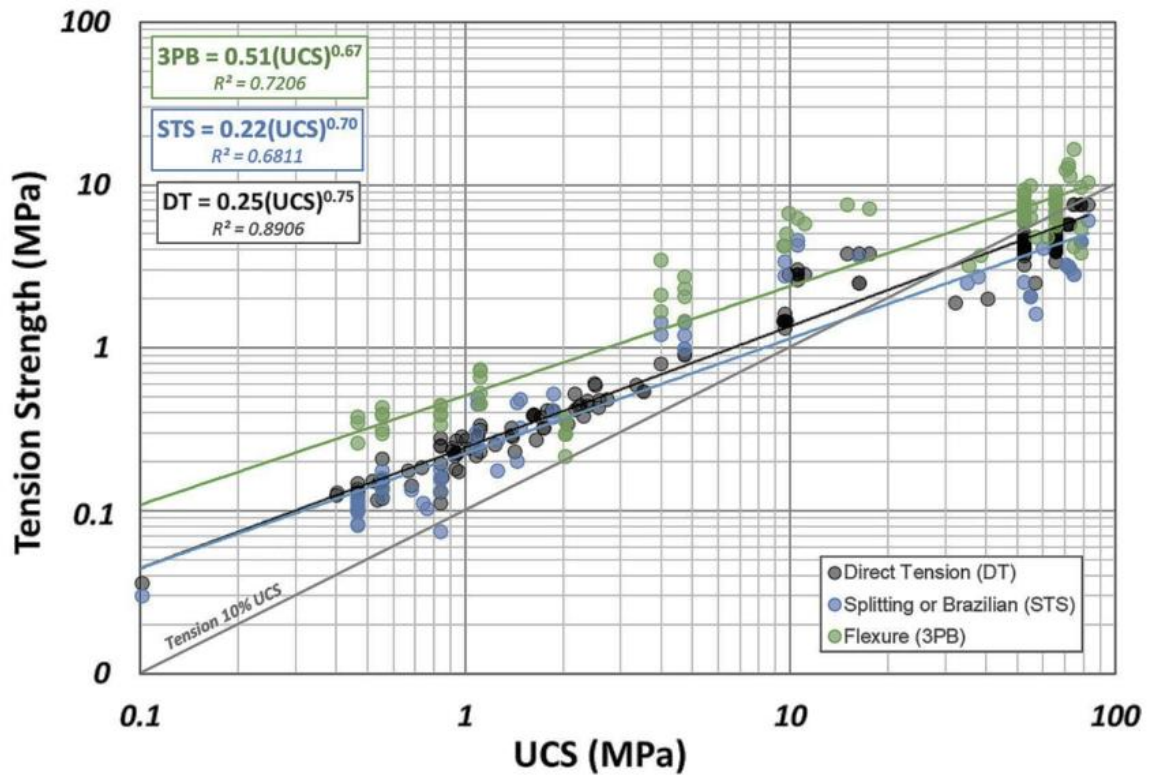Only for private and internal use!   Updated: 12 August 2024

Fig. 3.10.5: Tensile strength vs. UCS obtained by different methods to determine tensile strength (direct tensile test, Brazilian test, 3-point-bending test) [Sainsbury & McDonald, 2023]
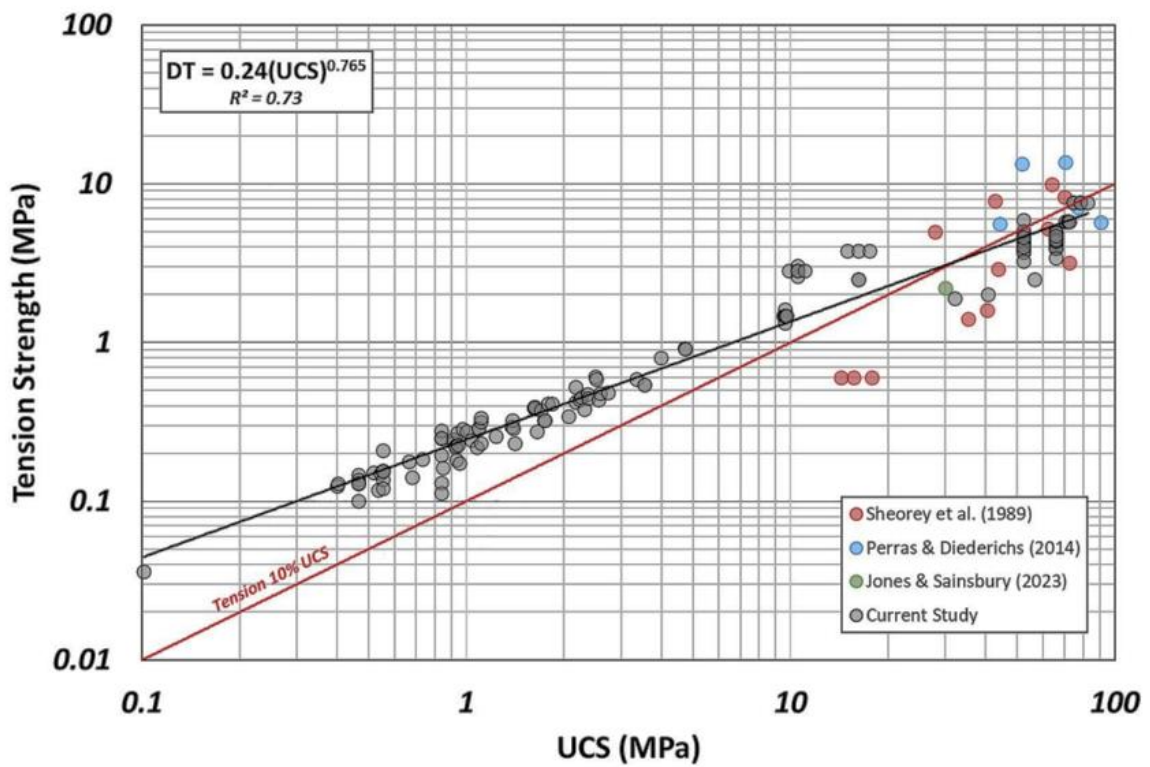

Fig. 3.10.5: Tensile strength vs. UCS [Sainsbury & McDonald, 2023]

Overview about rock mechanical lab testing – part I mechanical tests

Only for private and internal use!   Updated: 12 August 2024

3.11 Tilt test

Tilt tests are very simple and easy to perform tests on rock samples to estimate the basic friction angle. Fig. 3.11.1 shows different test arrangements (a, b and d are the most popular ones). Fig. 3.11.2 shows typical test devices. A corresponding ISRM recommendation (Alejano et al. 2018) describes the details of the test procedure. Gravity produces shear and normal forces on the inclined rock surface. The tilting has to be performed with a velocity between 10°/min to 20°/min.
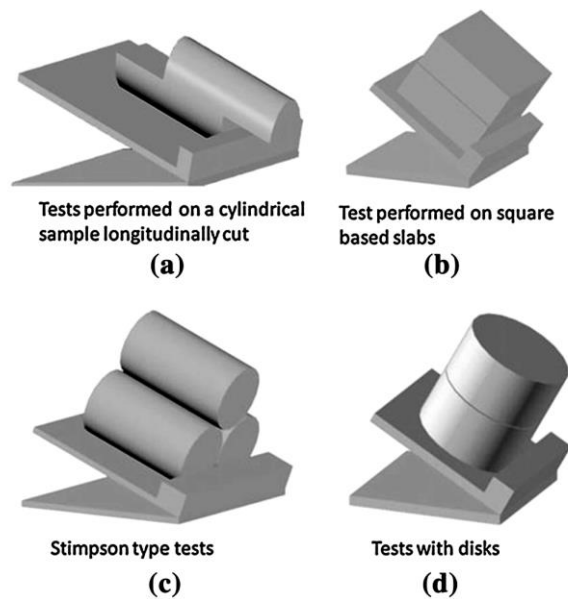

Fig. 3.11.1: Different tilt test arrangements (Jang et al., 2018; Alejano et al. 2012)

Fig. 3.11.2: Tilt test equipment (company material)

3.12 Triaxial test (Karman-type)

The Karman-type of testing is the most popular type of triaxial testing. This type of testing is designed for cylindrical specimen and characterized by circumferential and axial pressure ($\sigma_1 > \sigma_2 = \sigma_3$ for compressional testing and $\sigma_1 < \sigma_2 = \sigma_3$ for extensional testing). Requirements on sample preparation are similar to those already mentioned in chapter 3.6 (uniaxial compression testing). The axial pressure is applied by loading plates, the

Overview about rock mechanical lab testing – part I mechanical tests

Only for private and internal use!   Updated: 12 August 2024

circumferential load by oil pressure. This requiers, that the sample is encapsulated by a flexible rubber sleeve to avoid any direct contact between the pressurised oil and the rock sample. Sample size depends on triaxial cell size, but should follow a height to diameter ratio of about 2. Fig. 3.12.1 shows a sample prepared for triaxial testing including axial and circumferential strain measurement sensors. Triaxial testing can be performed in quite different ways, following different stress paths, deformation or stress controlled and using different loading velocities. Also, due to the existing servo-algorithm, the post-peak behaviour (strain softening) can be observed, if the machine frame provides sufficient stiffness (> 1 MN/mm). Fig. 3.12.3 illustrates the different stress paths, which can be applied (CTC: conventional triaxial compression, RTC: reduced triaxial compression, RTE: reduced triaxial extension, HC: hydrostatic compression, TE: triaxial extension, RTE: reduced triaxial extension). To determine the complete failure envelope different procedures can be applied: several single step tests, multi-stage tests or continuous failure state tests (Fig. 3.12.4 to 3.12.7). National and international recommendations (e.g. given by ISRM or DGGT) describe in detail the different procedures and demands for conducting triaxial tests. A comprehensive overview is given by Kwasniewski [2012].
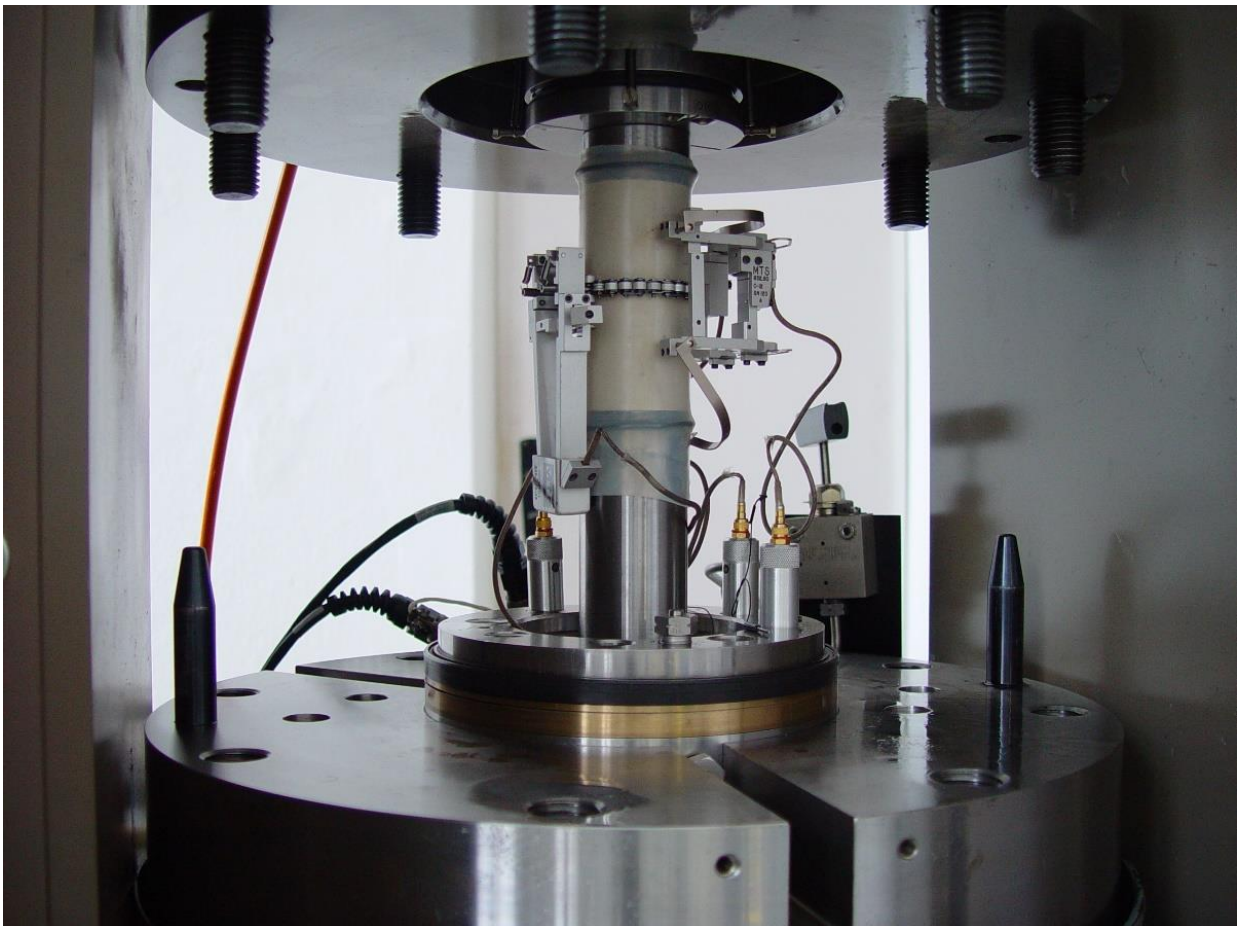
Fig. 3.12.1: Sample with rubber sleeve prepared for testing with sensors to measure axial and circumferential deformation [RML 2016]

Overview about rock mechanical lab testing – part I mechanical tests

Only for private and internal use!   Updated: 12 August 2024

Fig. 3.12.2: Typical triaxial testing device with loading frame and triaxial cell, pressure unit and data
        recording unit [RML 2016]
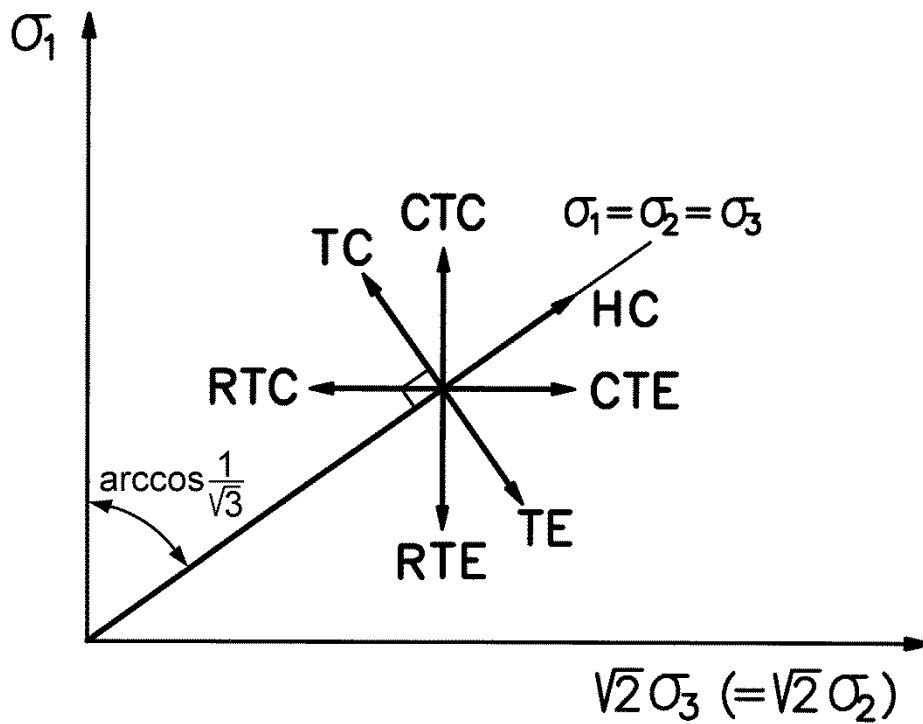
Fig. 3.12.3: Typical stress paths applied in Karman-type triaxial testing

Overview about rock mechanical lab testing – part I mechanical tests

Only for private and internal use!   Updated: 12 August 2024
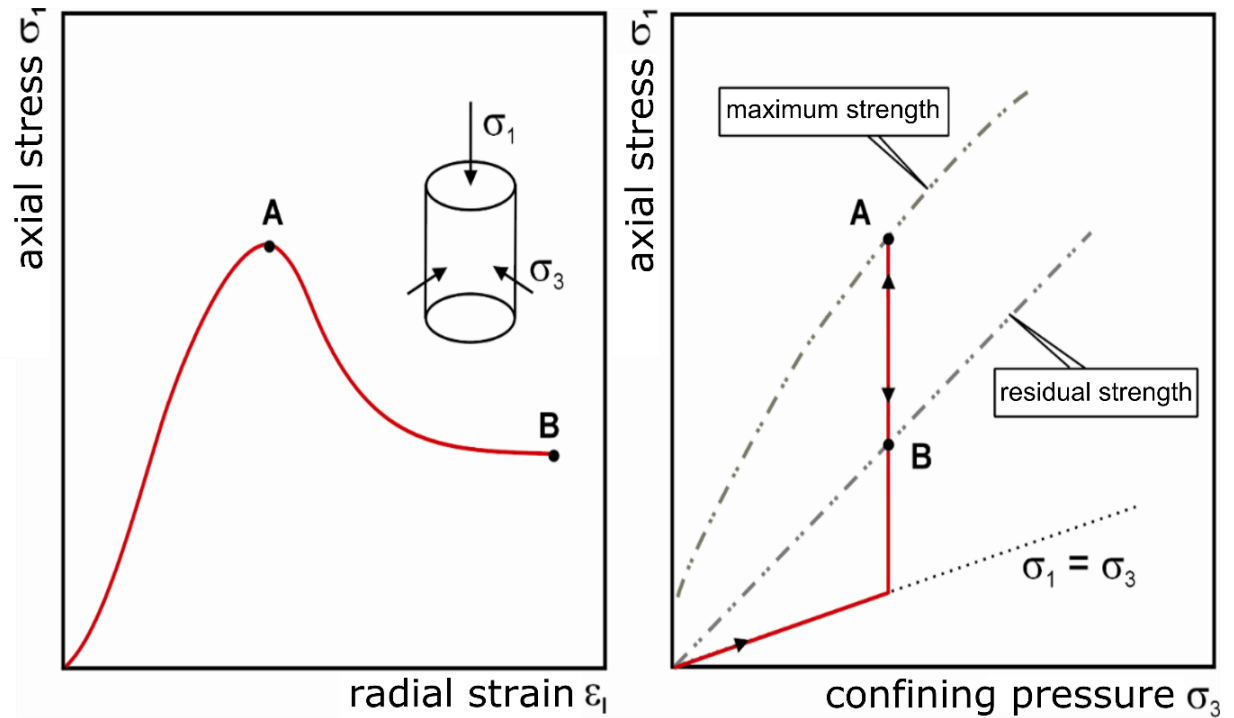
Fig. 3.12.4: Coventional single-stage test (axial pressure σ_1 versus axial deformation ε_1 or confining pressure σ_3)
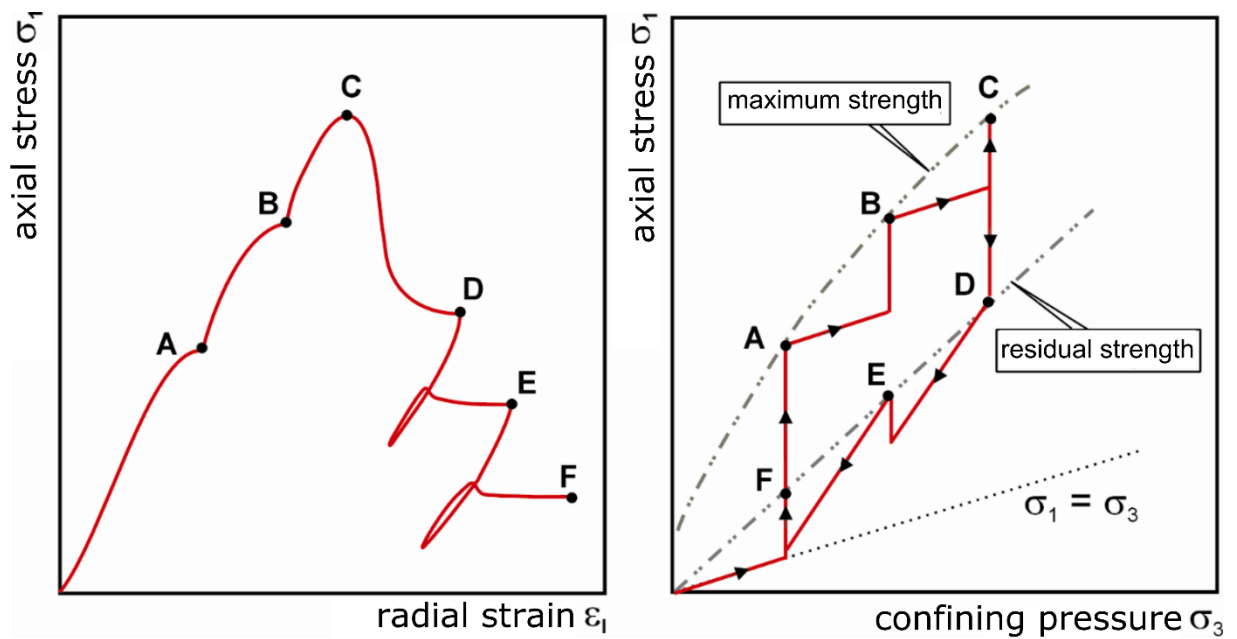
Fig. 3.12.5: Multi-stage test (axial pressure σ_1 versus axial deformation ε_1 or confining pressure σ_3)

Overview about rock mechanical lab testing – part I mechanical tests

Only for private and internal use!   Updated: 12 August 2024

Fig. 3.12.6: Triaxial single step and continuous failure state tests for determination of failure envelope for Postaer Sandstone, Germany (axial pressure σ_1 versus axial deformation ε_1 or confining pressure σ_3) [Baumgarten & Konietzky, 2012]

Overview about rock mechanical lab testing – part I mechanical tests

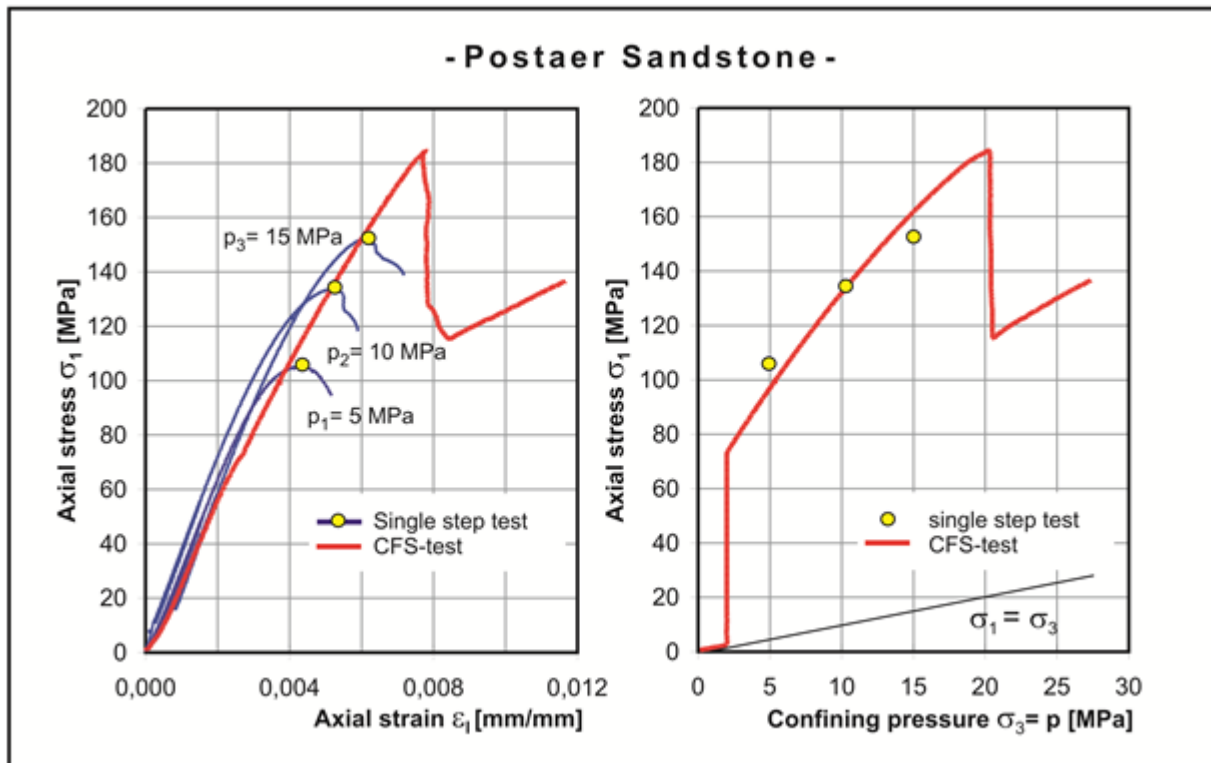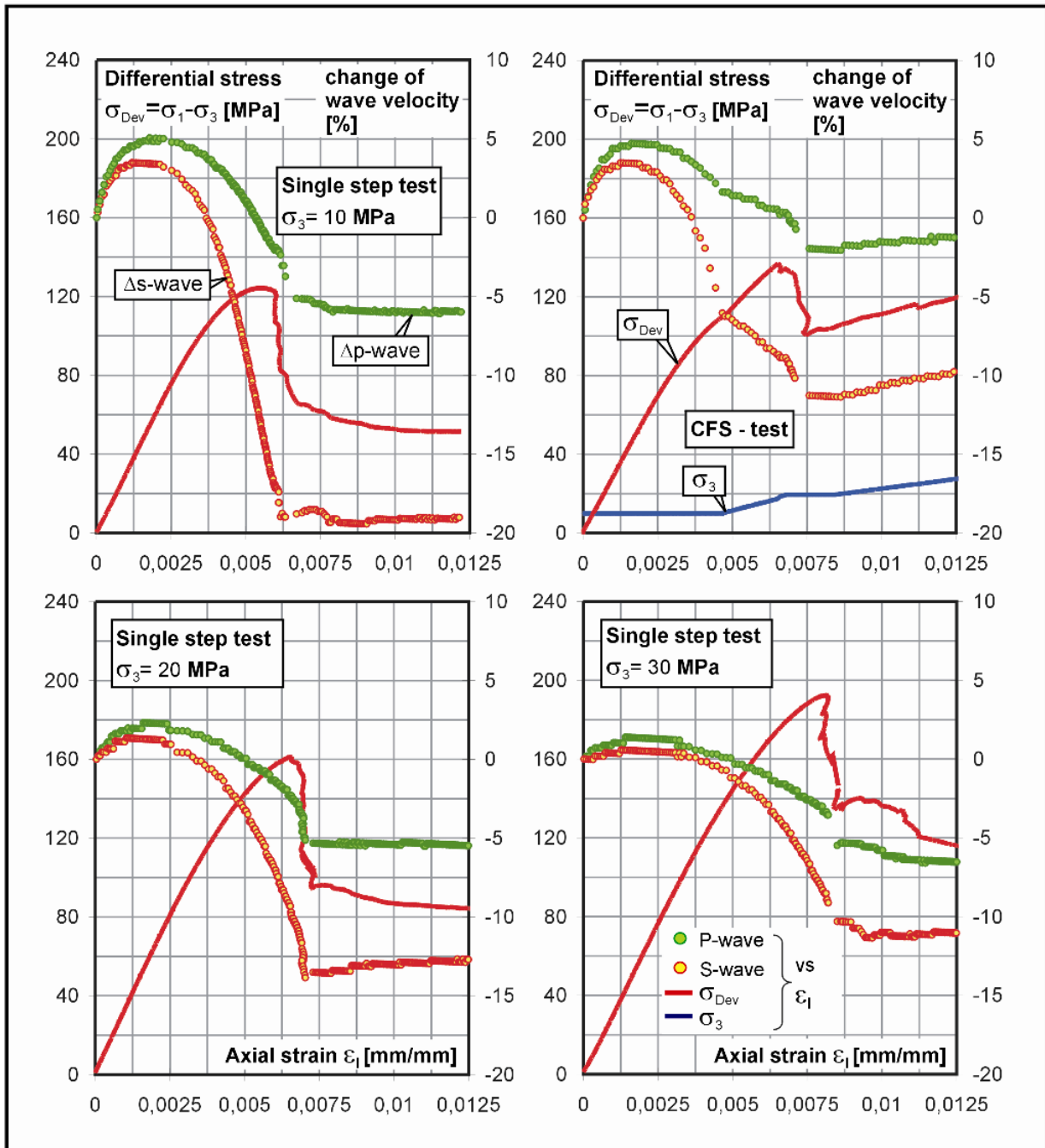Only for private and internal use!   Updated: 12 August 2024

Fig. 3.12.7: Change of compressional wave speed during triaxial testing of Postaer Sandstone, Germany [Baumgarten & Konietzky 2012]

3.13 True triaxial tests

True triaxial testing allows the application of three different principal stresses ($\sigma_1 > \sigma_2 > \sigma_3$) on cubical samples. Depending on the specific construction 3 to 6 hydraulic cylinders or pressure cells are necessary to apply the 3-dimensional stress state. True triaxial testing is necessary to investigate the effect of the intermediate principal stress on strength, failure pattern and deformation characteristics. More detailed information is given by Kwasniewski [2012]. Fig. 3.13.1. shows a typical true triaxial test device for cubic samples with size up to an edge length of 300 mm.
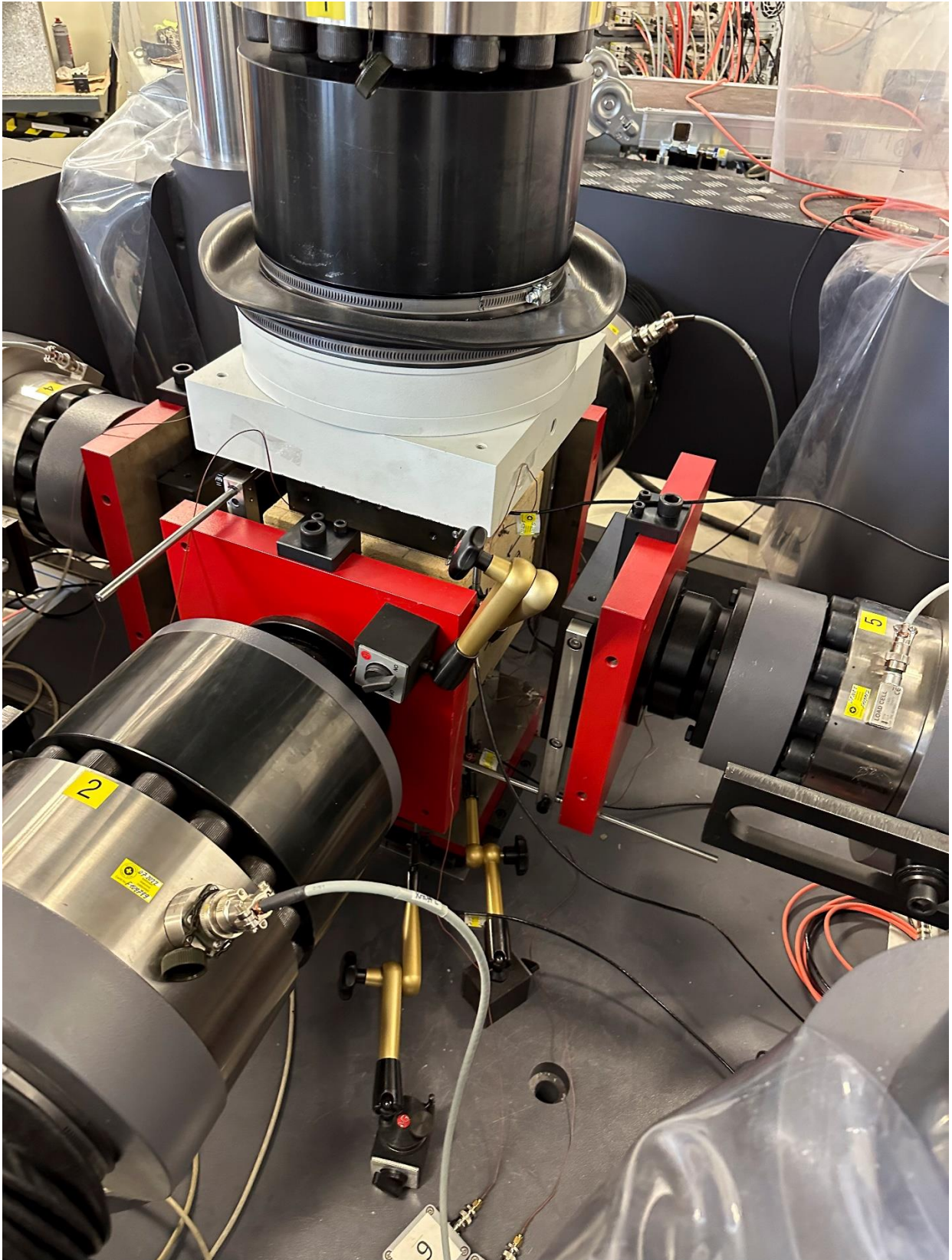
Overview about rock mechanical lab testing – part I mechanical tests

Only for private and internal use!   Updated: 12 August 2024

Fig. 3.13.1: Large true triaxial testing device [RML 2023]

Overview about rock mechanical lab testing – part I mechanical tests

Only for private and internal use!   Updated: 12 August 2024

3.14 Shear box tests

A shear box device consists of a loading frame, an upper and lower shear box and two pistons to apply shear force and normal force (Fig. 3.14.1). Fig. 3.14.2 shows a photo of the central part of a sophisticated shear box device including the empty upper and lower shear box. Inside these boxes the rock sample has to be placed. The fixation of the sample (either cuboidal or cylindrical) is performed with special grout of high strength and stiffness.
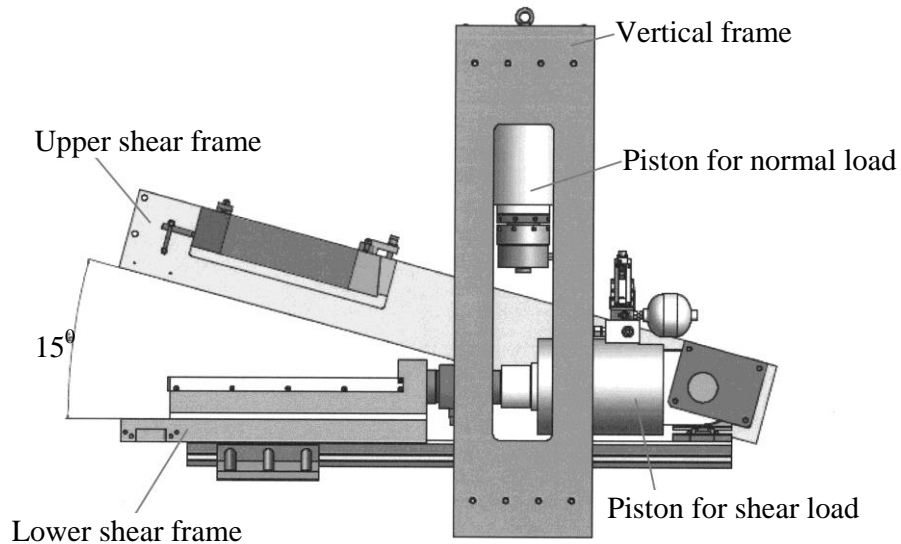

Fig. 3.14.1: Principal sketch of a shear box device [Konietzky et al. 2012]

Fig. 3.14.2: Foto of a shear box device and view into empty shear boxes [Konietzky et al. 2012]

Overview about rock mechanical lab testing – part I mechanical tests

Only for private and internal use!   Updated: 12 August 2024

Shear box testing can be performed in quite different manners:

- as a constant normal load (CNL) test or constant normal stiffness (CNS) test (Fig. 3.14.3)
- as a static, cyclic or dynamic test
- as a pure mechanical test or HM-coupled test
- as a test for intact rock samples or test of discontinuities (joints, fractures etc.)
- as a single-stage or multi-stage test
- as a test up to the peak strength or until the residual strength

During the test the following parameters should be monitored:

- axial and horizontal forces
- axial displacement and heave of loading plate (dilation measurement)

In addition surface roughness of shear plane can be scanned before and after the tests as well as during test breaks. Normal stress and shear stress can be determined by the recorded forces and the corresponding areas, whereby it should be considered, that effective shear area may be reduced with ongoing shear displacement and therefore, the normal stress should be updated continuously. Classical evaluation of shear tests include the determination of cohesion, friction and dilation. Cohesion and friction are determined using the Mohr-Coulomb theory by linear regression over several data pairs of normal and shear stresses (Fig. 3.14.4 and 3.14.5).
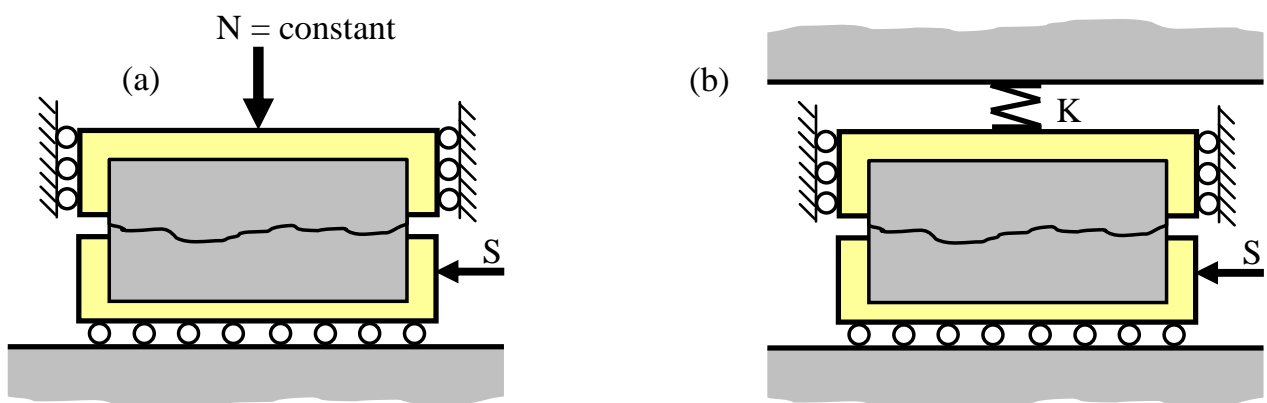

Fig. 3.14.3: Principle of CNL (left) and CNS (right) testing
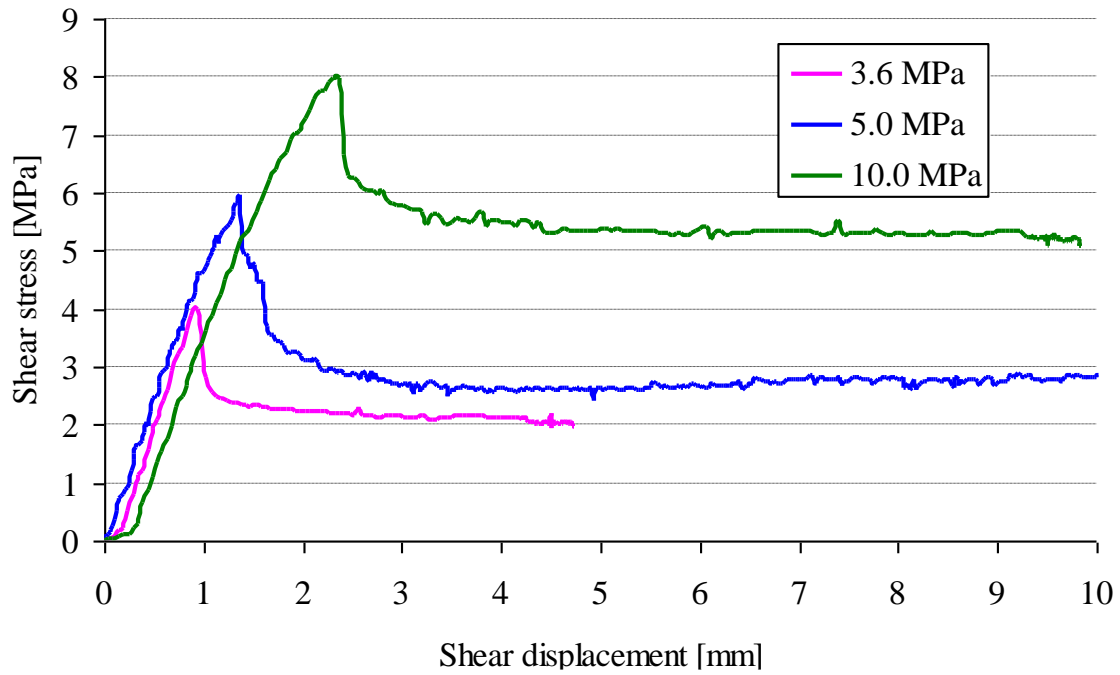
Fig. 3.14.4: Example: Shear test results for 3 tests with different normal stress of 3.6, 5.0 and 10.0 MPa

Fig. 3.14.5: Example: Determination of peak and residual strength for a slate by linear regression of 3 shear tests (peak cohesion = 2.5 MPa, peak friction angle 29°, residual cohesion = 0.16 MPa, residual friction = 27°)

The dilation Ψ is defined as ratio between measured vertical to horizontal displacement components (valid under the assumption, that the shear plane is horizontal):

$$\Psi = \frac{\Delta u_n}{\Delta u_s}$$

Overview about rock mechanical lab testing – part I mechanical tests
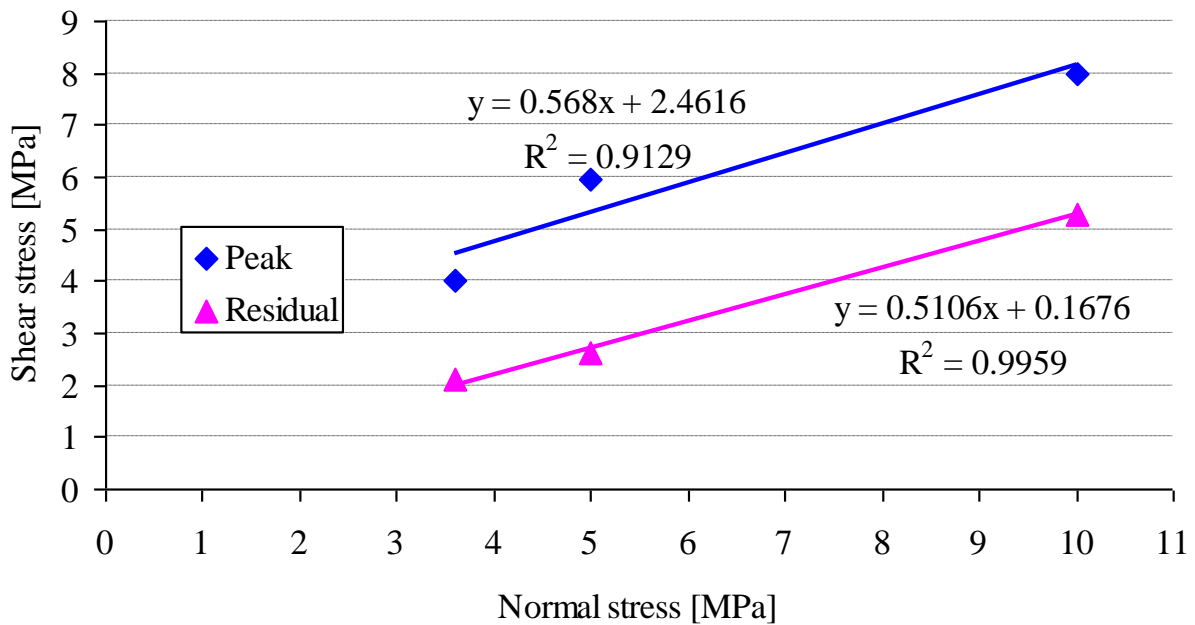
Only for private and internal use! Updated: 12 August 2024

However, one should take into consideration the actual orientation of the fracture plane. If the fracture plane is inclined, 'apparent' dilation is observed and the true value should be obtained by correction (Fig. 3.14.6).
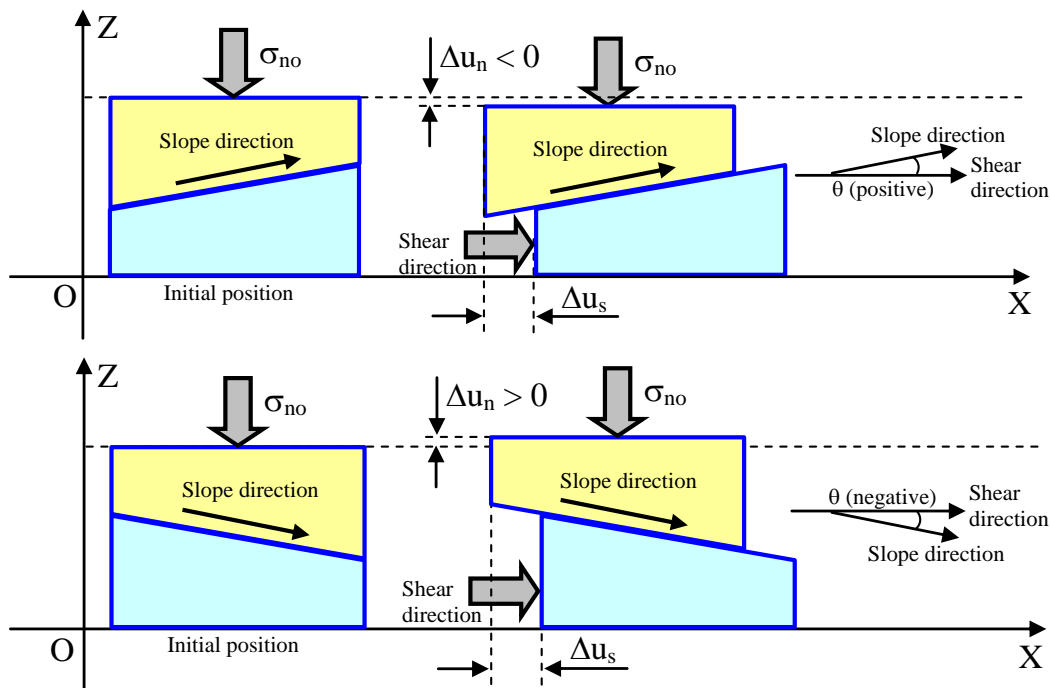

Fig. 3.14.6: Problem of 'apparent' dilation due to inclined fracture plane

3.15 Fracture toughness tests

Three different types of fracture toughness can be distinguished:

- Mode-I: tensile fracture
- Mode-II: in-plane shear fracture
- Mode-III: out-of-plane shear fracture (torsion fracture)

So far, for practical applications only Mode-I and Mode-II fracture propagations are considered. Therefore, lab testing concentrates on these two types:

- Determination of critical stress intensity factor (= fracture toughness) K_{IC}
- Determination of critical stress intensity factor (= fracture toughness) K_{IIC}

In material sciences several methods were developed to determine fracture toughness. Due to the specific material characteristics of rocks specific testing methods were developed in rock mechanics.

3.15.1 K_I fracture toughness tests

Most popular methods are:

- Chevron Bend Specimen (CBS) test
- Short Rod Specimen (SRS) test
- Cracked Chevron Notched Brazilian Disc (CCNBD) test
- Semi-circular bend (SCB) test

Overview about rock mechanical lab testing – part I mechanical tests

Only for private and internal use!   Updated: 12 August 2024

CBS test is similar to a 3-point-bending test, but needs a special prepared cylindrical sample (Fig. 3.15.1). A special shaped notch [Ulusay 2007] has to be created at the centre of the specimen opposite to the load entry point. The measurements can be conducted on two different levels:

- Level-1-testing: considers only load at failure and sample dimensions
- Level-2-testing: considers non-linearities during fracture propagation based on additional measurement of crack opening displacement and corresponding correction terms in calculating fracture toughness [Ulusay 2007]

K_{IC} based on level-1-testing is determined by the following formulae:

$$K_{IC} = \frac{AF}{D} \quad \text{where } [K_{IC}] = \text{MPa}\sqrt{m}$$

$$A = \left(1.835 + 7.15\frac{a}{D} + 9.85\left(\frac{a}{D}\right)^2\right)\frac{S}{D}$$

where:
F maximum load (load at failure) in kN
D diameter of specimen in cm
S distance between support points ($3.33 \cdot D$) in cm
A Chevron tip distance from specimen surface ($0.15 \cdot D$) in cm

Fig. 3.15.1: Test set-up for CBS test [RML 2016]

Overview about rock mechanical lab testing – part I mechanical tests

Only for private and internal use!   Updated: 12 August 2024

SRS tests are designed for using short rods (cylindrical core specimen of short length) with chevron-shaped notch cut along core axis. SRS test can also be performed as level-1 or level-2 test. K_{IC} based on level-1-testing is determined by the following formulae:

$$K_{IC} = 24 \frac{F}{D^{1.5}} \quad \text{where } [K_{IC}] = \text{MPa} \sqrt{\text{m}}$$

where:
F   maximum load (load at failure) in kN
D   diameter of specimen in cm

CCNBD testing is similar to the classical Brazilian test, but needs a special preparation of the sample: a special designed notch (Fig 3.15.2 and 3.15.3). K_{IC} is determined by the following formulae:

$$K_{IC} = \frac{P\sqrt{a}}{\sqrt{\pi R B}} N_I$$

R   radius of specimen
a   half crack length
P   load at failure
B   thickness of specimen
N_I special function depending on sample dimension and crack orientation α (see Chen & Konietzky [2014])

SCB tests is a special three-point bending test as shown in Fig. 3.15.4. More specific recommendations are given by Kuruppu et al. (2014).

$$K_{IC} = \frac{P\sqrt{\pi a}}{2rt} Y_I$$

where:
P   maximum load
a   notch length
r   radius of sample
t   thickness of specimen
Y_I special dimensionless function depending on sample dimension and crack orientation α according to Kuruppu et al. [2014]

Overview about rock mechanical lab testing – part I mechanical tests

Only for private and internal use!   Updated: 12 August 2024
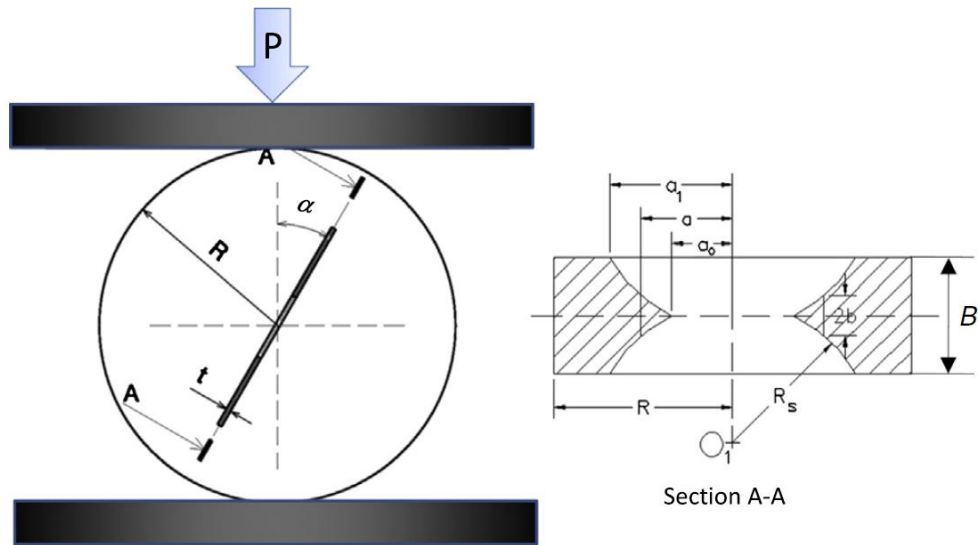

Fig. 3.15.2: CCNBD sample configuration [Aliha & Ayatollahi 2014]
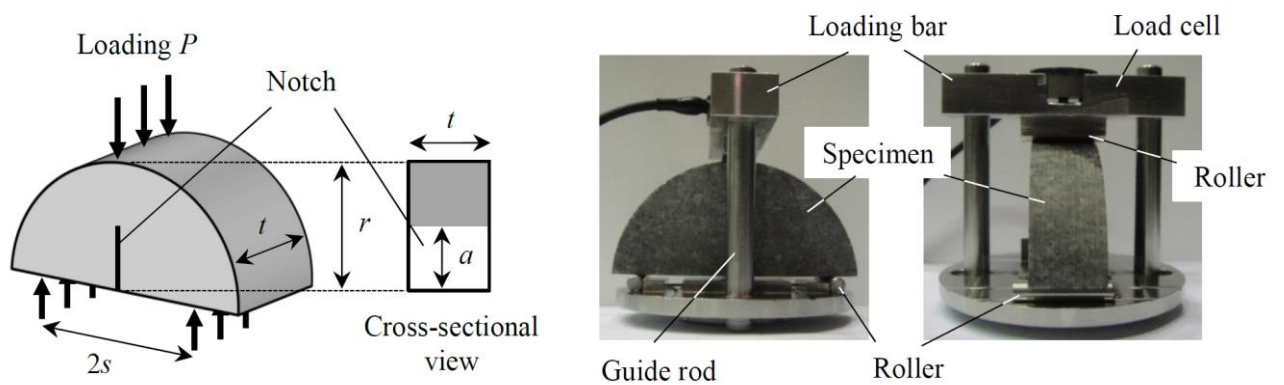

Fig. 3.15.3: Test set-up for CCNBD test [RML 2016]

Fig. 3.15.4: Test set-up for SCB test [Kataoka & Obara 2015]

Overview about rock mechanical lab testing – part I mechanical tests

Only for private and internal use!   Updated: 12 August 2024

3.15.2 K_{II} fracture toughness tests

Several test methods have been developed to measure K_{IIC} [e.g. Backers 2004, Backers & Stephansson 2012, Chen & Konietzky 2014, 2015, Ulusay 2015). Some common methods used in rock mechanics are illustrated in Fig. 3.15.5. The Central Cracked Notch Brazilian Disc (CCNBD) test is quite interesting, because easy to perform using the standard equipment for Brazilian tests. Also, the same test arrangement can be used to determine both, Mode-I and Model-II fracture toughness (Chen & Konietzky 2014, 2015).
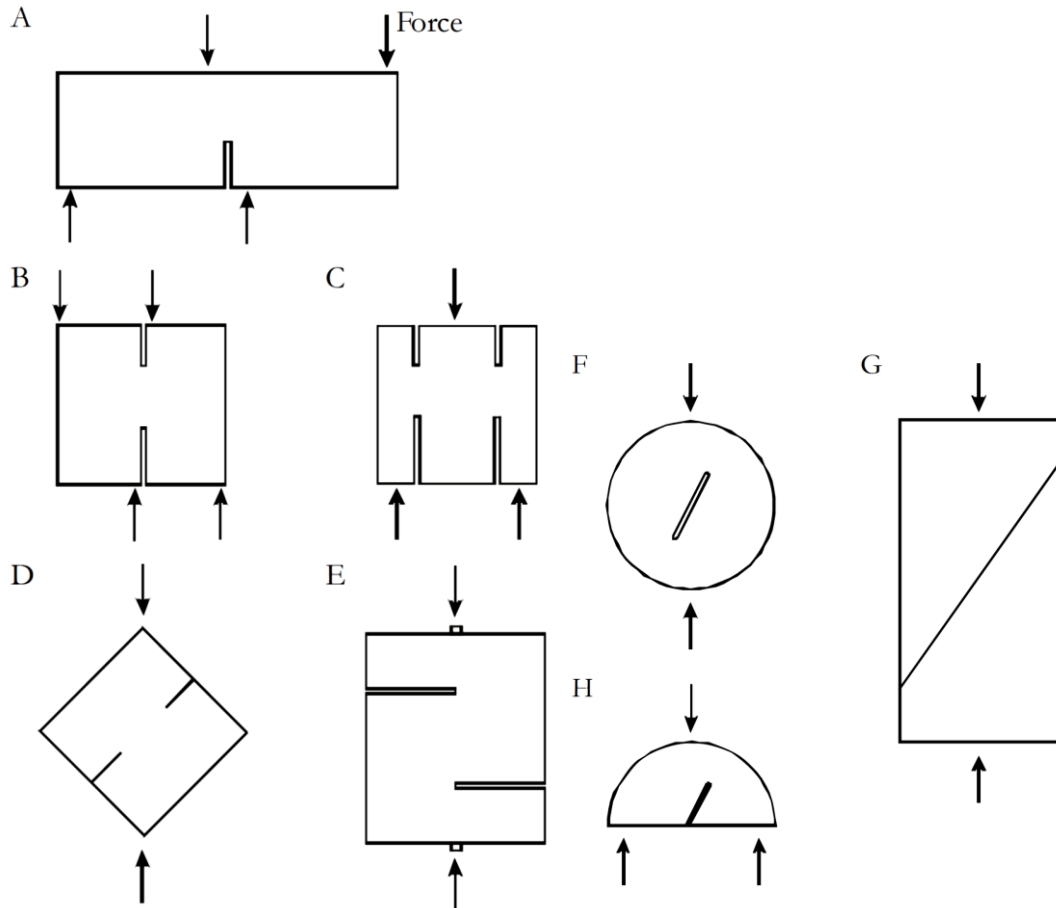

Fig. 3.15.5: Mode-II fracture toughness methods: A: antisymmetric four point bending, B: antisymmetric four point bending cube, C: punch through shear, D: compression shear cube, E: short beam compression, F: centrally cracked Brazilian disc, G: triaxial compression, H: three point bending semi disc [Backers 2004]

3.16 Macro-, Micro- and Nanoindentation tests

Micromechanical parameters can be determined via nano- or microindentation tests. During these tests small indenters are pushed into the rock with defined load and deformation/crack pattern is evaluated. These devices are usefull for parameter identification of grains or very fine rocks like claystone or shale (e.g. Wang et al. 2022). Ma et al. (2020) provide a good overview about the application of nano- and microindentation in rock mechanics.

Via nano- and microindentation information about the following items can be obtained:

- Hardness
- Elastic modulus
- Elasto-plasticity
- Residual stresses
- Yield strength
- Fracture toughness
- Creep and relaxation behaviour
- Fatigue

Different types of indenters are used as shown in Fig. 3.16.1. Nanoindentation is characterized by very small maximum indentations of up to 200 nm, but microindentation is characterized by indentations larger than 200 nm, but indentation forces smaller than 2 N. Fig. 3.16.2 shows typical parameters of micro- and nanoindentation testing devices. Fig. 3.16.3 shows a sample surface after 100 indentation tests.
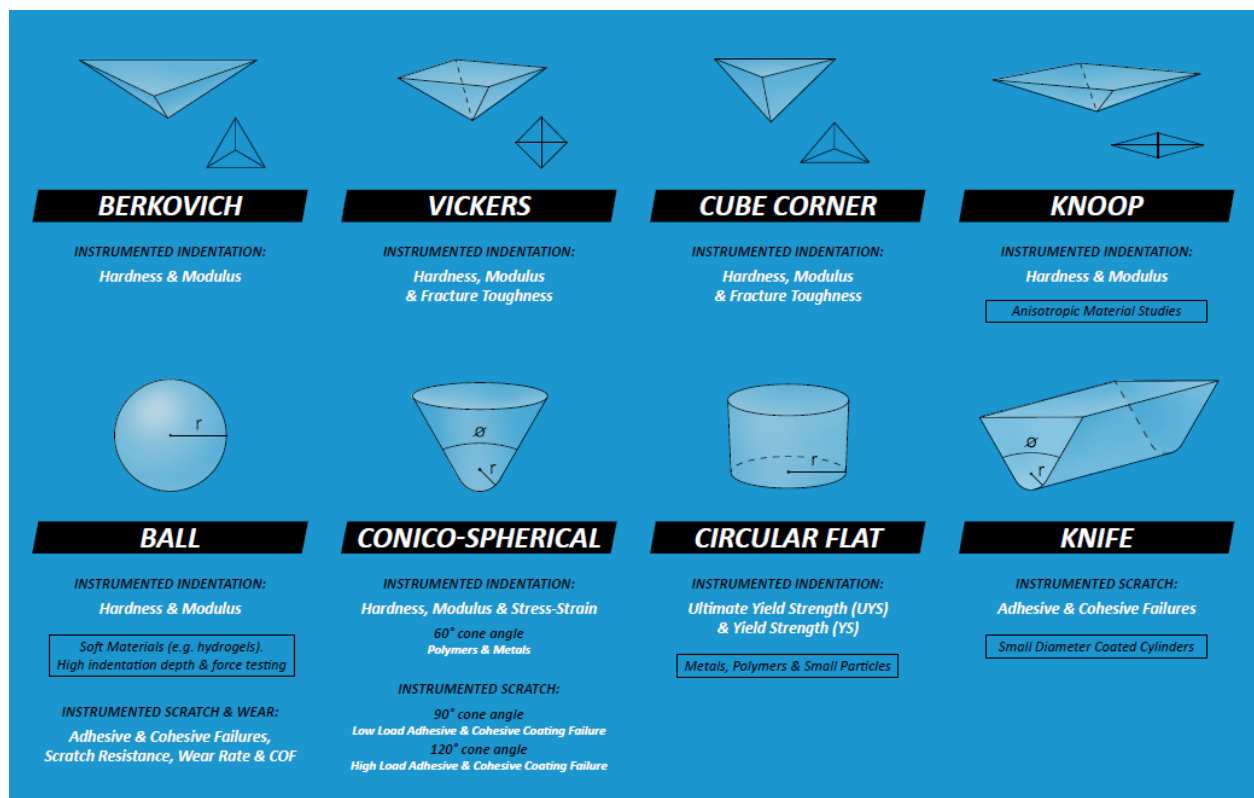

Fig. 3.16.1: Typical indenter types (Nanovea company material, 2022]

Overview about rock mechanical lab testing – part I mechanical tests

Only for private and internal use!   Updated: 12 August 2024

	NANO	MODULES	MICRO	
	Indentation, Scratch, Wear & Friction	MODES OF TESTING	Indentation, Scratch, Wear & Friction	
	Piezo Electric Actuator	LOADING SYSTEM	Ball Screw Servomotor	
	Ultra Precision Load Cell	LOAD SENSOR	Precision Load Cell	
	80 | 400 | 1800 | 4800 mN	LOAD RANGE	20 | 40 | 200 | 400 N	
	0.004 | 0.03 | 0.14 | 0.28 µN	LOAD RESOLUTION (24bit)	1.2 | 2.4 | 12 | 24 µN	
	0.12 | 1 | 4 |12 µN	LOAD NOISE FLOOR RMS	50 | 100 | 500 | 1000 µN	
	Capacitor Ring	DEPTH SENSOR	Large Area Capacitor	
	250 | 1500 µm	DEPTH RANGE	1 mm (extended range capability)	
	0.003 nm	DEPTH RESOLUTION (24bit)	0.01 nm	
	0.04 nm	DEPTH NOISE FLOOR RMS	0.15 nm	
	Ultra Precision Load Cell	FRICTION SENSOR	Precision Load Cell	
	50 | 400 |1800 mN	FRICTION RANGE	20 | 200 N	
	0.004 | 0.14 | 0.28 µN	FRICTION RESOLUTION	1.2 | 12 µN	
	0.3 | 6 | 12 µN	FRICTION NOISE FLOOR RMS	1.2 | 2 mN	
	150 - 400 kHz *	ACOUSTIC EMISSION FREQUENCIES	150 - 400 kHz	
	0.005 aJ	SENSITIVITY OF AE ABSOLUTE ENERGY	0.005 aJ	
	0.1 to 100 Hz	DMA / CSM FREQUENCIES	N/A	
	Yes	FREQUENCY & TEMPERATURE SWEEP AT CONSTANT LOAD	N/A	
	5 min (100 indents)	FASTMAP	12 min (100 indents)	
	275° | 450°C	HIGH TEMPERATURE	275° | 450° | 600°C	
	Down to -10°C | <-40°C	LOW TEMPERATURE	Down to -10°C | <-40°C	
	5% to Dew Point	HUMIDITY	5% to Dew Point	
	RT to 60ºC	LIQUID	RT to 60ºC	

Fig. 3.16.2: Typical specifications for micro- and nanoindentation equipment (Nanovea company material, 2022]
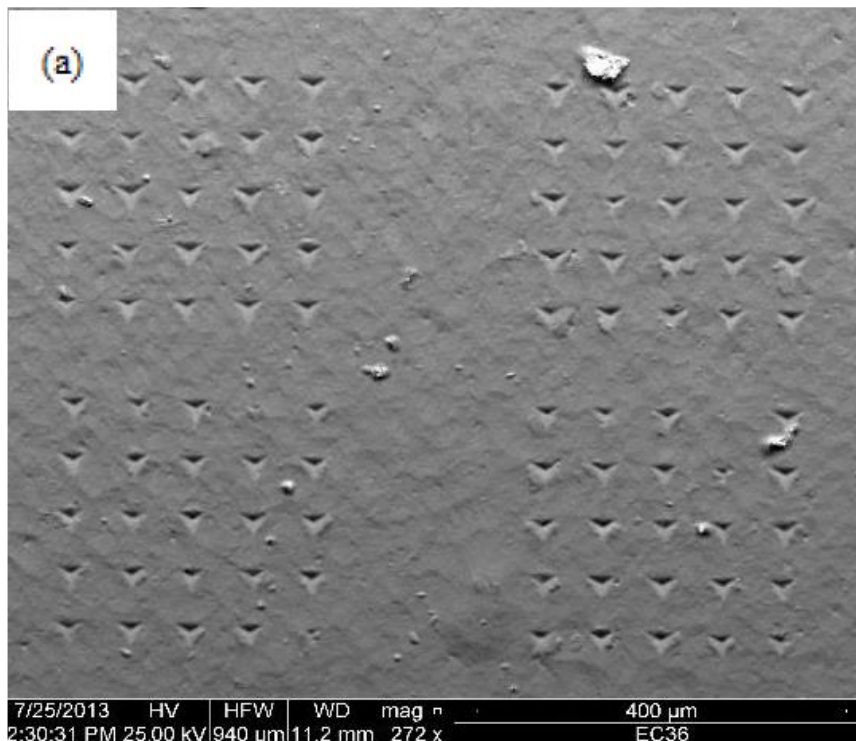

Fig. 3.16.3: Indentations on a shale sample (Shukla et al., 2015]

There are several methods to determine the microscopic fracture toughness or energy release rate using nano- or microindendation tests.

Fracture toughness Mode-I can be determined within 40% accuracy using the following formula:

$$K_{IC} = \alpha \sqrt{\frac{E}{H}} \left(\frac{P_{max}}{c^{3/2}} \right)$$

where:

α   dimensionless factor depending on indenter geometry
E   mean elastic modulus
H   mean hardness
P_{max} maximum indenter depth
C   crack length (see Fig. 3.16.4)

The means values of hardness and elastic modulus are typically determined by several (> 10) indendation tests. The same holds for c and P_{max}.
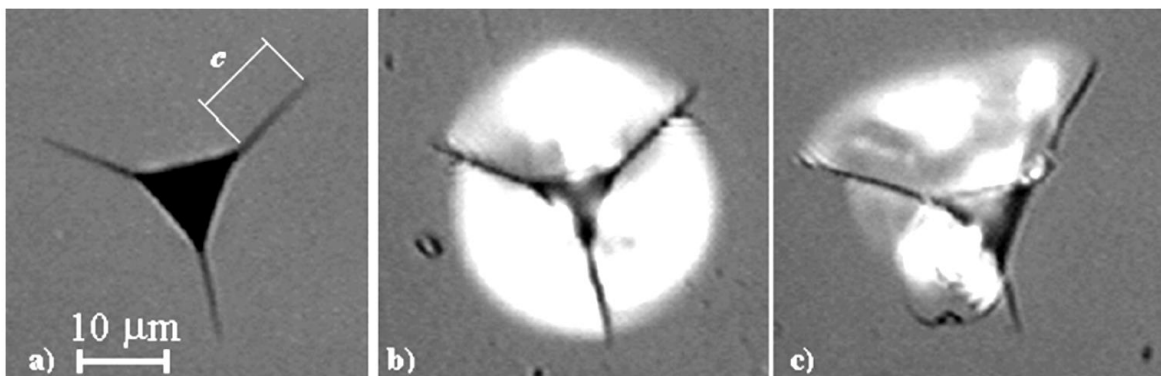

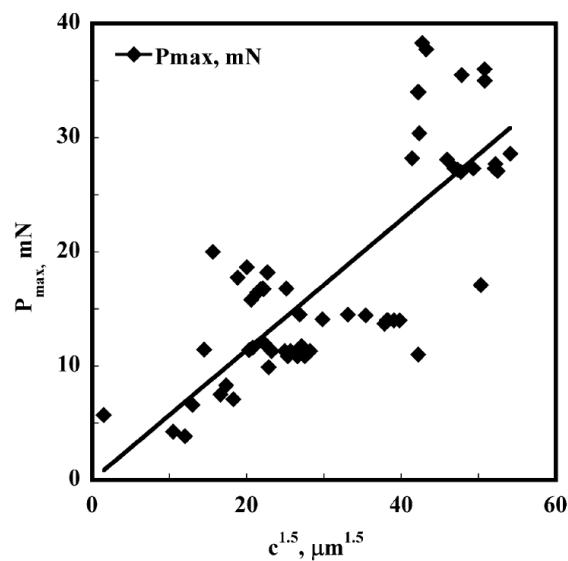Fig. 3.16.4: Optical micrographs of cube-corner indendations (Volinsky et al., 2003)

Fig. 3.16.5: Maximum indendation vs. crack length (Volinsky et al., 2003)

Besides nano- and microindendation also macroindentation is used, especially to investigate rock breaking processes like drilling and cutting. The principle test procedure is similar to that used for micro- or nanoindendations. However, the indenter size is much bigger (mm up to cm-range) and test equipment is simpler, easier to handle and much more robust in respect to environmental influences. Fig. 3.16.6 shows used macroidenter types. Fig. 3.16.7. shows the test set-up in principle as well as a typical force-displacemnt curve.
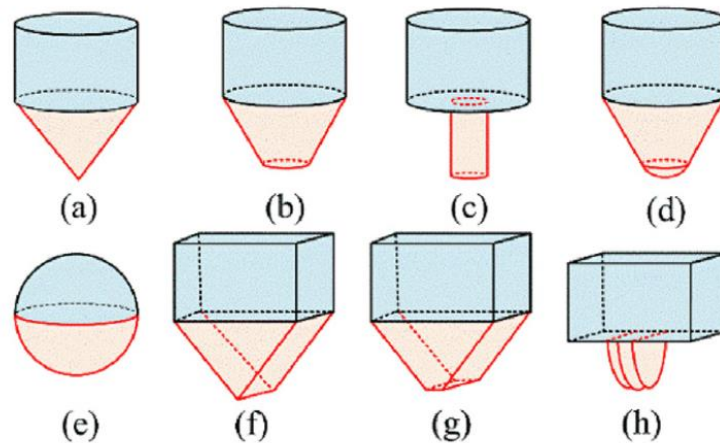

Fig. 3.16.6: Typical macroindeter types (Xie et al., 2024)
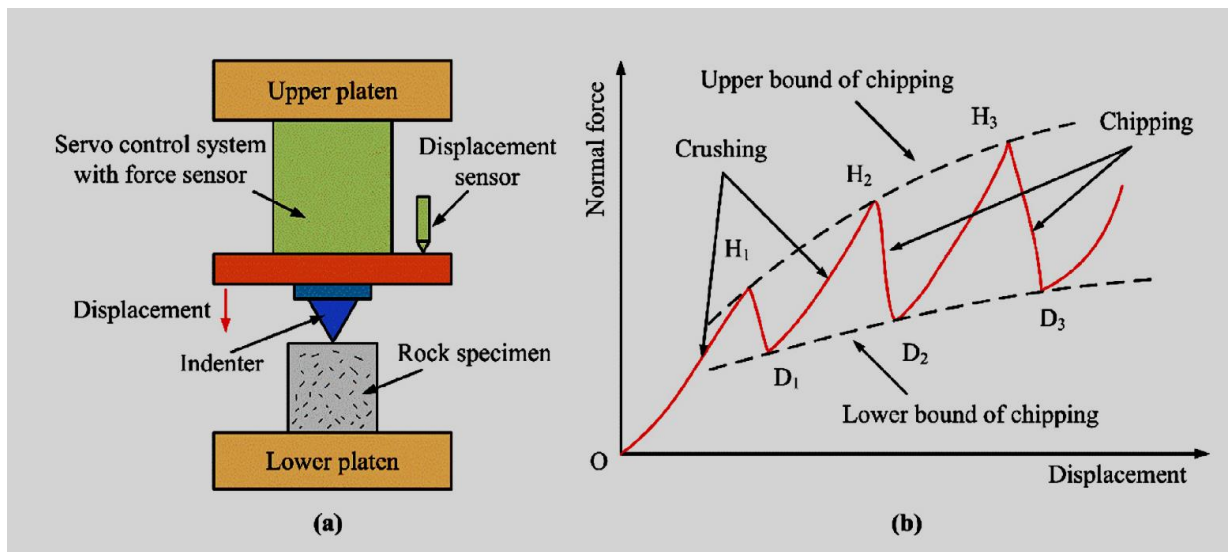
Fig. 3.16.7: Schematic of macroindenter device and typical force-displacement curve (Xie et al., 2024)

Xie et al. (2024) provide a comprehensive overview about theoretical concepts, empirical and analytical relations, simulation approaches and discuss several factors influencing the test results like sampel size, indentation rate, confinement, rock type or indenter type.

Fig. 3.16.8 and 3.16.9 show Discrete-Element based numerical simulations of a macroindenter test. These figures show the induced stresses (colored) as well as the fracture propagation (bold back lines).

Overview about rock mechanical lab testing – part I mechanical tests

Only for private and internal use!   Updated: 12 August 2024
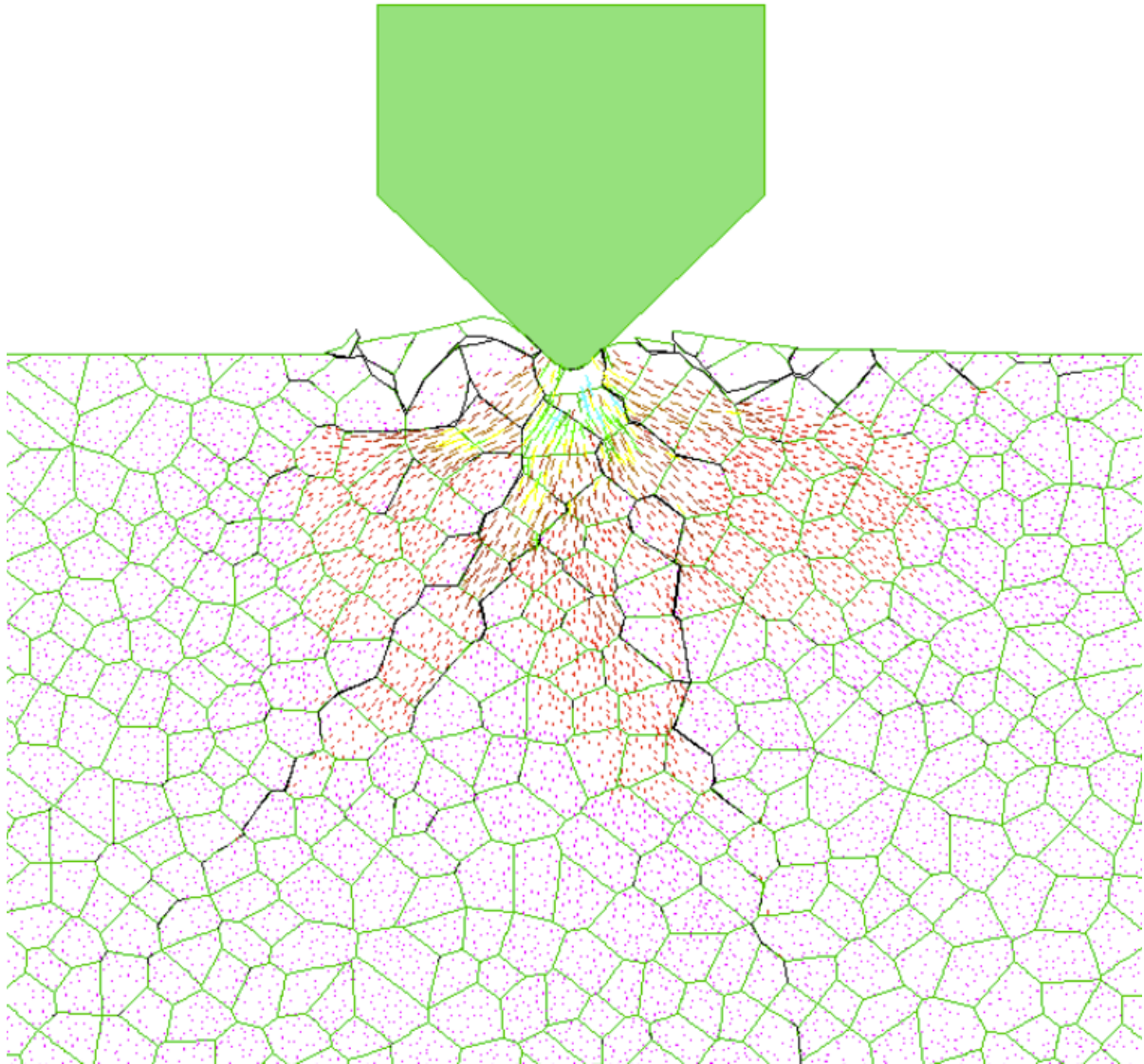
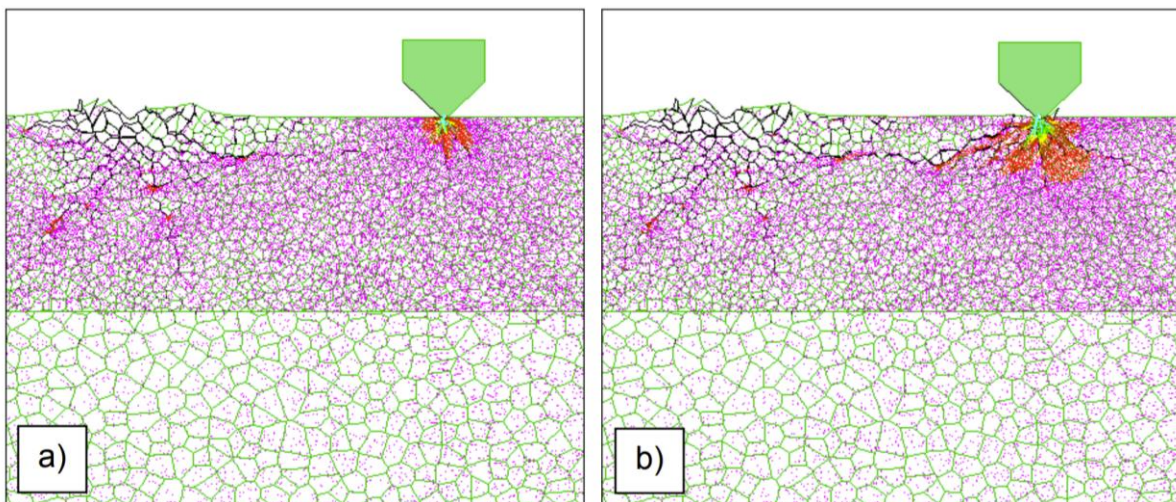Fig. 3.16.8: Macroindenter test: induced fractures and stresses (Lunow, 2014)

Fig. 3.16.9: Macroindenter test: induced fractures and stresses at different penetration depth of (a) 0,2 mm and (b) 0,6 mm (Lunow, 2014)

4   Acoustic emission monitoring

Crack development and fracture propagation are connected with radiation of seismic energy (seismic waves). Therefore, acoustic sensors can be used to monitor damage processes. Typical AE sensors have the following characteristics:

- frequency range between 10^3 Hz to 10^6 Hz
- velocity proportional registration (sometimes also acceleration proportional)
- sensors based on piezo-ceramic material
- sensor size: a few mm to a few cm

Sensors are either directly connected to the sample or fixed at the loading frame or loading plates. Monitoring can be performed in quite different ways, but in principal all applied techniques including data processing and evaluation are similar to earthquake monitoring. With one or just a very few sensors only event counting including some relative magnitude evaluation can be performed. If a complete network is installed, localization can be performed and seismic source parameters can be determined, e.g., seismic moment, magnitude, fault plane solution, stress drop, source dislocation and source dimensions. Localization can be performed with different techniques using first arrivals of P- and S-waves. Sophisticated AE analysis is described for instance by Stanchits et al. (2011, 2014 or Dresen et al. (2020)).

Typical AE systems consists of the following elements:

- Sensors

- Pre-amplifier

- Transient recorder

- Computer with software (on-line data evaluation and post processing)

To perform localization and seismic source parameter determination a roughly spherical network of at least 6 to 10 sensors is necessary. Also, noise level should be as low as possible, because only events above the noise level can be detected. Fig. 4.1 illustrates the parameters of a seismic event.
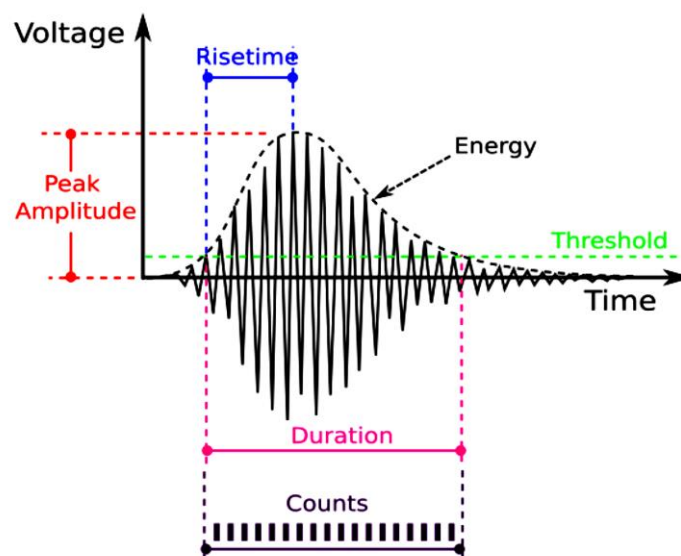

Fig. 4.1: Typical AE event parameters (Calabrese & Proverbio, 2020]

Overview about rock mechanical lab testing – part I mechanical tests

Only for private and internal use!   Updated: 12 August 2024

<u>Peak Amplitude</u> is the highest peak of the measured voltage signal and it is measured in decibels. <u>Threshold</u> is a setting parameter that is applied for the elimination of electronic and environmental background noises. Only AE waveforms with amplitude higher than the set threshold value will be recorded. <u>Duration</u> is defined as the interval between the first and last time the signal waveform crossing the threshold value. <u>Risetime</u> is the time interval between the first threshold crossing and the amplitude (maximum signal peak). <u>Energy</u> is the measure of the area under the envelope of the AE voltage signal waveform. <u>Counts</u> refers to the number of amplitude peaks greater than the threshold value.

Tab. 4.1: Typical AE event parameters (Calabrese & Proverbio, 2020)

Waveform Feature	Variable Name	Variable Description	Unit
Direct	Amplitude	Value of the maximum peak of the signal waveform. It indicates magnitude of the waveform.	dB
	Threshold	Threshold value such that signals with amplitude higher than this value will be recorded.	dB
	Duration	Time between the start and end of the signal referred to a predefined threshold	$\mu\sigma$
	Risetime	Time between the first overshoot of the defined threshold and the peak amplitude.	$\mu\sigma$
	Energy	Area under the envelope of the AE voltage signal waveform.	Eu or V^2s
	Counts	Number of time (counts) that AE signal crossed the amplitude threshold.	Absolute number
	Average Frequency	Ratio between Counts and Duration.	kHz
Indirect	RA	Ratio between Risetime and Amplitude. Useful to classify the type of cracks.	ms/V
	b-value; Ib-value	approach based on the event cumulative frequency–magnitude distribution	–
Cumulative	Cumulative	Cumulative value for specific parameters, such as hits, counts and energy	–

Fig. 4.2 to 4.4 show localization results. More sophisticated source parameters can be determined via seismic moment tensor inversion (see ebook chapter "Dynamic events in hard rocks" or in more detail Kwiatek et al., 2016).
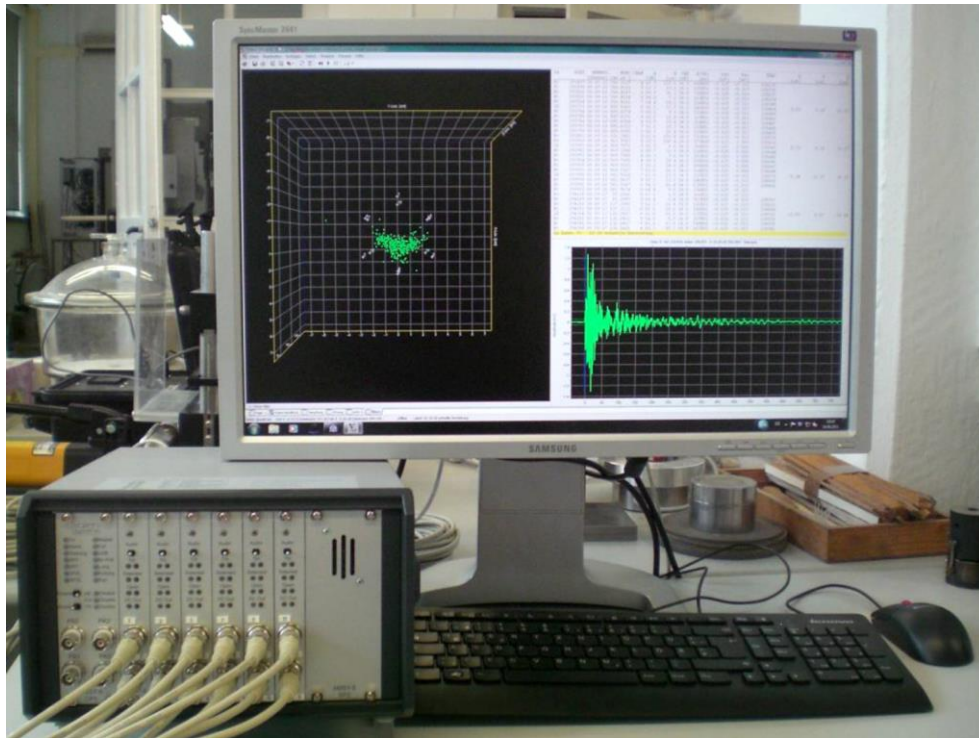
Fig. 4.2: Typical AE workplace with transient recorder (lower left side) and on-line display with single AE event and localization result [RML 2016]

(a) 20%   (b) 40%   (c) 60%

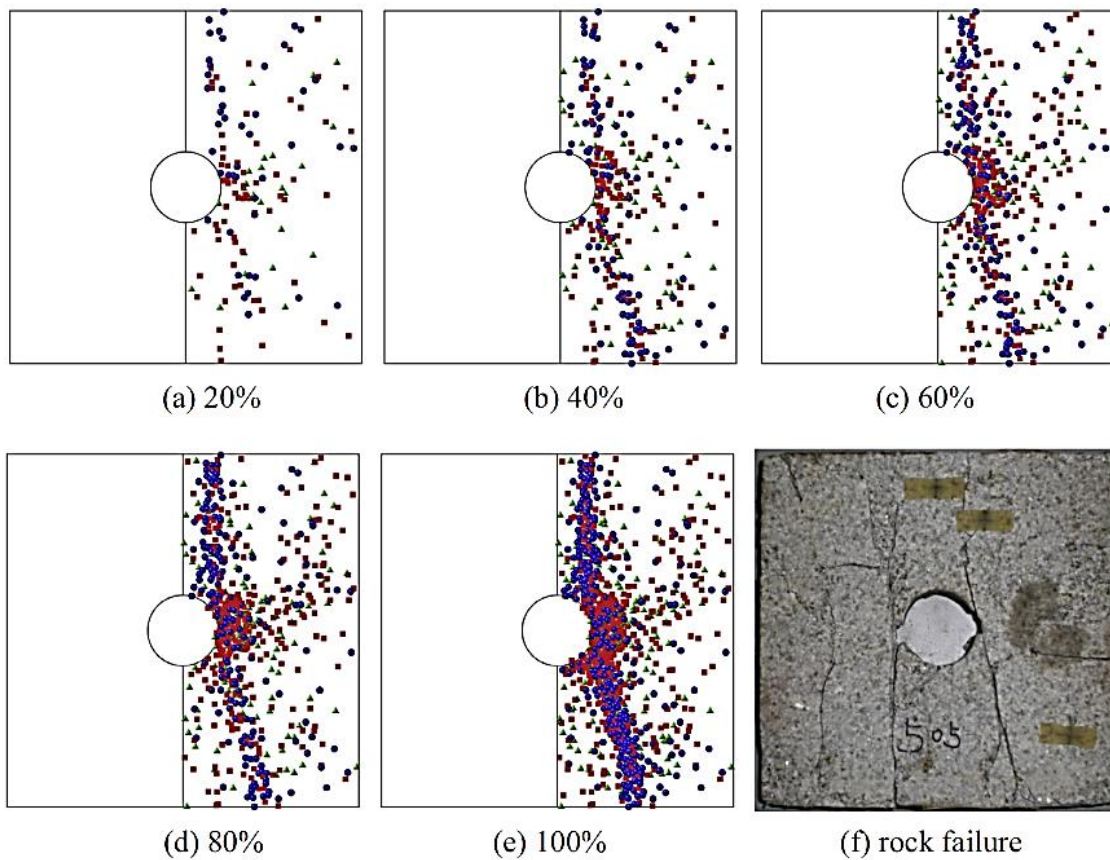(d) 80%   (e) 100%   (f) rock failure

Fig. 4.3: AE localization at different stress levels (percentage of failure stress) for uniaxial loading [Liu 2015].
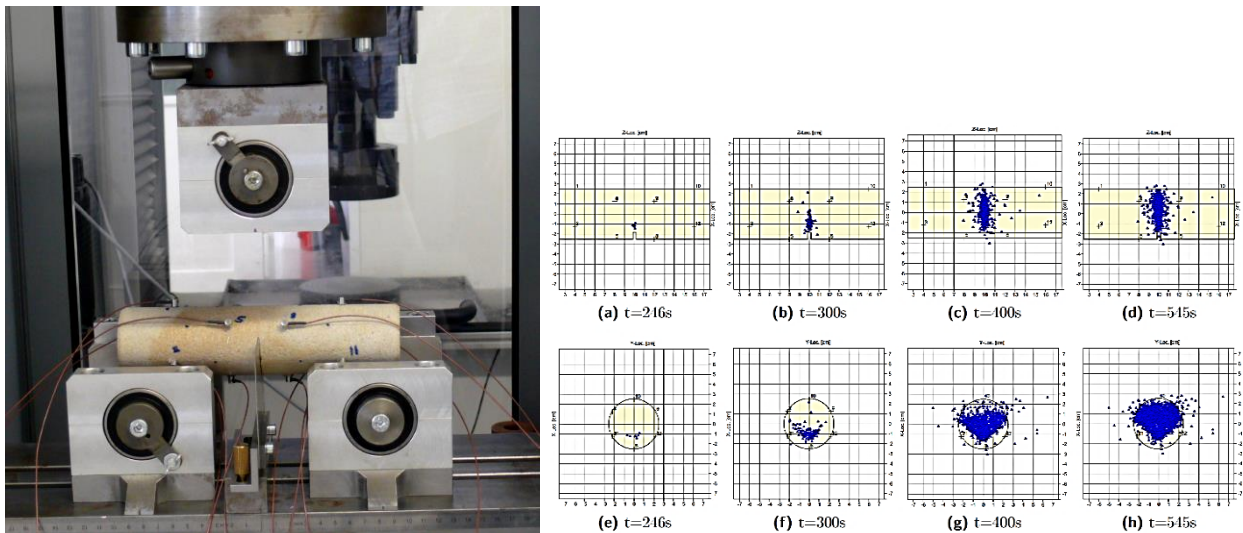
Fig. 4.4: Fracture toughness test with AE monitoring und localization [RML 2016]

5   Further dynamic testing methods

Several rock mechanical applications or processes demand the consideration of dynamic parameters, like earthquake engineering, blasting, explosions, rock bursts, drilling, impact and collision problems etc. Dynamic rock properties deviate significantly from static ones as exemplary demonstrated in Fig. 5.1. Dynamic rock parameters have to be always given together with the loading rate used during testing, because they are strongly depending on the loading rate. Most popular dynamic testing methods are [Xia & Yao 2015, Zhou et al. 2012]:

- Split Hopkinson pressure bar (SHPB) test
- Dynamic notched semi-circular bend (NSCB) test
- Dynamic Brazilian test
- Dynamic compression test

Main dynamic rock parameters are:

- Dynamic compressive strength
- Dynamic tensile strength
- Dynamic punch shear strength
- Dynamic bending strength
- Dynamic fracture toughness
- Dynamic Young's modulus
- Dynamic Poisson's ratio

Many of the dynamic tests are performed in the same way as the corresponding static tests are done, but on much higher loading rate. However, the very popular Split Hopkinson pressure bar test requires a special experimental set-up as exemplary shown in Fig 5.2 and 5.3. SHPB consists of three interacting bars: a striker bar, an incident bar and a transmitted bar. Via a special gun the striker bar is accelerated. The impact of the striker bar on the free surface of the incident bar induces longitudinal compressive waves in two

directions. The left propagation wave is fully released at the striker bar and forms the trailing edge of the incident compressive pulse. Reaching the incident bar – sample inter-face, part of the wave is reflected and the remainder passes through the specimen. Strain gauges are used to measure the stress wave pulse. The objective of SHPB tests is to determine the dynamic stress strain curves and to deduce dynamic strength and stiffness of the material. Fig. 5.3 shows the set-up of special SHPB device, which allows to test samples under confining pressure.
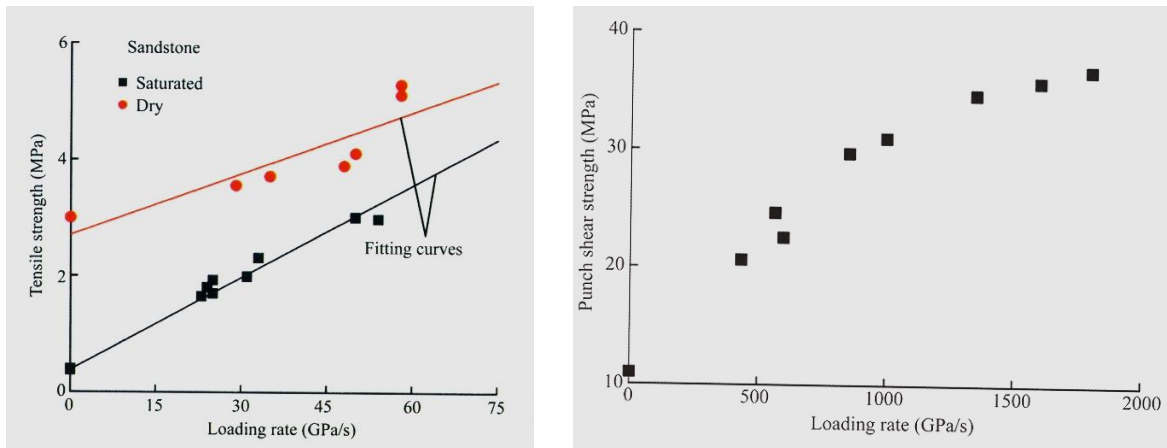

Fig. 5.1: Tensile (left) and punch shear strength (right) for sandstones as a function of loading rate [Xia & Yao 2015]
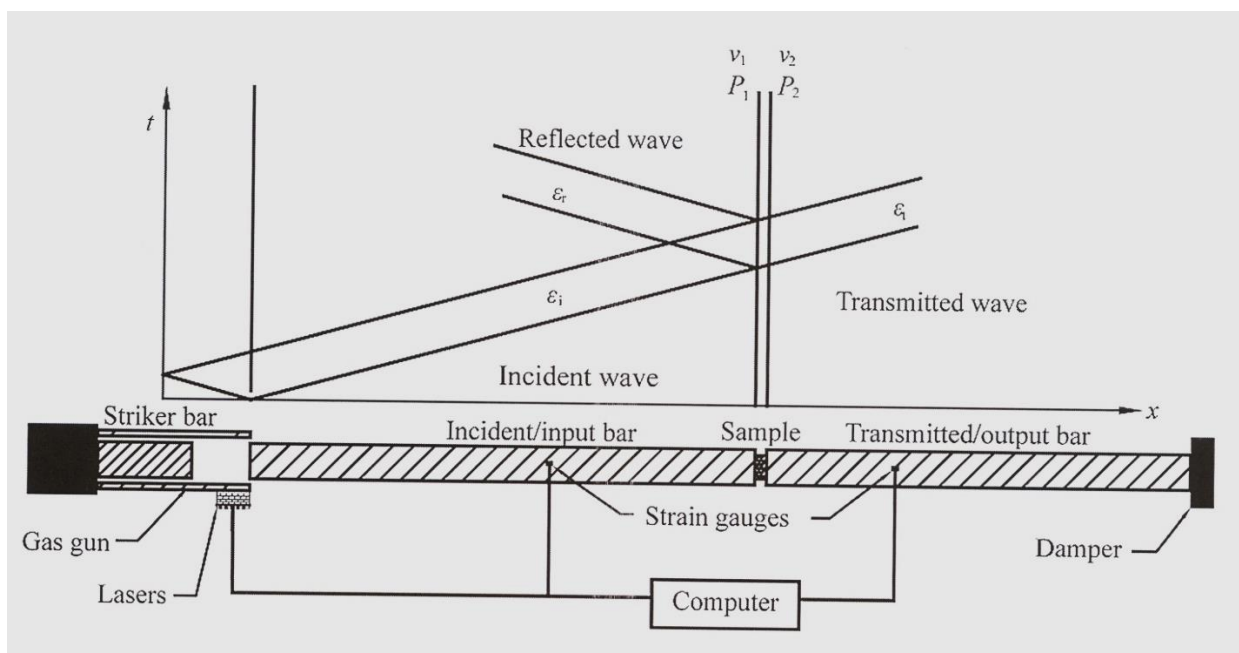

Fig. 5.2: Principal sketch of Split Hopkison pressure bar device [Xia et al. 2015]
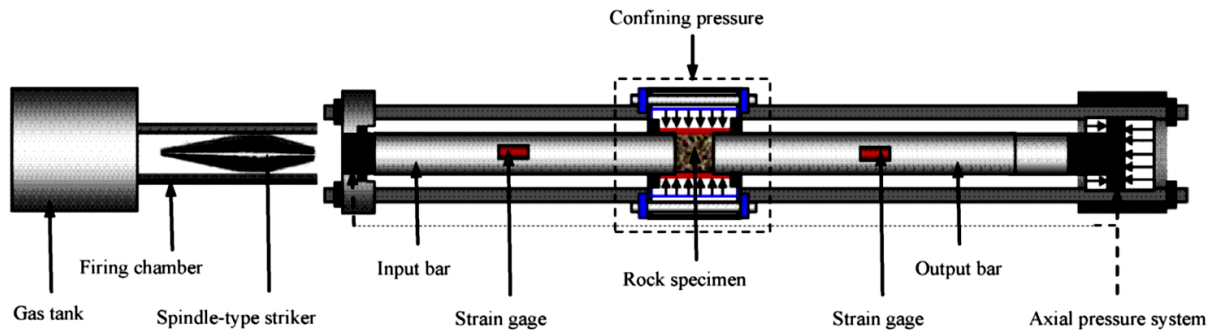
Fig. 5.3: Advanced Split Hopkinson pressure bar device with sample under confining pressure [Li et al. 2017]

6   Drilling resistance measurement

Drilling resistance (DR) measurement is a micro-destructive technique (e.g. Pamplona & Koher, 2007; Dumitrescu et al., 2017). Forward and rotational speed of a small drill bit are kept constant and drilling resistance (force) is measured or force is kept constant and penetration speed is measured. It is a popular method for evaluation of strength or weathering state of natural and artificial stones, masonry materials and wood. Correlations exist between DR and strength values. Typical drill bit diameter is between 3 and 7 mm. Typical drilling depth is up to about 100 mm, mostly shorter. Fig. 6.1 shows corresponding equipment and Fig. 6.2 typical values for different types of rock.
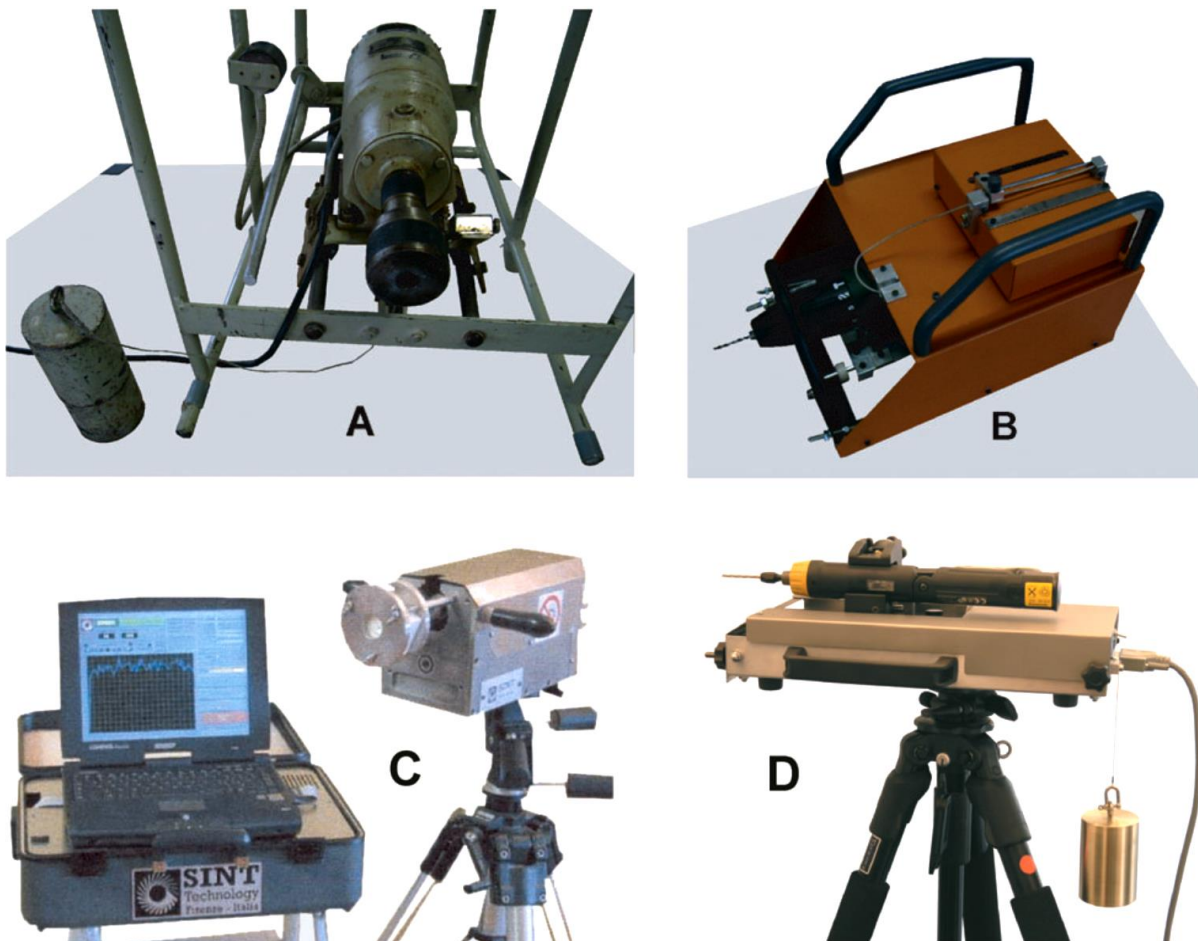
Fig. 6.1: Drilling resistance measurement equipment (Pamplona & Kocher, 2007)

Overview about rock mechanical lab testing – part I mechanical tests

Only for private and internal use!   Updated: 12 August 2024

l = drill bit Ø	DR$_m$ [N]				DR$_i$ [N/mm]			
	3 mm	5 mm	7 mm	10 mm	3 mm	5 mm	7 mm	10 mm
Talc	2.3	4.4	5.3	8.8	0.8	0.9	0.8	0.9
ARS	4.8	8.8	10.8	16.3	1.6	1.8	1.5	1.6
Gypsum	6.9	11.3	17.0	25.6	2.3	2.3	2.4	2.6
Calcite	15.6	26.1	38.5	60.1	5.2	5.8	5.5	5.9
Macor	16.4	28.1	41.4	67.7	5.5	5.6	5.9	6.8

Fig. 6.2: Measured and converted DR values (Pamplona & Kocher, 2007)

Sensitivity of DR measurements is impressively displayed in Fig. 6.3 for a piece of wood. Fig. 6.4 shows a correlation between drilling resistance and biaxial flexural strength for unweathered rocks.

Fig. 6.3: Measured drilling resistance in a piece of wood (company material)

Fig. 6.4: Drilling resistance vs. biaxial fluxeral strength for rocks (Pamplona & Kocher, 2007)

Overview about rock mechanical lab testing – part I mechanical tests
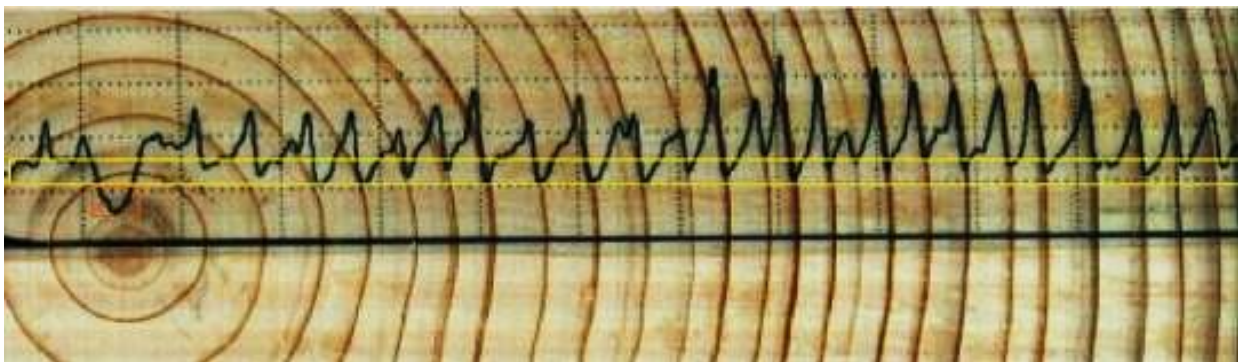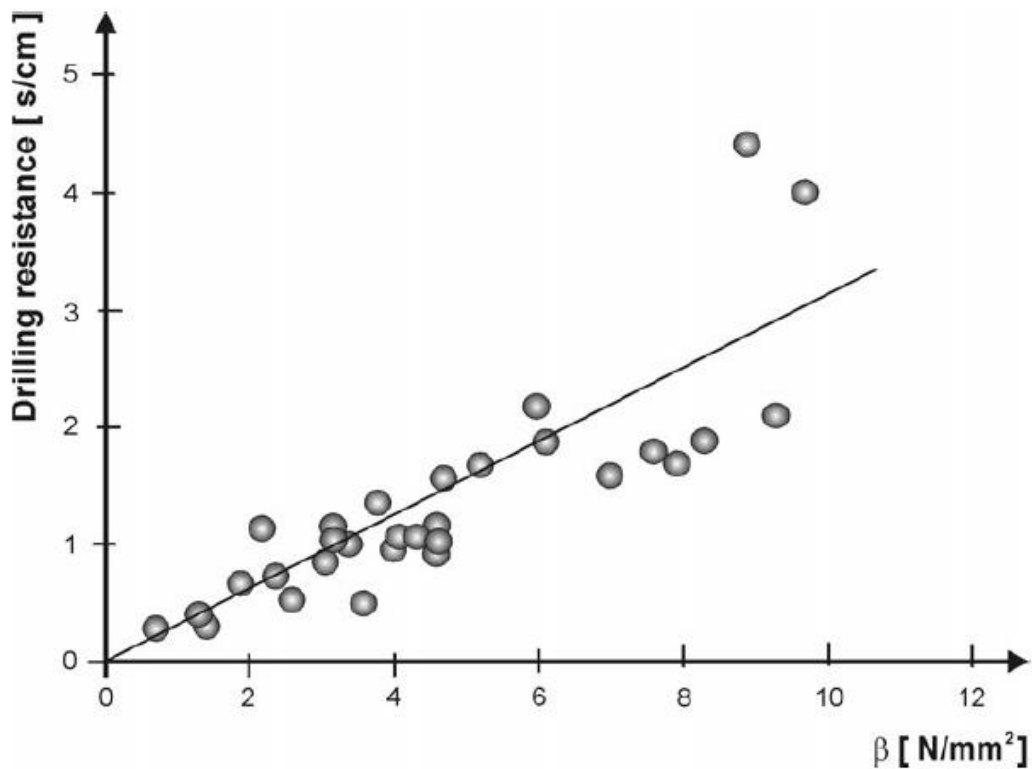
Only for private and internal use!   Updated: 12 August 2024

7   Mercury intrusion porosimetry

Porosity (effective porosity) can be determined based on the density determination as described in chaper 2. However, this simple technique has two major restrictions: (a) no information about the pore size/volume distribution can be obtained and (b) this technique can cover only pores above a certain minimum size. The mercury intrusion porosimetry (MIP) uses the non-wetting liquid mercury and is able to detect pores over a range of a few nm up to about 1000 µm, and allows to deduce pore size distributions well above 500 nm. Further information which can be deduced from MIP measurements is: skeletal and apparent density, total open porosity and specific surface area. Fig. 7.1 illustrates the application range of MIP in comparison with other techniques.
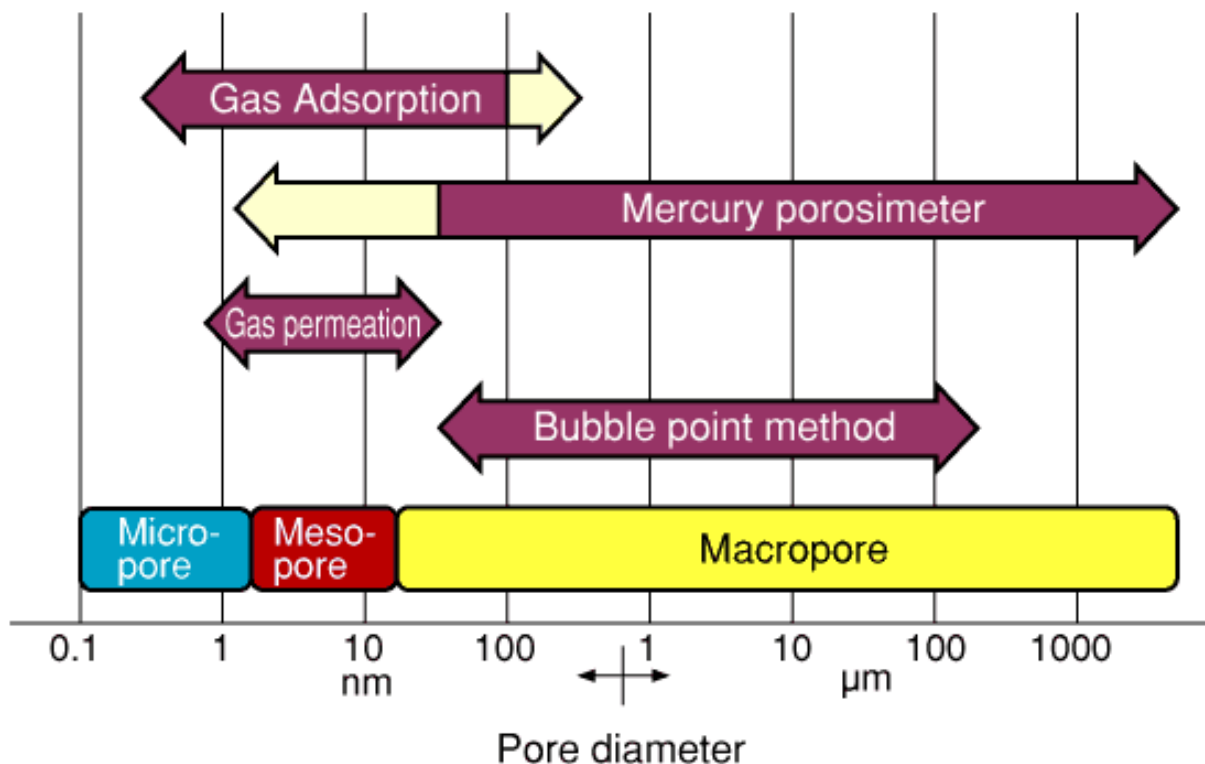
Fig. 7.1: Application range of MPI in comparison to other techniques (company material)

Depending on mercury pressure, pores of certain size are filled. Fig. 7.2 illustrates one complete mercury intrusion-extrusion cycle. If different pressure levels are applied the pore size (diameter) and volume distribution can be deduced as exemplary shown in Fig. 7.3. The higher the pressure on the mercury, the smaller the pores (characterized by pore diameter) can be entered by the mercury.

Overview about rock mechanical lab testing – part I mechanical tests

Only for private and internal use!   Updated: 12 August 2024
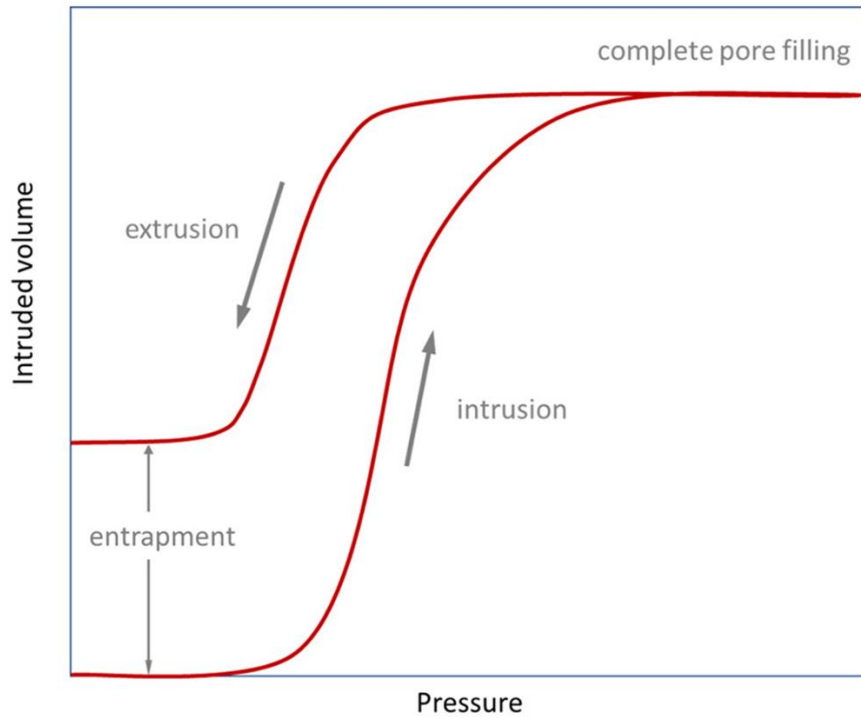
Fig. 7.2: One complete MIP intrusion – extrusion cycle indicating hysteresis (company material)
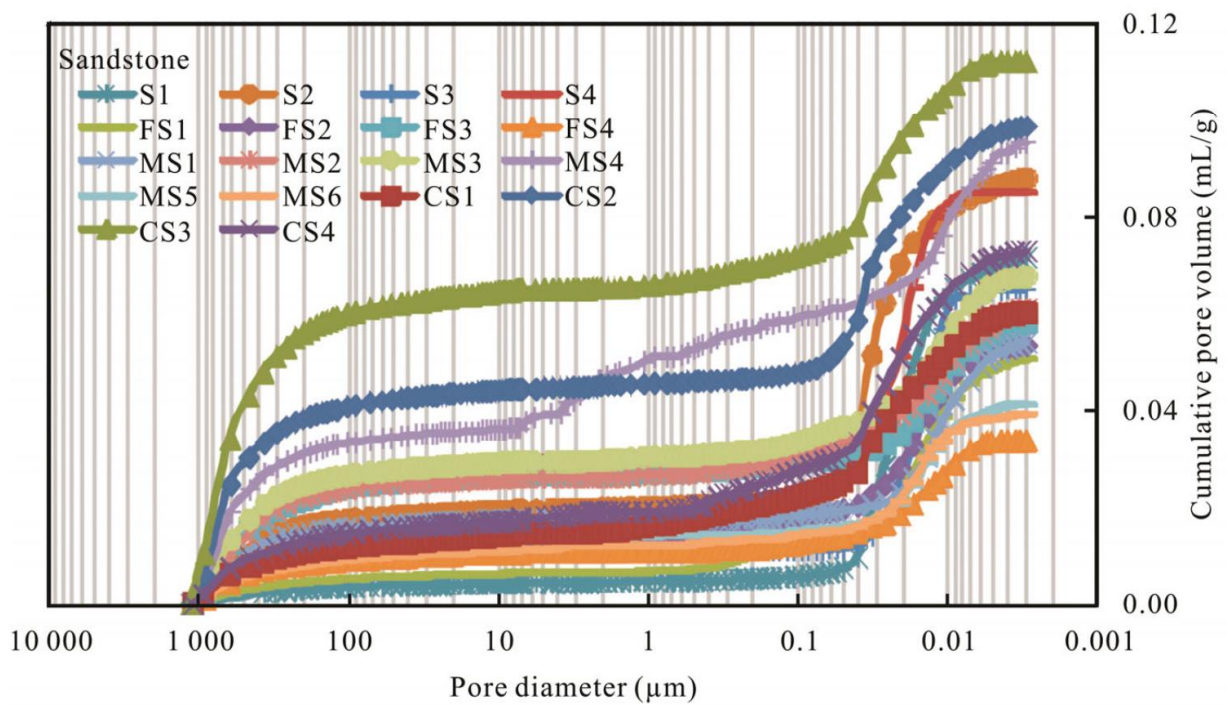
Fig. 7.3: Pore size and volume distribution of different types of sandstone (Zhang et al. 2026)

Overview about rock mechanical lab testing – part I mechanical tests

Only for private and internal use!   Updated: 12 August 2024

8   Gas pyknometer measurements

Gas pyknometer measurements are more precise compared to classical density determination like described in chapter 2. They have also the big advantage to perform measurements on small and irregular shaped samples. Fig. 8.1 shows a corresponding device.

Fig. 8.1: Gas pyknometer (company material)

A $\rho_F = \dfrac{m}{V_F}$

B $\rho_R = \dfrac{m}{(V_F + V_P)}$

C $\rho_S = \dfrac{m}{(V_F + V_S)}$

D $\rho_S = \dfrac{m}{(V_F + V_P + V_S)}$

V_F Volume of the solid
V_P Pore volume
V_S Inter-particle volume
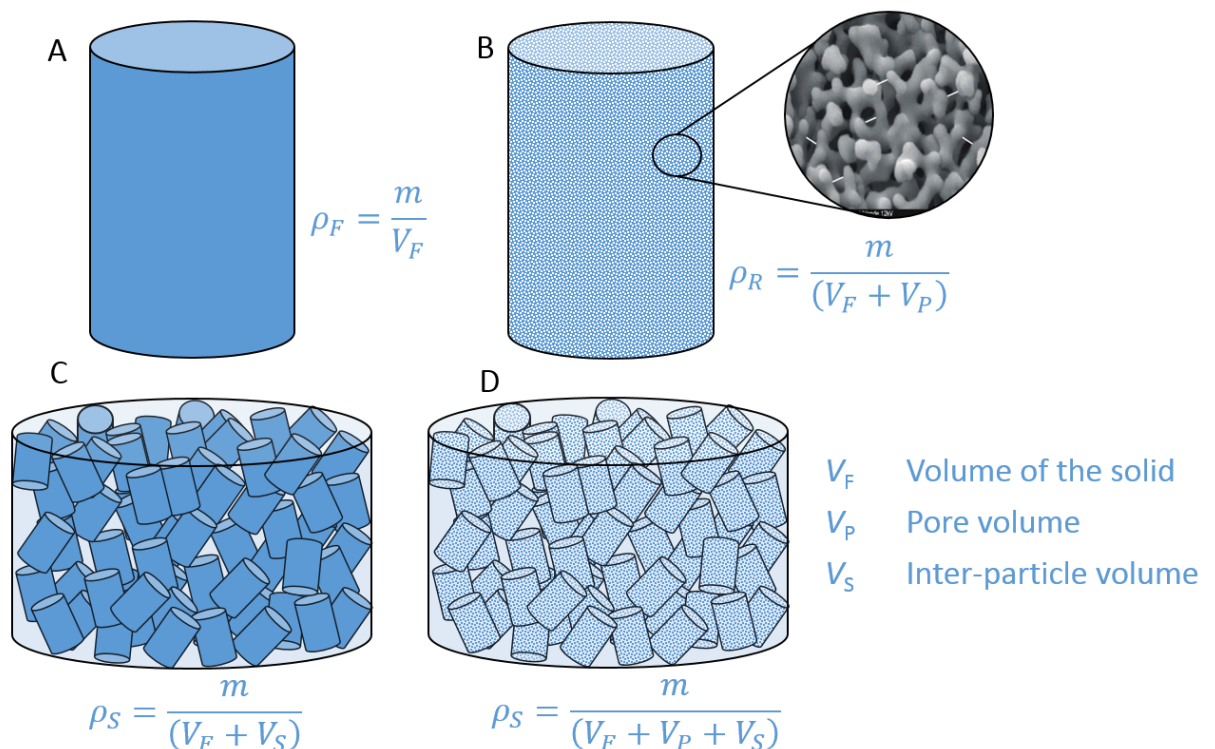
Fig. 8.2: Background of gas pyknometer measurements (company material)

Overview about rock mechanical lab testing – part I mechanical tests

Only for private and internal use!   Updated: 12 August 2024
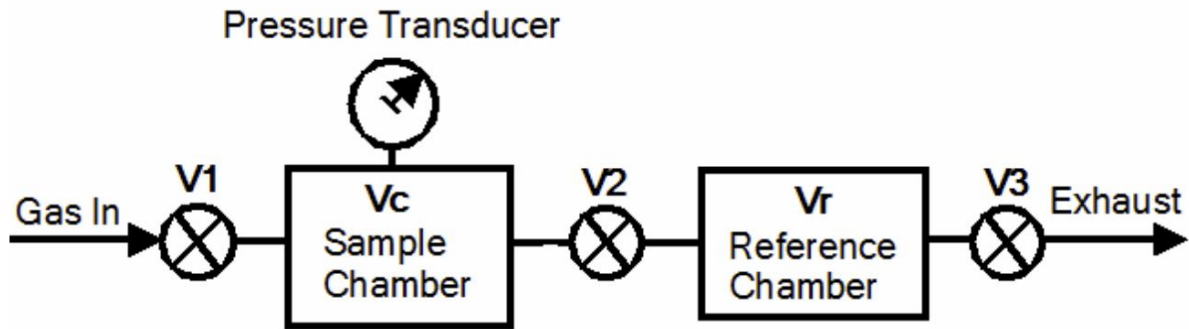
Fig. 8.3: Sketch illustrating the measuring principle of gas pyknometer (company material)

The gas pyknometer determines primarily the solid sample volume V_{solid} (density can be determined by measuring the weight additionally). The basic equation is:

$$V_{solid} = V_C - \frac{V_r(P_a - P_b)}{P_c - P_a}$$

Where:

V_{solid} -   Volume of sample
V_C -   Volume of sample chamber
V_r -   Volume of reference chamber
P_a -   Equilibrium pressure, when sample chamber and reference chamber are connected
P_b -   Atmospheric pressure (ambient pressure)
P_c -   Enhanced gas pressure in sample chamber

In principle, the measurement is conducted by the following steps:

(1) Pressurize the sample chamber up to P_c
(2) Connect sample and reference chamber and measure final pressure P_a (same pressure in both chambers)
(3) Measure atmospheric pressure P_b

The accuracy fo gas pyknometer measurements are in the order of 10^{-5} g/cm^3. Gas pyknometer measurements are standardized (ASTM or DIN).

Overview about rock mechanical lab testing – part I mechanical tests

Only for private and internal use! Updated: 12 August 2024

9 Large-scale testing (physical models)

The aim of large-scale experiments is to investigate scale effects, bigger rock blocks or the behaviour of more complex systems. Large scale experiments consist of large loading frames. Two types of tests can be distinguished:

- Physical models based on up-scaling of complex systems under consideration of the laws of physical equivalence (e.g. mining systems or dam constructions)
- Test of geotechnical elements in real size (e.g. railroad systems, support elements or huge rock blocks)

In most cases these tests are unique and need special designed measuring and loading arrangements. Large scale testing is very time and cost consuming and therefore often replaced or at least supported by numerical simulations.

Fig. 9.1: Loading frame with physical model of tunnel with installed anchors (State key lab, Zhengzhou, China)

Overview about rock mechanical lab testing – part I mechanical tests

Only for private and internal use!   Updated: 12 August 2024

Fig. 9.2: Static and dynamic loading rig for testing of railway foundation in real size (CSU, Changsha, China)

Fig. 9.3: True triaxial cell for large samples up to 3 x 3 x 3.5 m (State key lab, Zhengzhou, China)

10 Literature

Alejano, L.R. et al. (2018): ISRM suggested method for determining the basic friction angle of planar rock surfaces by means of tilt tests, Rock Mech. Rock Eng., 51: 3853-3859

Alejano, L.R. et al. (2017): A benchmark experiment to assess factors affecting tilt test results for sawcut rock surfaces, Rock Mech. Rock Eng., 50: 2547-2562

Alejano, L.R. et al. (2012): Compasrion of different techniques of tilt testing and basic friction angle variability assessment, Rock Mech. Rock Eng., 45(6): 1023-1035

Aliha, M.R.M.; Ayatollahi, MN.R. (2014): Rock fracture toughness study using cracked chevron notched Brazilian disc specimen under pure modes I and II loading – A stochastical approach, Theoretical and Applied Fracture Mechanics, 69: 17-25.

Backers, T. (2004): Fracture toughness determination and micromechanics of rock under mode I and mode II loading, PhD thesis, University Potsdam, Germany

Backers, T.; Stephansson, O. (2012): ISRM suggested method for the determination of model II fracture toughness, Rock Mech Rock Eng, 45: 1011-1022

Baumgarten, L.; Konietzky, H. (2012): Stress-strain, strength and failure behavior of Postaer Sandstone in tension and compression tests – laboratory investigations and numerical modelling with PFC^{3D}, Veröffentl. Institut f. Geotechnik (ed. H. Konietzky), TU Bergakademie Freiberg, Heft 2012-1, pp. 41-61

Baumgarten, L. (2015): Gesteinsmechanische Versuche und petrophysikalische Untersuchungen – Laborergebnisse und numerische Untersuchungen, PhD-Thesis, Institut für Geotechnik, TU Bergakademie Freiberg

Burbach, U. (2021): Zum Einfluss der Belastungsgeschwindigkeit auf die Ergebnisse einaxialer Druckversuche und Folgen für die Abgrenzung von Homogenbereichen, 24. Symposium Felsmechanik und Tunnelbau, DGGT (unpublished)

Calabrese, L. & Proverbio, E. (2020): A review on the application of acoustic emission technique in the study of stress corrosion cracking, Corros. Mater. Degrad., 2: 1-30

Chen, W., Konietzky, H. (2014): Simulation of heterogeneity, creep, damage and life time for loaded brittle rocks, Tectonophysics, 633: 164-175

Chen, W., Konietzky, H. (2015): Numerical simulation of time-independent and time-dependent fracturing in sandstone, *Engineering Geology*, 193: 118-131

Dinh, Q.D. (2011): Brazilian test on anisotropic rocks – laboratory experiment, numerical simulation and interpretation, Veröffentl. Institut Geotechnik (ed. H. Konietzky), TU Bergakademie Freiberg, Heft 2011-2

Dinh, Q.D; Konietzky, H.; Herbst, M., (2013): Brazilian Tensile Strength Tests on some Anisotropic Rocks, Int. J. Rock Mech. Mining Sci., 58: 1-7.

Overview about rock mechanical lab testing – part I mechanical tests

Only for private and internal use!   Updated: 12 August 2024

Dinh, Q.D.; Konietzky, H. (2014): Numerical simulations and interpretations of Brazilian tensile tests on transversely isotropic rocks, Int. J. Rock Mech. Min. Sci., 71: 53-63

Dresen, G. et al. (2020): Seismic and aseismic preparatory processes before large stick-slip failure, Pure Appl. Geophys., 117: 5741-5760

Dumiterscu, T.F. et al. (2017): Optimization of drilling resistance measurements (DRM) user-controlled variables, Materials and Structures, 50: 243

Germaine, J.T & Germaine, A.V. (2009): Geotechnical laboratory measurements for engineers, John Wiley & Sons, 368 p.

Giesche, H. (2006): Mercury porosimetry: a general (practical) overview, Part. Part. Syst. Charact., 23: 1-11

Jang, H.-S. et al. (2018): Determination of the basic friction of rock surfaces by tilt tests, Rock Mech. Rock Eng., 51: 989-1004

Kataoka, M. & Obara, Y. (2015): Anisotropy in fracture toughness of sedimentary and crystalline rocks estimated by semi-circular bend test, Proc. of ISRM Regional Symposium – EUROCK 2015, Salzburg, Austria

Konietzky, H.; Frühwirt, T.; Luge, H., (2012): A new large dynamic rockmechanical direct shear box device, Rock Mech. Rock Eng., 45(3): 427-432.

Kuruppu, M.D., Obara, Y., Ayatollahi, M.R., Chong, K.P. & Funatsu, T. (2014): ISRM-suggested method for determining the mode I static fracture toughness using semi-circular bend specimen, Rock Mech. Rock Eng., 47: 267-274

Kwasniewski, M. (2012): Recent advances in studies on the strength of rocks under general triaxial compression conditions, Veröffentl. Institut Geotechnik (ed. H. Konietzky), TU Bergakademie Freiberg, Heft 2012-2, p. 77-104

Kwiatek, G. et al. (2016): HybridMT: a mathlab/shell environment package for seismic moment tensor inversion and refinement, Seismological Research Letters, 87(4): 964-976

Li, X., Gong, F., Tao, M., Dong, L., Du, K., Ma, C., Zhou, Z. & Yin, T. (2017): Failure mechanism and coupled static-dynamic loading theory in deep hard rock mining: a review, J. Rock Mech. Geotechn. Eng., 9(4): 767-782

Liu, J., Li, Y.-h., Xu, S.-d., Xu, S., Jin, C.-h., Liu, Z.-s. (2015): Moment tensor analysis of acoustic emission for cracking mechanisms in rock with a pre-cut circular hole under uniaxial compression, Eng. Fracture Mechanics, 135: 206-218

Lunow, C. (2014): Simulation von gesteinsmechanischen Bohr- und Schneidprozessen mittels der Diskreten-Elemente-Methode, PhD Thesis, TU Bergakademie Freiberg, Germany

Ma, Z. et al. (2020): Application of nanoindentation technology in rocks: a review, Geomech. Geophys. Geo-energ. Geo.-resour., 6: 60

Overview about rock mechanical lab testing – part I mechanical tests

Only for private and internal use!   Updated: 12 August 2024

Mittelbach, L.; Konietzky, H.; Baumgarten, L., (2012): Ultrasonic wave measurements during triaxial tests - laboratory tests and numerical simulations, BAW-Mitteilungen, 95: 71-78.

Nguyen, V.M. (2013): Static and dynamic behavior of joints in schistose rock: Lab testing and numerical simulation, Veröffentl. Institut Geotechnik (ed. H. Konietzky), TU Bergakademie Freiberg, Heft 2013-3

Nguyen, V.M; Konietzky, H.; Frühwirt, T., (2014): New Methodology to Characterize Shear Behavior of Joints by Combination of Direct Shear Box Testing and Numerical Simulations. Geotech Geol Eng., 32(4): 829-846

Pamplona, M. & Kocher, M. (2007): Drilling resistance: overview and outlook, Zeitschrift der DGG, 158/3, 665-676

Perras, M.A. & Diederichs, M.S. (2014): A review of the tensile strength of rock: concepts and testing, Geotechnical and Geological Engineering, 32(2): 525-546

Perez-Rey, I., Muniz-Mendenez, M., Fruehwirt, T., Konietzky, H., Jacobsson, L., Perras M.A., Atefi-Monfared, K., Mas Ivars, D., Sanchez Juncal, A., Alejano, L.R. (2024): Assessment of direct tensile strength tests in rock through a multi-laboratory benchmark experiment, Rock Mech. Rock Eng., 57: 3617-3634

Pinto da Cunha, A., (1990): Scale Effects in Rock Masses. International Workshop, 7. & 8.6.1990, Leon, Norway, Balkema

Plinninger, R.; Käsling, H.; Thuro K.; Spaun, B. (2003): Testing conditions and geomechanical properties influencing the Cherchar abrasiveness index (CAI), Int. J. Rock Mech. Mining Sci., 40(2): 259-263.

Rabat, A. et al. (2020): Evaluation of strength and deformability of soft sedimentary rocks in dry and saturated conditions through needle penetration and point load tests: a comparative study, Rock Mech. Rock Eng., 53: 2701-2726

RML (2022): Rock Mechanical Laboratory, Chair for Rock Mechanics, Geotechnical Institute, TU Bergakademie Freiberg, Germany

Ruffolo, R.M. & Shakoor, A. (2009): Variability of unconfined compressive strength in relation to number of test samples, Engineering Geology, 108: 16-23

Sainsbury, B. & McDonald, A. (2023): Cosnideration of the accuracy of empirical and indirect laboratory methods for the characterization of tension strength, Geotech. Geol. Eng., 42: 4679-4692

Shukla, P. et al. (2015): Nanoindentation measurements on rocks, Proc. 5. Conference of Society for Experimental Mechanics, Springer

Stanchits, S., Mayr, S., Shapiro, S., Dresen, G., (2011): Fracturing of porous rock induced by fluid injection, Tectonophysics, 503(1-2): 129-145

Overview about rock mechanical lab testing – part I mechanical tests

Only for private and internal use!   Updated: 12 August 2024

Stanchits, S., Surdi, A., Gathogo, P., Edelman, E., Suarez-Rivera, R., (2014): Onset of hydraulic fracture initiation monitored by acoustic emission and volumetric deformation measurements, Rock Mech. Rock Eng., 47(5): 1521-1532

Tan, X.; Konietzky, H.; Frühwirt, T., (2014): Laboratory observation and numerical simulation of permeability evolution during progressive failure of brittle rocks., Int. J. Rock Mech. Mining Sci., 68: 167-176

Thuro, K. (2008): The new suggested Method No. 5 of the AK 3.3. – Point Load Index Tests on Rocks Samples, Veröffentl. Institut Geotechnik (ed. H. Konietzky), TU Bergakademie Freiberg, Heft 2008-3, p. 23-36

Ulusay, R. & Hudson, J.A., (2007): The complete ISRM suggested methods for rock characterization, testing and monitoring: 1974-2006. Suggested Methods Prepared by the Commission on Testing Methods.

Ulusay, R. et al. (2014): ISRM suggested method for the needle penetration test, Rock Mech. Rock Eng., 47: 1073-1085

Ulusay, R. (2015): The ISRM suggested methods for rock characterization, testing and monitoring: 2007-2014, Springer International Publishing, 293 p.

Vervoort, A.; K.-B., Min; Konietzky, H.; Cho, J.-W; Debecker, B.; Dinh, Q. D.; Frühwirt, T.; Tavallali, A., (2014): Failure of transversely isotropic rock under Brazilian test conditions., Int. J. Rock Mech. Mining Sci., 70: 343-352

Volinsky, A.A. et al. (2003): Fracture toughness, adhesion and mechanical properties of low-K dielectric thin films measured by nanoindentation, Thin Solid Films, 429: 201-210

Wang, J. et al. (2022): Using nanoindentation to characterize the mechanical and creep properties of shale: load and loading strain rate effects, ACS Omega, 7: 14317-14331

Wong, L.N.Y., Li, Z., Kang, H.M., the, C.I., (2017): Dynamic loading of Carrara marble in a heated state, Rock Mech. Rock Eng., 50(6): 1487-1505

Xia, K.; Yao, W (2015): Dynamic rock test using split Hopkinson (Kolsky) bar system – A review, Journal of Rock Mech. Geotechn. Eng., 7: 27-59

Xie, W. et al. (2024): A review of rock macro-indentation: theories, experiments, simulations and applications, J Rock Mech. Geotechn. Eng., 16: 2351-2374

Zhang, N. et al. (2016): Pore structure characteristics and permeability pf deep sedimentary rocks determined by mercury intrusion porosimetry, J. Earth Sciences, 27(4): 670-676

Zhou, Y.X., Xia, K., Li, X., Dai, F. (2012): Suggested methods for determination the dynamic strength parameters and mode-I fracture toughness of rock materials, Int. J. Rock Mech. Min. Sci., 49: 105-112